

**BARIUM AND LITHIUM IN FORAMINIFERA:
GLACIAL-INTERGLACIAL CHANGES IN THE NORTH ATLANTIC**

A Dissertation

Submitted to the Graduate Faculty of the
Louisiana State University and
Agricultural and Mechanical College
in partial fulfillment of the
requirements for the degree of
Doctor of Philosophy

in

The Department of Geology and Geophysics

by

Jenney M. Hall

B.S., Southern Utah University, 1996

M.S., University of Kansas, 1998

August, 2002

Dedicated to Jack and Otis

ACKNOWLEDGEMENTS

First, I would like to thank the members of my dissertation committee, Laurie Anderson, Ajoy Baksi, Phil Bart, Jeff Hanor, Robert Rohli, and John Wrenn. I am also grateful for the assistance given by Barun Sen Gupta in foraminiferal identification and nomenclature. Above all, I would like to thank my advisor Lui Chan (a.k.a. Dragon Lady) who inspired me with her integrity, work ethic, patience, and her endless supply of energy.

I would like to thank the many people and institutions that generously provided samples for this work. Richard Z. Poore provided sediment samples from the Arctic Ocean, William B. Curry and the Woods Hole Oceanographic Institution allowed me to sample the Bahama Bank cores and provided the North Atlantic transect samples. The Deep-Sea Sample Repository at the Lamont-Doherty Earth Observatory provided the Caribbean core. Special thanks to Yair Rosenthal for providing solutions from the Sierra Leone Rise and for sharing his insights. I also thank Karen L. Von Damm for the opportunity to participate in Indian Ocean cruise KN162-13.

I would also like to thank Alan Shiller, Arnold R. Warren, and Zhongxing Chen and the University of Southern Mississippi for use of the ICP-MS facility. I am also grateful for the assistance given by Tommy Blanchard, Wanda LeBlanc, Dorinda Ostermann, Kassia Pavich, Suzanne Perron-Cashman, Ellen Roosen, and Walter Joyce.

This work was supported by grants from the Geological Society of America, Gulf Coast Association of Geological Societies, and the Paleontological Society.

TABLE OF CONTENTS

DEDICATION	ii
ACKNOWLEDGEMENTS	iii
ABSTRACT	vii
CHAPTER 1. INTRODUCTION	1
1.1. Foraminiferal Geochemistry	1
1.2. Foraminiferal Barium	2
1.2.1. Glacial-interglacial Changes in the Upper North Atlantic	3
1.2.2. Deglacial Changes in the North Atlantic	4
1.3. Foraminiferal Lithium	5
1.4. Dissertation Overview and Objectives	6
1.5. References	7
CHAPTER 2. BA/CA IN BENTHIC FORAMINIFERA: RECONSTRUCTION OF THERMOCLINE AND MID-DEPTH CIRCULATION IN THE NORTH ATLANTIC DURING THE LAST GLACIATION	11
2.1. Introduction	11
2.1.1. Glacial-interglacial Changes within the Thermocline	13
2.1.2. Glacial-interglacial Changes at Mid-depth	14
2.1.3. Oceanographic Setting	15
2.2. Materials and Methods	15
2.2.1. Sample Preparation and Analysis	15
2.2.2. Chronology	19
2.3. Results	20
2.3.1. Bahama Banks	20
2.3.2. Caribbean	26
2.4. Discussion	29
2.4.1. The Last Glacial Maximum	34
2.4.1.1. Lower Thermocline Water	34
2.4.1.2. Intermediate Water	34
2.4.2. Deglaciation	36
2.5. Conclusions	38
2.6. References	39
CHAPTER 3. BA/CA IN NEOGLOBOQUADRINA PACHYDERMA AS AN INDICATOR OF MELT-WATER DISCHARGE INTO THE WESTERN ARCTIC OCEAN	44
3.1. Introduction	44
3.2. Materials and Methods	46
3.3. Results	49
3.3.1. Ba/Ca and $\delta^{18}\text{O}$	49
3.3.2. Reconstruction of Meltwater Input Using $\delta^{18}\text{O}$	54

3.3.3. Reconstruction of Surface Ba	56
3.3.4. Reconstruction of Meltwater Input Using Ba	57
3.4. Discussion	58
3.5. Conclusions	61
3.6. References	62
CHAPTER 4. LI/CA IN MULTIPLE SPECIES OF BENTHIC AND PLANKTONIC FORAMINIFERA: THERMOCLINE, LATITUDINAL, AND GLACIAL-INTERGLACIAL VARIATION	67
4.1. Introduction	67
4.1.1. Sediment Samples and Oceanographic Setting	68
4.2. Methods	71
4.2.1. Sample Preparation and Analysis	71
4.2.2. Chronology	74
4.3. Results	75
4.3.1. Down-core Variation in Bahamas and Caribbean	75
4.3.2. Sierra Leone Rise	79
4.3.3. North Atlantic Transect	84
4.3.4. Bahama Bank Margins	84
4.3.5. Interspecies Differences	89
4.4. Discussion	93
4.4.1. Water Depth	93
4.4.2. Dissolution	94
4.4.3. Temperature	95
4.4.4. Interspecies Incorporation Behavior	96
4.4.5. Calcification Rate	97
4.5. Conclusions	99
4.6. References	100
CHAPTER 5. DETERMINATION OF THE LITHIUM ISOTOPIC COMPOSITION OF FORAMINIFERAL TESTS AND ITS APPLICATION AS A PALEO-SEAWATER PROXY	104
5.1. Introduction	104
5.2. Materials and Methods	107
5.2.1. Lithium Composition of Seawater	107
5.2.2. Foraminiferal Cleaning and Li/Ca	107
5.2.3. Lithium Isotopic Analyses	108
5.3. Results and Discussion	110
5.3.1. Lithium in Seawater	110
5.3.2. Lithium in <i>O. universa</i>	112
5.4. Conclusions	115
5.5. References	116
CHAPTER 6. SUMMARY AND CONCLUSIONS	118
6.1. Benthic Ba/Ca Record of North Atlantic Circulation Changes	118
6.2. Planktonic Ba/Ca Record of Arctic Meltwater Discharge	119

6.3. Lithium in Foraminifera: A New Paleocean Tracer?	120
6.4. Foraminiferal Lithium Isotopic Composition	121
6.5. Future Work	122
APPENDIX 1. FORAMINIFERAL MN/CA DATA SUMMARY	124
APPENDIX 2. DETERMINATION OF THE Y-Z BOUNDARY	128
VITA	131

ABSTRACT

The trace element content of calcareous foraminifera provides a powerful tool to the study of glacial-interglacial changes in the physical and chemical properties of the ocean. Foraminifera incorporate barium in direct proportion to its concentration in seawater. Using barium as a nutrient proxy, Ba/Ca in benthic *Planulina wuellerstorfi* is used to reconstruct changes in thermocline ventilation and mid-depth circulation in the North Atlantic during the last glacial and deglacial time. Rivers are concentrated in barium compared to surface seawater. Therefore, barium in planktonic *Neogloboquadrina pachyderma* is used to identify deglacial meltwater in the Arctic Ocean. Foraminiferal Li/Ca was analyzed to elucidate factors influencing incorporation behavior, including interspecies differences, temperature, pressure, dissolution, and shell mass. To investigate the use of lithium isotopes as a proxy for paleo-seawater chemistry, $\delta^6\text{Li}$ was determined in planktonic *Orbulina universa*.

During the last glacial maximum, nutrients in the thermocline and the intermediate water of the North Atlantic was lower than today due to increased ventilation and the presence of nutrient-depleted Glacial North Atlantic Intermediate Water (GNAIW). During deglacial time, GNAIW was replaced by southern component water, resulting in an enrichment of nutrients in the mid-depth Atlantic water. Increased Ba/Ca in the surface Arctic Ocean indicates an increase in meltwater discharge between 12.4 and 11.3 ^{14}C ka BP. This may have triggered an increase in the export of freshwater to the North Atlantic, contributing to a shutdown in GNAIW production, and leading to the onset of the Younger Dryas. A second meltwater event at 9.4 ^{14}C ka BP may be the result of glacial Lake Agassiz draining through the Clearwater spillway to the Mackenzie River. Foraminiferal Li/Ca shows systematic glacial-interglacial variation coincident with $\delta^{18}\text{O}$. The incorporation behavior of lithium in foraminifera does not appear to be dominated by

changes in temperature, pressure, dissolution, or shell mass, but is potentially controlled by changes in growth conditions, including calcification rate. Preliminary work indicates that $\delta^6\text{Li}$ remained constant throughout the Holocene and the last glacial maximum at $-30.5 \pm 1.1\%$. Further developmental studies are necessary to fully engage lithium isotopes as a tracer of seawater composition.

CHAPTER 1: INTRODUCTION

1.1. Foraminiferal Geochemistry

A primary goal of paleoceanography is to reconstruct changes in thermohaline circulation through climatic transitions. Of the tools used by paleoceanographers, calcareous foraminifera are perhaps the most useful. Foraminifera are particularly sensitive to their surrounding conditions, occur throughout the Phanerozoic, are abundant, widespread, and have an excellent preservation potential. The taxonomic distribution of foraminifera has long been recognized as an indicator of oceanic environmental conditions. In the past two decades, geochemical investigations of foraminiferal tests have greatly enhanced our understanding of physical and geochemical changes in ancient oceans.

Calcareous foraminifera incorporate accessory cations into their tests (Lea, 1999). Elements such as magnesium and strontium are incorporated in minor amounts, whereas cadmium, barium, and lithium are incorporated in trace amounts. The resulting carbonate composition reflects both seawater chemistry and environmental conditions (e.g.; temperature and pressure) of the waters in which they live. These elements can therefore be used as paleoceanographic proxies.

Foraminifera sequester some elements, such as cadmium and barium, in proportion to their concentration in the surrounding seawater (Boyle et al., 1976; Lea and Boyle, 1989). Because the oceanic circulation of cadmium and barium in seawater resemble nutrients, their distributions can be used to identify watermasses because northern component watermasses are nutrient-poor whereas southern component watermasses are nutrient-rich. The chemical signatures of ancient watermasses preserved within the foraminiferal test can therefore be used to reconstruct ocean circulation in the past. In contrast, the incorporation behaviors of

geochemically conservative elements, such as magnesium, are dominated by environmental conditions like temperature (Rosenthal et al., 1997; Lea et al., 1999). These elements are therefore used to reconstruct paleoenvironmental conditions. As different proxies have different utilities and limitations, it is important to have a multi-proxy approach to paleoceanography. It is equally important to develop new proxies to provide fresh insights. In this work, a nutrient-type element, barium, and a conservative element, lithium, are investigated as paleoceanographic proxies.

1.2. Foraminiferal Barium

Nutrients in the ocean are depleted in the surface water and regenerated with depth (Broecker and Peng, 1982). The regeneration of labile nutrients (phosphate and nitrate) occurs from the decomposition of organic tissue, while refractory nutrients (silica and alkalinity) are dissolved from skeletal debris, resulting in slightly deeper regeneration. Foraminiferal $\delta^{13}\text{C}$ and Cd/Ca have a linear correlation with phosphate in seawater and are widely used as proxies for labile nutrients (e.g.; Boyle et al., 1976; Boyle, 1988; Marchitto et al., 1998). The distribution of barium in the global ocean has a linear relationship with alkalinity and silica, making it a proxy for refractory nutrients (Chan et al., 1977; Lea and Boyle, 1989). The incorporation of barium in foraminiferal tests occurs in direct proportion to seawater concentration and does not appear to vary with temperature or salinity (Lea and Boyle, 1991; Lea and Spero, 1992, 1994). As such, barium can be used to identify watermasses based on their nutrient content. Because refractory nutrients have a different oceanic distribution than labile nutrients, the use of barium in benthic foraminifera provides additional constraints on glacial-interglacial circulation changes.

In addition to being a watermass tracer, barium is also useful in tracking river water discharge into the ocean (e.g.; Guay and Faulker, 1997). Barium is removed from the surface

ocean due to biological activities (Chan et al., 1976; Bishop, 1988), but is concentrated in rivers as a result of continental weathering (Martin and Meybeck, 1979). Therefore, high levels of barium in surface seawater are indicative of a continental origin. This association enables barium in planktonic foraminifera to be used as an independent meltwater proxy to estimate salinity changes in the surface ocean.

1.2.1. Glacial-interglacial Changes in the Upper North Atlantic

There is increasing evidence that extensive reorganization in ocean circulation occurred during climatic transitions. A primary focus of this work is to address glacial-interglacial changes in the circulation history of the thermocline and mid-depth layers of the North Atlantic during the last glaciation, using foraminiferal Ba/Ca as paleo-nutrient proxy. The thermocline is a zone that separates the surface ocean mixed layer from the deeper watermasses that are driven by thermohaline circulation. The vertical distribution and cycling of nutrients within the thermocline respond to glacial-interglacial changes in climate, atmospheric composition, and biological productivity. The deeper watermasses can be distinguished from one another, because southern component watermasses such as Antarctic Intermediate Water (AAIW) and Antarctic Bottom Water are nutrient-rich while northern component watermasses such as North Atlantic Deep Water (NADW) and Glacial North Atlantic Intermediate Water (GNAIW) are nutrient-poor.

The thermohaline circulation of the modern North Atlantic is largely controlled by the formation of NADW, which is created by the cooling of surface waters in the Nordic Sea and the Labrador Sea (Broecker, 1991). Previous studies have shown that the production of NADW was greatly reduced during the last glaciation (Boyle and Keigwin, 1987; Oppo and Fairbanks, 1987; Duplessy et al., 1988; deMenocal et al., 1992; Oppo and Lehman, 1993). It is important to

understand changes in the production of NADW, because deepwater formation in the northern ocean affects global thermohaline circulation and climate.

Today, the mid-depth Atlantic is dominated by the presence of upper NADW between 1000 and 2000 m water depth, with minor amounts of AAIW and Mediterranean Overflow Water (deMenocal et al., 1992; Slowey and Curry, 1995). While the production of NADW was greatly reduced during the last glacial maximum, GNAIW was enhanced (Boyle and Keigwin, 1987; Oppo and Fairbanks, 1987; Duplessy et al., 1988; deMenocal et al., 1992; Oppo and Lehman, 1993). GNAIW formed at the expense of NADW when the subarctic surface water was unable to achieve the density required for deepwater formation and sank only to mid-depths. As a result, GNAIW replaced NADW in the intermediate depth North Atlantic during the last glacial maximum (Boyle and Keigwin, 1982, 1987; Oppo and Fairbanks, 1990; Marchitto et al., 1998) and southern component water filled the Atlantic basin up to 2000 m water depth (Oppo and Fairbanks, 1987; Duplessy et al., 1988; Oppo and Lehman, 1993). Previous work, based on benthic foraminiferal Cd/Ca and $\delta^{13}\text{C}$, indicates that this major redistribution in watermass circulation resulted in an increase in ocean ventilation, which caused a decrease in nutrients within the thermocline layer (Slowey and Curry, 1992, 1995; Marchitto et al., 1998) and in the mid-depth North Atlantic (Boyle and Keigwin, 1987; Oppo and Fairbanks, 1987, 1990; Zahn et al., 1987). This investigation utilizes foraminiferal Ba/Ca as a proxy of refractory nutrients, in comparison to labile nutrient proxies such as Cd/Ca and $\delta^{13}\text{C}$. It represents the first paleo-barium data from the thermocline layer.

1.2.2. Deglacial Changes in the North Atlantic

This work also aims to elucidate the changes that occurred during the last deglacial transition by using foraminiferal Ba/Ca to track meltwater discharge and related circulation

changes in the Atlantic Ocean. The high flux of meltwater from the Laurentide Ice Sheet significantly affected ocean circulation and climate by interrupting deepwater formation (Broecker et al., 1985; Boyle and Keigwin, 1987). The presence of a freshwater lens in the northern ocean may have halted the production of GNAIW (Venz et al., 1999; Rühlemann et al., 1999; Flower et al., 2000; Willamowski and Zahn, 2000) and triggered the Younger Dryas cold interval (Broecker et al., 1989). However, relatively little is known about the timing and extent of circulation changes during deglacial time.

1.3. Foraminiferal Lithium

Foraminiferal Li/Ca and lithium isotopic ratios have the potential to be used as proxies for changes in the lithium concentration and isotopic composition of seawater. Lithium exhibits conservative behavior in the ocean. It has an oceanic residence time of about 1.5 Ma (Huh et al., 1998) and currently has a constant concentration (26 μM) and isotopic composition (-32‰ $\delta^6\text{Li}$) throughout the world oceans (Chan and Edmond, 1988; You and Chan, 1996; James and Palmer, 2000). The major sources of lithium to the ocean are rivers (Huh et al., 1998) and hydrothermal interaction with oceanic crust (Von Damm et al., 1985; Chan et al., 1993). Because hydrothermal and river fluxes have distinctly different isotopic signatures, at -7‰ (Chan et al., 1993; Bray, 2001) and -23‰ $\delta^6\text{Li}$ (Huh et al., 1998) respectively, changes in the lithium concentration and isotopic composition of seawater would reflect changes in hydrothermal input and continental weathering over geologic time, provided the removal processes and rate constants do not change.

In order to develop foraminiferal Li/Ca and $\delta^6\text{Li}$ as new paleocean proxies, it is essential to understand factors that influence incorporation of lithium and its isotopes in foraminiferal tests. Previous investigations on the use of foraminiferal Li/Ca as a paleoceanographic proxy are

limited to date (Delaney et al., 1985; Delaney and Boyle, 1986), while the study of foraminiferal $\delta^6\text{Li}$ has been hampered by analytical difficulties (You and Chan, 1996; Hoefs and Sywall, 1997; Košler et al., 2001). This work examines several parameters that potentially influence foraminiferal Li/Ca, namely temperature, pressure, interspecies differences, and dissolution. It is also directed towards the development of methods for the reliable determination of lithium isotopic composition of foraminiferal tests.

1.4. Dissertation Overview and Objectives

Chapter 2 describes the use of barium in the benthic foraminifer *Planulina wuellerstorfi* to reconstruct changes in thermocline ventilation and mid-depth thermohaline circulation in the North Atlantic from the last glacial maximum to the Present. This work presents the first foraminiferal Ba/Ca data from the thermocline layer and focuses on the lesser known changes that occurred during the last deglacial transition. Chapter 3 demonstrates the use of barium in the planktonic foraminifer *Neogloboquadrina pachyderma* sinistral as a new independent proxy of meltwater discharge to the surface waters of the Arctic Ocean during deglacial time. Chapter 4 documents the glacial-interglacial variation in foraminiferal Li/Ca, and investigates the factors influencing lithium incorporation into foraminiferal tests including interspecies differences, temperature, pressure, dissolution, and shell mass. This study suggests that increased calcification rate may be the dominant factor controlling the Li/Ca content of foraminiferal calcite. Comparisons are also made to magnesium and strontium incorporation behavior from the same samples. Chapter 5 summarizes the development of a mass spectrometric technique for lithium isotope analyses of foraminiferal tests and applies the use of lithium isotopes in the planktonic foraminifer *Orbulina universa* as a paleo-lithium seawater proxy. This work presents

preliminary foraminiferal $\delta^6\text{Li}$ data, and the first seawater lithium isotope analyses from the Indian Ocean.

1.5. References

- Bishop J.K.B. (1988) The barite-opal-organic carbon association in oceanic particulate matter. *Nature* **332**, 341-343.
- Boyle E.A. (1988) Cadmium: Chemical tracer of deepwater paleoceanography. *Paleoceanography* **3**, 471-489.
- Boyle E.A. and Keigwin L.D. (1982) Deep circulation of the North Atlantic over the last 200,000 years: Geochemical evidence. *Science* **218**, 784-787.
- Boyle E.A. and Keigwin L.D. (1987) North Atlantic thermohaline circulation during the past 20,000 years linked to high-latitude surface temperature. *Nature* **330**, 35-40.
- Boyle E.A., Sclater F., and Edmond J.M. (1976) On the marine geochemistry of cadmium. *Nature* **263**, 42-44.
- Bray A. (2001) The geochemistry of boron and lithium in mid-ocean ridge hydrothermal vent fluids. Ph.D. dissertation, University of New Hampshire.
- Broecker W.S. (1991) The great ocean conveyor. *Oceanography* **4**, 79-89.
- Broecker W.S. and Peng T.-H. (1982) *Tracers in the Sea*. Eldigio Press.
- Broecker W.S., Kennett J.P., Flower B.P., Teller J.T., Trumbore S., Bonani G., and Wolfli W. (1989) Routing of meltwater from the Laurentide Ice Sheet during the Younger Dryas cold episode. *Nature* **341**, 318-321.
- Broecker W.S., Peteet D.M., and Rind D. (1985) Does the ocean-atmosphere system have more than one stable mode of operation? *Nature* **315**, 21-26.
- Chan L.-H., Drummond D., Edmond J.M., and Grant B. (1977) On the barium data from the GEOSECS expedition. *Deep-Sea Research* **24**, 613-649.
- Chan L.-H. and Edmond J.M. (1988) Variation of lithium isotope composition in the marine environment: A preliminary report. *Geochimica et Cosmochimica Acta* **52**, 1711-1717.
- Chan L.-H., Edmond J.M., Stallard R.F., Broecker W.S., Chung Y.C., Weiss R.F., and Ku T.L. (1976) Radium and barium at GEOSECS stations in the Atlantic and Pacific. *Earth and Planetary Science Letters* **32**, 259-267.

- Chan L.-H., Edmond J.M., and Thompson G. (1993) A lithium isotope study of hot springs and metabasalts from mid-ocean ridge hydrothermal systems. *Journal of Geophysical Research* **98**, 9653-9659.
- deMenocal P.B., Oppo D.W., Fairbanks R.G., and Prell W.L. (1992) Pleistocene $\delta^{13}\text{C}$ variability of North Atlantic Intermediate Water. *Paleoceanography* **7**, 229-250.
- Duplessy J.-C., Shackleton N.J., Fairbanks R.G., Labeyrie L., Oppo D.W., and Kallel N. (1988) Deepwater source variations during the last climatic cycle and their impact on the global deepwater circulation. *Paleoceanography* **3**, 343-360.
- Delaney M.L., Bé A.W.H., and Boyle E.A. (1985) Li, Sr, Mg, and Na in foraminiferal calcite shells from laboratory culture, sediment traps, and sediment cores. *Geochimica et Cosmochimica Acta* **49**, 1327-1341.
- Delaney M.L. and Boyle E.A. (1986) Lithium in foraminiferal shells: Implications for high-temperature hydrothermal circulation fluxes and oceanic crustal generation rates. *Earth and Planetary Science Letters* **80**, 91-105.
- Flower B.P., Oppo D.W., McManus J.F., Venz K.A., Hodell D.A., and Cullen J.L. (2000) North Atlantic intermediate to deep water circulation and chemical stratification during the past 1 Myr. *Paleoceanography* **15**, 388-403.
- Guay C.K. and Falkner K.K. (1997) Barium as a tracer of Arctic halocline and river waters. *Deep-Sea Research II* **44**, 1543-1569.
- Hoefs J. and Sywall M. (1997) Lithium isotope composition of Quaternary and Tertiary biogenic carbonates and a global lithium isotope balance. *Geochimica et Cosmochimica Acta* **13**, 2679-2690.
- Huh Y., Chan L.-H., Zhang L., and Edmond J.M. (1998) Lithium and its isotopes in major world rivers: Implications for weathering and the oceanic budget. *Geochimica et Cosmochimica Acta* **62**, 2039-2051.
- James R.H. and Palmer M.R. (2000) The lithium isotope composition of internal rock standards. *Chemical Geology* **166**, 319-326.
- Košler J., Kučera M., and Sylvester P. (2001) Precise measurement of Li isotopes in planktonic foraminiferal tests by quadrupole ICPMS. *Chemical Geology* **181**, 169-179.
- Lea D.W. (1999) Trace elements in foraminiferal calcite. In: *Modern Foraminifera* (ed. B. Sen Gupta), pp. 259-277. Dordrecht, Kluwer.
- Lea D.W. and Boyle E.A. (1989) Barium content of benthic foraminifera controlled by bottom-water composition. *Nature* **338**, 751-753.

- Lea D.W. and Boyle E.A. (1991) Barium in planktonic foraminifera. *Geochimica et Cosmochimica Acta* **55**, 3321-3331.
- Lea D.W., Mashiotta T.A., and Spero H.J. (1999) Controls on magnesium and strontium uptake in planktonic foraminifera determined by live culturing. *Geochimica et Cosmochimica Acta* **63**, 2369-2379.
- Lea D.W. and Spero H.J. (1992) Experimental determination of barium uptake in shells of the planktonic foraminifera *Orbulina universa* at 22°C. *Geochimica et Cosmochimica Acta* **56**, 2673-2680.
- Lea D.W. and Spero H.J. (1994) Assessing the reliability of paleochemical tracers: Barium uptake in the shells of planktonic foraminifera. *Paleoceanography* **9**, 445-452.
- Marchitto T.M., Curry W.B., and Oppo D.W. (1998) Millennial-scale changes in North Atlantic circulation since the last glaciation. *Nature* **393**, 557-561.
- Martin J.M. and Meybeck M. (1979) Elemental mass-balance of material carried by major world rivers. *Marine Chemistry* **7**, 173-206.
- Oppo D.W. and Fairbanks R.G. (1987) Variability in the deep and intermediate water circulation of the Atlantic Ocean during the past 25,000 years: Northern Hemisphere modulation of the Southern Ocean. *Earth and Planetary Science Letters* **86**, 1-15.
- Oppo D.W. and Fairbanks R.G. (1990) Atlantic Ocean thermohaline circulation of the last 150,000 years: Relationship to climate and atmospheric CO₂. *Paleoceanography* **5**, 277-288.
- Oppo D.W. and Lehman S.J. (1993) Mid-depth circulation of the subpolar North Atlantic during the last glacial maximum. *Science* **259**, 1148-1152.
- Rosenthal Y., Boyle E.A., and Labeyrie L. (1997) Last glacial maximum paleochemistry and deepwater circulation in the Southern Ocean: Evidence from foraminiferal cadmium. *Paleoceanography* **12**, 787-796.
- Rühlemann C., Mulitza S., Müller P.J., Wefer G., and Zahn R. (1999) Warming of the tropical Atlantic Ocean and slowdown of thermohaline circulation during the last deglaciation. *Nature* **402**, 511-514.
- Slowey N.C. and Curry W.B. (1992) Enhanced ventilation of the North Atlantic subtropical gyre thermocline during the last glaciation. *Nature* **358**, 665-668.
- Slowey N.C. and Curry W.B. (1995) Glacial-interglacial differences in circulation and carbon cycling within the upper western North Atlantic. *Paleoceanography* **10**, 715-732.

- Venz K.A., Hodell D.A., Stanton C., and Warnke D.A. (1999) A 1.0 myr record of Glacial North Atlantic Intermediate Water variability from ODP site 982 in the northeast Atlantic. *Paleoceanography* **14**, 42-52.
- Willamowski C. and Zahn R. (2000) Upper ocean circulation in the glacial North Atlantic from benthic foraminiferal isotope and trace element fingerprinting. *Paleoceanography* **15**, 515-527.
- Von Damm K.L., Edmond J.M., Grant B., Measures C.I., Walden B., and Weiss R.F. (1985) Chemistry of submarine hydrothermal solutions at 21°N, East Pacific Rise. *Geochimica et Cosmochimica Acta* **49**, 2197-2220.
- You C.-F. and Chan L.H. (1996) Precise determination of lithium isotopic composition in low concentration natural samples. *Geochimica et Cosmochimica Acta* **60**, 909-915.
- Zahn R., Sarnthein M., and Erlenkeuser H. (1987) Benthic isotope evidence for changes of the Mediterranean outflow during the late Quaternary. *Paleoceanography* **2**, 543-559.

CHAPTER 2. BA/CA IN BENTHIC FORAMINIFERA: RECONSTRUCTION OF THERMOCLINE AND MID-DEPTH CIRCULATION IN THE NORTH ATLANTIC DURING THE LAST GLACIATION

2.1. Introduction

Much of our current geochemical knowledge of paleoceanography comes from paleo-nutrient proxies such as $\delta^{13}\text{C}$, Cd/Ca, and Ba/Ca from benthic foraminifera (e.g.; Boyle and Keigwin, 1987; Oppo and Fairbanks, 1987; Lea and Boyle, 1989, 1990a, b; deMenocal et al., 1992; Sarnthein et al., 1994; Slowey and Curry, 1995; McIntyre et al., 1999; Venz et al., 1999; Flower et al., 2000). Although prior studies have investigated glacial-interglacial changes in the deep and intermediate depth North Atlantic, relatively little is known about differences in ventilation and watermass circulation within shallower waters. This investigation utilizes the barium content of benthic foraminifera as a nutrient proxy to reconstruct changes in lower thermocline ventilation (800 to 1000 m) and mid-depth watermass circulation (1000 to 2000 m) in the western North Atlantic during the last glacial cycle.

Previous studies reconstructing thermocline and mid-depth glacial-interglacial changes utilized foraminiferal $\delta^{13}\text{C}$ (Slowey and Curry, 1995) and Cd/Ca (Boyle and Keigwin, 1987; Marchitto et al., 1998) as proxies of labile nutrients. Foraminiferal Ba/Ca can be used to study refractory nutrient distribution in comparison to labile nutrients. This investigation represents the first paleo-barium data from the thermocline layer and elucidates the changes that occurred during the deglacial transition. Because refractory nutrients have a different oceanic distribution than labile nutrients, the study of barium in benthic foraminifera provides additional constraints on glacial-interglacial circulation changes.

Labile nutrients (phosphate and nitrate) regenerate through the decomposition of organic tissue (Broecker and Peng, 1982). As such, labile nutrients tend to have relatively shallow

regeneration as the majority of organic matter is oxidized at around 800 to 1000 m water depth. Boyle et al. (1976) established that there is a positive linear correlation between phosphorous and cadmium in ocean water. Therefore, benthic foraminiferal Cd/Ca is widely used as a proxy for labile nutrients in paleoceanographic studies (e.g.; Boyle, 1988; Marchitto et al., 1998).

Refractory nutrients (silica and alkalinity) are dissolved from skeletal debris in the water column, resulting in deeper regeneration compared to labile nutrients. The distribution of barium in the global ocean has a positive correlation with alkalinity and silica in that it is depleted in surface waters and regenerated at depth, making it a proxy for refractory nutrients (Chan et al., 1977; Lea and Boyle, 1989). The removal of barium from the surface water is attributed to barite (BaSO_4) precipitation, although the biological processes involved are not fully understood (Dehairs et al., 1980; Bishop, 1988; Paytan and Kastner, 1996).

Watermasses can be distinguished from one another based on their nutrient content, as southern component watermasses such as Antarctic Intermediate Water (AAIW) and Antarctic Bottom Water (AABW) are nutrient-rich whereas northern component watermasses such as North Atlantic Deep Water (NADW) and Glacial North Atlantic Intermediate Water (GNAIW) are nutrient-poor. Figure 2.1 shows the distribution of barium in a north-south section of the present day western Atlantic Ocean (after Chan et al., 1977). Barium is enriched in nutrient-rich southern component watermasses, but depleted in nutrient-poor northern component watermasses. Its distribution pattern shows the presence of barium-poor NADW wedged between barium-rich AAIW and AABW.

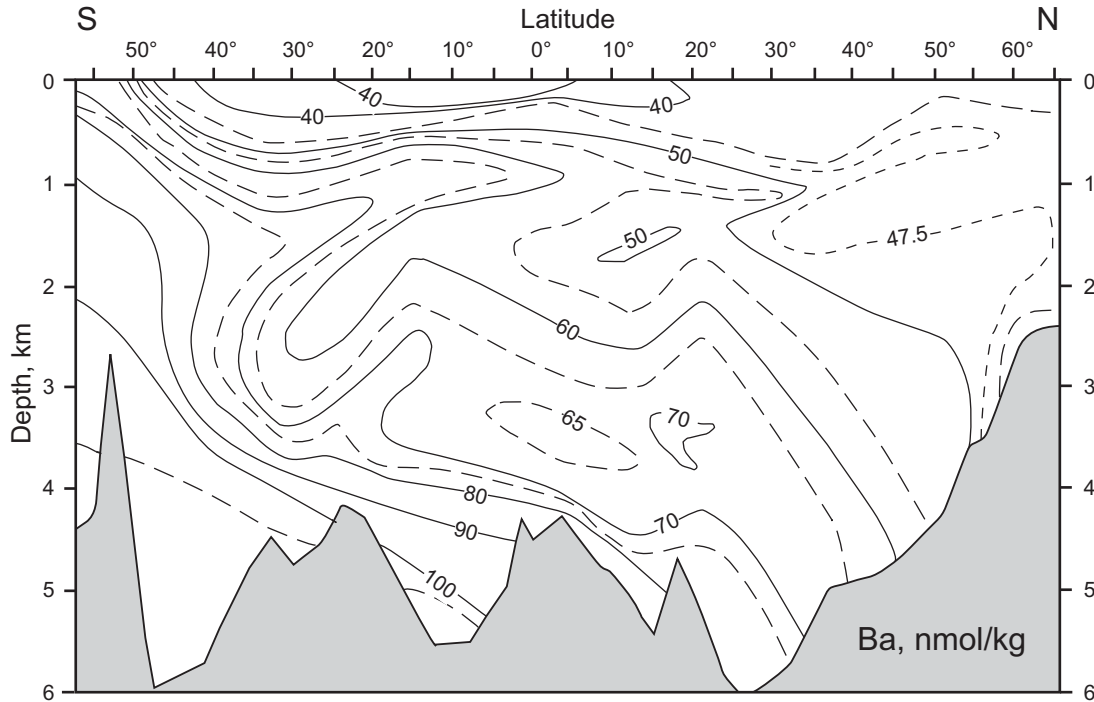


Figure 2.1. The distribution of seawater barium in a north-south section of the present day western Atlantic Ocean versus water depth (after Chan et al., 1977).

2.1.1. Glacial-interglacial Changes within the Thermocline

The thermocline is a zone that separates the surface ocean from deeper thermohaline circulated watermasses (Fig. 2.2) and is characterized by a rapid decrease in temperature with depth. Thermocline waters of the North Atlantic subtropical gyre outcrop in northern latitudes. Waters that originate here flow along the deepening isopycnals and gain nutrients due to the decomposition of organic matter, leading to a phosphate maximum and an oxygen minimum at the base of the thermocline. The vertical distribution and cycling of nutrients within the thermocline respond to climate change, related sea surface conditions (e.g.; wind and temperature), and biological productivity. Previous work utilizing benthic foraminiferal Cd/Ca and $\delta^{13}\text{C}$ indicates that during the last glacial maximum (LGM), increased ventilation of the western Atlantic thermocline caused a decrease in nutrients in thermocline waters, resulting in

the disappearance of the nutrient maximum and the oxygen minimum zone (Slowey and Curry, 1992, 1995; Marchitto et al., 1998). This work investigates refractory nutrient distribution, in comparison to labile nutrients, and represents the first paleo-barium data from the thermocline layer.

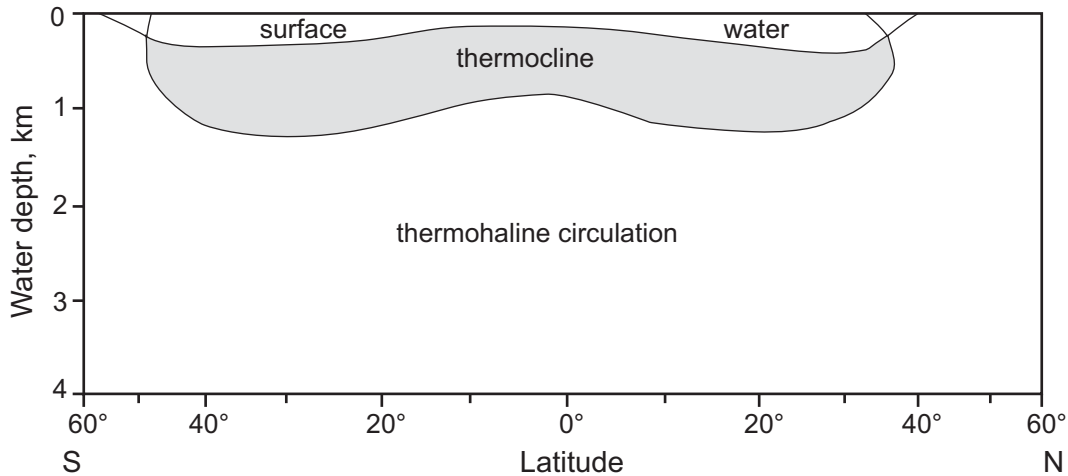


Figure 2.2. A north-south section of thermocline waters in the present day western Atlantic Ocean (after Weihaupt, 1979).

2.1.2. Glacial-interglacial Changes at Mid-depth

Previous work using foraminiferal Cd/Ca and $\delta^{13}\text{C}$ has shown a depletion of nutrients during the LGM in the mid-depth North Atlantic as seen by an enrichment of $\delta^{13}\text{C}$ (Oppo and Fairbanks, 1987, 1990; Zahn et al., 1987; Slowey and Curry, 1992, 1995) and a depletion of Cd/Ca (Boyle and Keigwin, 1987; Marchitto et al., 1998). GNAIW formed at the expense of NADW when the surface waters of the subarctic were unable to achieve the density required for deepwater formation and sank only to mid-depths (Boyle and Keigwin, 1987; Oppo and Fairbanks, 1987; Duplessy et al., 1988; deMenocal et al., 1992; Oppo and Lehman, 1993). During the LGM, GNAIW filled the North Atlantic above about 2000 m (Boyle and Keigwin,

1982, 1987; Oppo and Fairbanks, 1990; Marchitto et al., 1998), while southern component water occupied the deeper Atlantic basin (Oppo and Fairbanks, 1987; Duplessy et al., 1988; Oppo and Lehman, 1993). This redistribution in watermass circulation contributed to a decrease of nutrients in intermediate waters and an increase in deep waters (Boyle and Keigwin, 1985; Boyle, 1988; Curry et al., 1988; Lea and Boyle, 1990a; Martin and Lea, 1998). This work further investigates mid-depth circulation changes in the western Atlantic, but focuses on deglacial time.

2.1.3. Oceanographic Setting

Sediments from the Bahama Banks offer the unique opportunity to study the thermocline because the bank margins intersect the North Atlantic subtropical gyre thermocline waters above 1000 m water depth (Fig. 2.3). Oxygen-rich, nutrient-depleted upper NADW dominates the waters between 1000 and 2000 m, with less than 5% contribution from AAIW (Slowey and Curry, 1995). The Atlantic intermediate water adjacent to the Caribbean Sea sills (e.g.; the Windward passage) consists of 85% upper NADW, 10% AAIW, and 5% Mediterranean Overflow Water (MOW) (deMenocal et al., 1992). This water flows over the sills and fills the deep basins of the Caribbean Sea. In this work, foraminiferal Ba/Ca, Cd/Ca, and $\delta^{13}\text{C}$ from the Bahama Banks and the Caribbean Sea are used to reconstruct changes in watermass circulation in the mid-depth North Atlantic and the vertical distribution of nutrients in the lower thermocline layer during glacial, deglacial, and Holocene times.

2.2. Materials and Methods

2.2.1. Sample Preparation and Analysis

Sediment cores used in this study include a suite of cores recovered from the Bahama Banks between 423 to 1535 m water depths (Slowey and Curry, 1995) and a core from the

Columbia Basin of the Caribbean Sea from 3400 m water depth (Prell, 1978). The locations of the cores are given in Table 2.1.

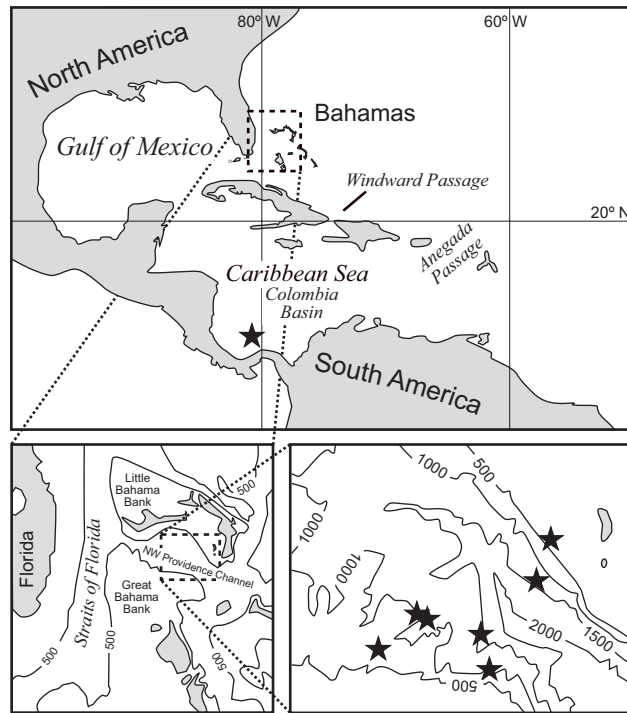


Figure 2.3. Core localities (stars) from the Northwest Providence Channel of the Bahama Banks and the Columbia Basin of the Caribbean Sea. See Table 2.1 for core descriptions.

Down-core samples typically were taken every 3 to 5 cm from sediments representing deglacial and glacial time and otherwise at 10 cm intervals. Sediments were disaggregated in distilled water on a shaker table and then wet-sieved through a 150 μm polypropylene mesh. The coarse fraction remaining in the sieve was then dried in an oven for 30 minutes to an hour at 55 to 60°C. Sediments were picked for benthic foraminifera including *Planulina wuellerstorfi* (synonymous with *Cibicidoides wuellerstorfi*), *Cibicidoides cicatricosus*, *Cibicidoides incrassatus* (synonymous with *Cibicidoides corpulentus*), *Cibicidoides pachyderma* (synonymous with *Cibicidoides floridanus*), and *Cibicidoides robertsonianus*.

Table 2.1. Sediment core descriptions; jumbo piston core (JPC), piston core (PC), and giant gravity core (GGC).

Core	Latitude, °N	Longitude, °W	Water Depth (m)	Core Number
<i>Bahama banks:</i>				
OC205-2-149JPC	26.26	77.67	423	1
OC205-2-108GGC	25.98	78.18	743	2
OC205-2-103GGC	26.07	78.06	965	3
OC205-2-100GGC	26.06	78.03	1057	4
OC205-2-97JPC	25.94	77.85	1183	5
OC205-2-7JPC	26.14	77.74	1320	6
OC205-2-117JPC	26.03	77.88	1535	7
<i>Caribbean:</i>				
VM28-129PC	11.12	80.40	3400	8

For chemical analyses, a 0.5 mg sample containing 4 to 25 individuals was used. Foraminiferal tests were gently crushed and then purified following modified procedures from Lea and Boyle (1993). Samples were ultrasonically cleaned four times with distilled water and twice with methanol to remove detrital grains and fine clay particles. Metal oxide coatings were reduced in a solution consisting of anhydrous-hydrazine, citric-acid, and ammonium-hydroxide and organic matter was oxidized in a solution of hydrogen-peroxide and sodium-hydroxide. Sedimentary barite was dissolved in alkaline diethylenetriamine-pentaacetic acid (DTPA). Any remaining adsorbed metals were leached with 0.001 N nitric acid. All dilute nitric acids used in this study were prepared from SEASTAR™ high purity acid. The remaining shell material was then dissolved in 0.1 N nitric acid and simultaneously analyzed for barium, cadmium, manganese, and calcium using a ThermoQuest Finnigan Element 2 inductively coupled plasma mass spectrometer (ICP-MS) at the University of Southern Mississippi in accordance with procedures of Rosenthal et al. (1999).

Following the method developed by Rosenthal et al. (1999), element to calcium ratios were determined from intensity ratios of appropriate isotopes with mass discrimination corrected using an external matrix matched standard. The multi-element standard was prepared with ICP-MS grade High-Purity Standards. This solution was standardized for barium by isotope dilution using a Finnigan MAT 262, thermal ionization mass spectrometer (TIMS) and procedures adapted from Chan et al. (1977). Cadmium and manganese were standardized by the standard additions method using ICP-MS, and calcium with PerkinElmer Optima 3300DV inductively coupled plasma optical emission spectrometry (ICP-OES). Replicate analyses of an external $^{135}\text{Ba}/^{138}\text{Ba}$ gravimetric standard that was calibrated using TIMS were performed to monitor the reproducibility and accuracy of the method. Long-term precision was within 2.8% and differed by less than 1% from values obtained using TIMS. Replicate analyses of *Planulina wuellerstorfi* yield an external precision (1σ) of about 5.5% for $^{138}\text{Ba}/^{43}\text{Ca}$. The analytical reproducibility is comparable to 7 to 10% standard deviation for foraminiferal samples reported by Lea and Boyle (1990b).

Some data were rejected from this study based on several criteria. Foraminiferal Mn/Ca was analyzed to monitor the effectiveness of the cleaning procedures (Appendix 1). Mn-carbonate overgrowths and Mn-oxide coatings contain a variety of other elements and therefore, must be removed before chemical analyses (Boyle, 1981, 1983). Samples with Mn/Ca ratios above 100 $\mu\text{mol/mol}$ are considered to be contaminated and were eliminated from consideration. However, Ba/Ca samples with Mn/Ca ratios above 100 $\mu\text{mol/mol}$ were retained if foraminiferal Ba/Ca from duplicate analyses was reproducible within 0.3 $\mu\text{mol/mol}$. Additionally, as the cleaning procedures were quite rigorous, some amount of shell material was inevitably lost.

Cleaned sample with excessively low yields were rejected from the data set as well as samples that were obviously contaminated with sedimentary barite ($> 4 \mu\text{mol/mol Ba/Ca}$).

2.2.2. Chronology

The Y-Z boundary is a biostratigraphic designation defined by the first consistent appearance of the *Globorotalia menardii* complex and represents the Pleistocene/Holocene boundary (Ericson and Wollin, 1956). Core sediments from a $>150 \mu\text{m}$ sieved fraction were dried, weighed, and then picked for the *G. menardii* complex. The frequency of the *G. menardii* complex was then calculated by dividing the number of individuals by the weight of the sample (Appendix 2). The radiocarbon age of the Y-Z boundary in the Gulf of Mexico, Caribbean Sea, and in the Bahamas is $11,000 \pm 500 \text{ yr BP}$ (Ericson and Wollin, 1956; Broecker et al., 1960; Ericson and Wollin, 1968). The Y-Z boundary for Caribbean core VM28-129PC was determined by Prell (1978) based on the carbonate and coarse fraction contents. Corrected radiocarbon ages from *Globigerinoides sacculifer* analyzed by accelerator mass spectrometry (AMS) were reported for Bahaman core 100GGC by Slowey and Curry (1995) assuming a 400 year reservoir age.

Stable isotopic measurements on *G. sacculifer* were made for Caribbean core V28-129PC at the Woods Hole Oceanographic Institution using a Finnigan MAT 252 mass spectrometer with a Kiel device. Stable isotopic analyses on the Bahaman cores, also using a Finnigan MAT 252 mass spectrometer, were performed on several species of benthic foraminifera and are reported by Slowey and Curry (1995). According to the oxygen isotope records, Caribbean core V28-129PC includes Holocene, deglacial, and LGM sediments whereas the cores taken from the Bahama Banks include the Holocene, deglacial, and LGM, with some cores extending into

oxygen isotope stage 3. The isotope stratigraphy of V28-129PC is in accordance with the stratigraphy based on percent carbonate and coarse-fraction (Prell, 1978).

2.3. Results

2.3.1. Bahama Banks

Ba/Ca was measured on *P. wuellerstorfi* from four Bahaman cores spanning water depths from 1057 to 1535 m (Table 2.2). Down-core Ba/Ca distributions are shown with $\delta^{18}\text{O}$ and $\delta^{13}\text{C}$ data from multiple benthic species (Slowey and Curry, 1995) in Fig. 2.4. Also shown are available radiocarbon ages for core 100GGC. Foraminiferal Ba/Ca is enriched in each of the cores during deglacial time corresponding to the $\delta^{13}\text{C}$ minimum, which is most clearly seen in the 100GGC profile (Fig. 2.4a). Figure 2.5 shows Holocene and core top measurements of Ba/Ca from multiple species of benthic foraminifera from the Bahama Banks between 423 and 1535 m water depths (Table 2.3). Foraminiferal Ba/Ca in Fig. 2.5 is plotted with equivalent seawater Ba/Ca from Geochemical Ocean Sections Study (GEOSECS) station 33 in the western Atlantic (21°N, 54°W). The equivalent seawater Ba/Ca is calculated from seawater barium concentrations (Chan et al., 1977) and a distribution coefficient for barium in mixed benthic species of 0.37 ± 0.06 (Lea and Boyle, 1989) according to Eqn. 2.1. This is possible because the incorporation of barium in foraminiferal tests occurs in direct proportion to seawater concentration and does not appear to vary with temperature or salinity (Lea and Boyle, 1991; Lea and Spero, 1992, 1994). Fig. 2.5 demonstrates that barium concentrations at GEOSECS station 33 are similar to those found at the Bahamas at equivalent water depths.

$$D_{Ba} = \frac{(Ba / Ca)_{foram}}{(Ba / Ca)_{sw}} \quad (\text{Eqn. 2.1})$$

Table 2.2. Ba/Ca in $\mu\text{mol/mol}$ in *Planulina wuellerstorfi* and *Orbulina universa* from Bahaman cores 100GGC, 97JPC, 7JPC, and 117JPC.

OC205-2-100GGC, 1057 m		OC205-2-97JPC, 1183 m		OC205-2-117JPC, 1535 m	
Core Depth (cm)	Ba/Ca <i>P. wuellerstorfi</i>	Core Depth (cm)	Ba/Ca <i>P. wuellerstorfi</i>	Core Depth (cm)	Ba/Ca <i>P. wuellerstorfi</i>
43.5	1.59	39.5	1.81	17	1.82
90	1.74	43	1.93	24.5	1.75
100	1.75	43	1.62	30	1.58
110	1.74	47	1.69	30	1.63
110	1.68	50	1.85	40	1.62
114.5	1.88	53	1.75	50	1.92
114.5	2.01	57	2.09	53	2.16
118.5	1.77	60	1.50	53	1.82
118.5	1.86	63	1.56	55.5	2.24
118.5	1.79	73	1.66	59	2.60
126	1.79	77	1.72	61.5	2.25
129	1.67	80	1.75	65.5	2.15
131.5	1.70	83	1.58	67.5	2.02
134.5	1.64	87	2.21	74	1.82
137	1.54	90	1.60	81	1.87
137	1.55	94.5	2.31	87	1.76
156	1.65	99.5	1.46	87	1.67
156	1.54	104.5	1.50	92.5	1.93
167	1.66	110	1.41	103.5	1.73
167	1.54			110	1.67
176.5	1.54			120	1.77
190	1.39			130	1.65
210	1.41			140	1.56
220	1.43			150	1.71
230	1.61			160	1.77
240	1.48			170	1.60
250	1.60			180	1.74
260.5	1.69			190	1.44
271	1.71			200	1.65
280.5	1.59			200	1.51
				220	1.60
				230	1.47
				240	1.47
				240	1.65
				247	1.56
				247	1.53
				247	1.61

Table 2.2 continued

OC205-2-7JPC, 1320 m		
Core Depth (cm)	Ba/Ca <i>P. wuellerstorfi</i>	Ba/Ca <i>O. universa</i>
11.5	1.50	0.63
18.5	1.36	0.74
28.5	1.38	0.72
38.5	1.52	0.65
38.5	1.53	---
48.5	1.47	0.66
54.5	1.84	0.71
60	1.70	0.54
60	1.57	---
63.5	1.49	---
63.5	1.71	---
67.5	1.37	0.56
77.5	1.43	0.56
79	1.51	0.63
79	1.44	---
85	---	0.62
90	1.77	0.73
97.5	1.58	0.67
108.5	1.68	0.67
121.5	1.78	0.82
121.5	1.36	---
121.5	1.29	---
131.5	1.87	0.67
144	1.57	0.77
150	---	0.73
160	---	0.86
170	1.57	0.74
190	1.66	---
210	1.64	---
220	1.77	---
240	1.68	---
250	1.83	---
260	1.80	---

Table 2.2 continued

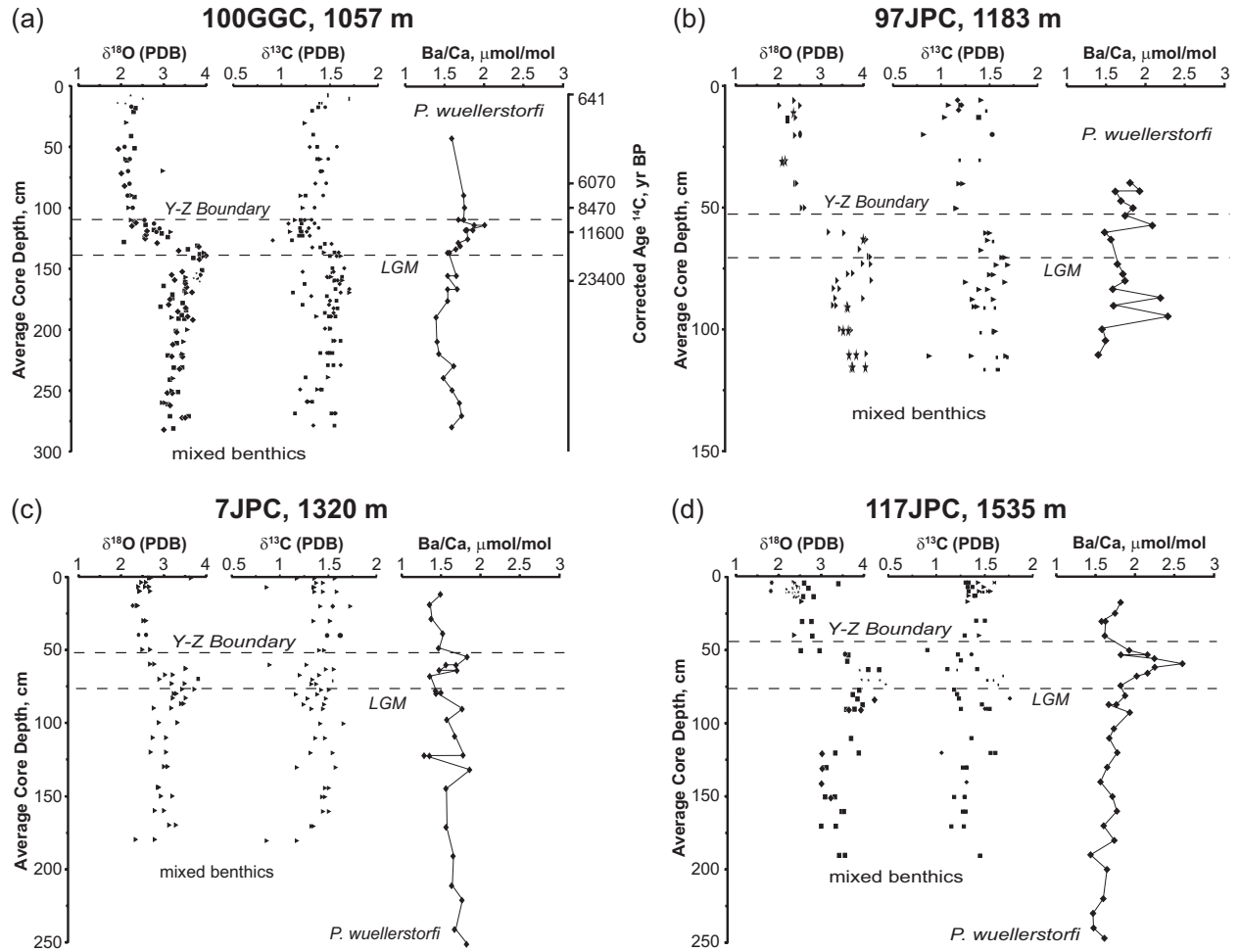


Figure 2.4. Ba/Ca in *Planulina wuellerstorfi* from Bahaman cores (a) 100GGC, (b) 97JPC, (c) 7JPC, and (d) 117JPC. See Table 2.2 for data summary. Slowey and Curry (1995) reported $\delta^{18}\text{O}$ and $\delta^{13}\text{C}$ from mixed benthic species and radiocarbon AMS ages from *Globigerinoides sacculifer*. $\delta^{18}\text{O}$ is used to identify the LGM while the Y-Z boundary is based on the *Globorotalia menardii* complex (Appendix 2; Ericson and Wollin, 1956).

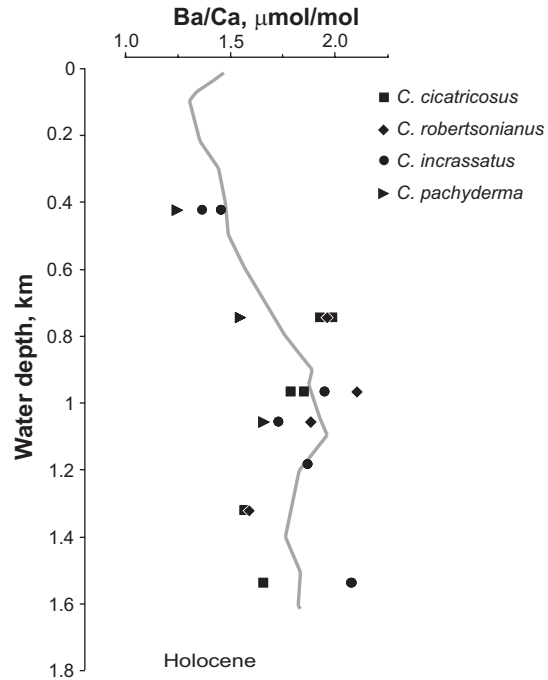


Figure 2.5. Ba/Ca in multiple species of benthic foraminifera from surface and Holocene sediments of the Bahama Banks between 423 and 1535 m water depths. See Table 2.3 for data summary. For comparison, equivalent Ba/Ca in seawater from GEOSECS station 33 (21°N, 54°W) is shown as gray line (Chan et al., 1977).

Table 2.3. Holocene and core top measurements of Ba/Ca in *Cibicidoides cicatricosus*, *Cibicidoides robertsonianus*, *Cibicidoides incrassatus*, and *Cibicidoides pachyderma* from the Bahama Banks between 423 and 1535 m water depths.

Water Depth (m)	Ba/Ca ($\mu\text{mol/mol}$)
▪ <i>C. cicatricosus</i>	
743	1.96
743	1.94
965	1.79
965	1.85
1320	1.56
1535	1.66
♦ <i>C. robertsonianus</i>	
743	1.94
965	2.27
965	2.10
1057	1.88
1320	1.58
• <i>C. incrassatus</i>	
423	1.36
423	1.45
965	1.95
1057	1.73
1183	1.86
1535	2.07
▶ <i>C. pachyderma</i>	
423	1.24
743	1.54
1057	1.66

Previous studies have shown that distribution coefficients may vary with water depth (McCorkle et al., 1995; Rosenthal et al., 1997; Buerkert, 1999). McCorkle et al. (1995) observed a 25% decrease in foraminiferal Ba/Ca and a 50% decrease in Cd/Ca at water depths greater than 2.5 km at the Ontong Java Plateau owing to increased dissolution with depth. As Bahaman and Caribbean waters are saturated with respect to calcite (Broecker and Peng, 1982; Haddad and

Droxler, 1996), D_{Ba} should not be affected by dissolution. Using *P. wuellerstorfi* from the Gulf of Mexico, Buerkert (1999) calculated a distribution coefficient of 0.37 ± 0.02 for water depths above 3200 m. Thus, the effects of water depth, due to dissolution or pressure, are considered to be negligible for the Ba/Ca variation observed in the present study.

Figure 2.6 shows Holocene, deglacial, and LGM barium values in *P. wuellerstorfi* with seawater barium from GEOSECS station 33. Barium concentrations are calculated from foraminiferal Ba/Ca according to Eqn. 2.1 using a distribution coefficient of 0.37 ± 0.06 (Lea and Boyle, 1989). The benthic foraminifer *P. wuellerstorfi* is a deep-water species, and is therefore not present at shallow depths and is relatively scarce in Holocene sediments compared to glacial. The foraminiferal Ba/Ca values used to calculate the average for each period from the various cores are listed in Table 2.4. Water depths for samples from the LGM are shifted upward by 120 m to correct for lower sea level (Fairbanks, 1989), and deglacial water depths are estimated to be 60 m shallower relative to modern water depths. Compared to the Holocene, the LGM was depleted in barium by 9 to 19% between 937 and 1200 m paleo-depth (Fig. 2.6, Table 2.4). At 1415 m paleo-depth, foraminiferal Ba/Ca from the LGM is similar to Holocene values from approximately the same depth. Following the LGM, there was a deglacial enrichment extending up to 1 km water depth, with the greatest change occurring at 1475 m paleo-depth, increasing by 41%.

2.3.2. Caribbean

Caribbean sediments provide a record of the intermediate waters (1600 – 1800 m) of the western North Atlantic that flow over the sills into the basin (Wüst, 1963). Down-core measurements of $\delta^{18}O$ from *G. sacculifer* from Caribbean core VM28-129PC show that these

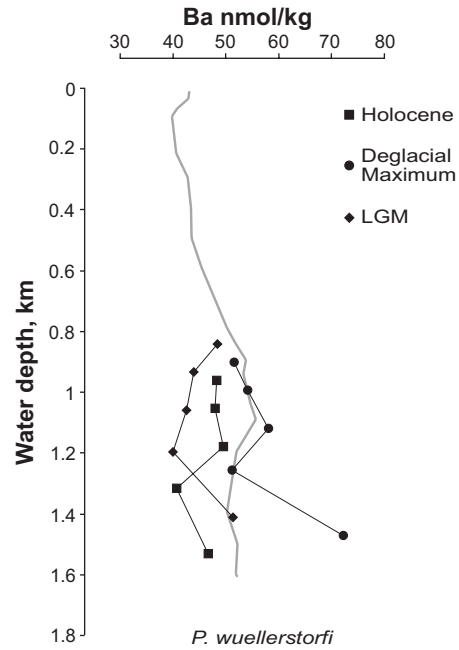


Figure 2.6. Barium seawater concentration reconstructed from Ba/Ca in *Planulina wuellerstorfi* from Bahama Bank margin sediments representing the Holocene, deglacial maximum, and last glacial maximum. See Table 2.4 for data summary. For comparison, barium in seawater from GEOSSECS station 33 (21°N, 54°W) is shown as gray line (Chan et al., 1977).

Table 2.4. Ba/Ca in $\mu\text{mol/mol}$ from *Planulina wuellerstorfi* from the Holocene, deglacial maximum, and last glacial maximum from the Bahama Banks and Caribbean Sea. See Table 2.1 for core descriptions.

Core Number	Water Depth (m)	Core Depth (cm)	Ba/Ca <i>P. wuellerstorfi</i>	Core Number	Water Depth (m)	Core Depth (cm)	Ba/Ca <i>P. wuellerstorfi</i>
Holocene				Deglacial Maximum			
3	965	82	1.80	3	905	109.5	1.87
3	965	101.5	1.66	3	905	114	1.83
4	1057	43.5	1.59	4	997	114.5	1.88
4	1057	90	1.74	4	997	114.5	2.01
4	1057	90	1.83	5	1123	57	2.09
4	1057	100	1.75	6	1260	54.5	1.84
4	1057	110	1.74	7	1475	59	2.60
4	1057	110	1.68	8	3340	53	2.57
5	1183	39.5	1.81	8	3340	53	2.92
5	1183	43	1.93	8	3340	53	3.10
5	1183	43	1.62	8	3340	53	2.62
5	1183	47	1.69	8	3340	57	2.29
5	1183	50	1.85	8	3340	57	2.61
6	1320	11.5	1.50	8	3340	57	2.32
6	1320	18.5	1.36	8	3340	61	2.56
6	1320	28.5	1.38	8	3340	67	2.49
6	1320	38.5	1.52				
6	1320	38.5	1.53	Last Glacial Maximum			
6	1320	48.5	1.47	3	845	119.5	1.72
7	1535	17	1.82	3	845	131	1.76
7	1535	24.5	1.75	4	937	129	1.67
7	1535	30	1.58	4	937	131.5	1.70
7	1535	30	1.63	4	937	134.5	1.64
7	1535	40	1.62	4	937	137	1.54
8	3400	3.5	2.56	4	937	137	1.55
8	3400	9	2.37	5	1063	60	1.50
8	3400	13	2.17	5	1063	63	1.56
8	3400	17	2.26	6	1200	67.5	1.37
8	3400	21	2.09	6	1200	77.5	1.43
8	3400	25	2.34	6	1200	79	1.51
8	3400	25	2.29	6	1200	79	1.44
8	3400	29	2.58	7	1415	74	1.82
8	3400	33	2.40	7	1415	81	1.87
8	3400	33	2.46	7	1415	87	1.76
8	3400	37	2.55	7	1415	87	1.67
8	3400	37	2.54	8	3280	75	1.92
8	3400	37	2.40	8	3280	83	1.92
8	3400	41	2.81	8	3280	89	2.01
8	3400	41	2.91	8	3280	93	1.93
8	3400	41	2.33				
8	3400	45	2.38				
8	3400	45	2.52				
8	3400	45	2.33				
8	3400	49	3.34				
8	3400	49	2.52				

sediments extend into oxygen isotope stage 2 (Fig. 2.7). Three nutrient proxies were analyzed in this core: $\delta^{13}\text{C}$ from *G. sacculifer*, and Ba/Ca and Cd/Ca from *P. wuellerstorfi* (Table 2.5). During the LGM, $\delta^{13}\text{C}$ depicts a general maximum, while Ba/Ca and Cd/Ca are at a minimum. During deglacial time, there is considerable fluctuation in $\delta^{13}\text{C}$ and Ba/Ca, but on the average $\delta^{13}\text{C}$ is depleted compared to glacial time and the mean Ba/Ca ($2.61 \pm 0.26 \mu\text{mol/mol}$) is at a maximum during this interval. During the late Holocene, Ba/Ca is depleted compared to deglacial time, whereas Cd/Ca steadily increases throughout the length of the core.

There is a great deal of scatter in foraminiferal Ba/Ca and $\delta^{13}\text{C}$ during the Holocene. Based on measurements at GEOSECS station 33 (Chan et al., 1997), the barium concentration of Caribbean overflow water at 1800 m water depth is about 55 nmol/kg, which should correspond to a foraminiferal Ba/Ca value of approximately 2 $\mu\text{mol/mol}$. The average foraminiferal Ba/Ca value for the top 25 cm of the core equals $2.29 \pm 0.15 \mu\text{mol/mol}$, which is consistent with the shallowest *P. wuellerstorfi* value from Caribbean core KNR64-5PG at 2.26 $\mu\text{mol/mol}$ (Lea and Boyle, 1990b). These values are within 13 to 15% of the expected value.

2.4. Discussion

As the residence time of barium in the ocean, estimated around 10 ka (Chan et al., 1976), is on the same timescale as the last glacial transition, it is possible that the observed variations in foraminiferal Ba/Ca represent changes in the barium inventory of the world oceans. Oceanic barium inventory is directly related to the concentration of surface ocean water and therefore can be monitored by Ba/Ca in planktonic foraminifera (Lea and Boyle, 1990b). The average Ba/Ca value from the planktonic foraminifer *Orbulina universa* in Bahaman core 7JPC from Holocene, deglacial, and glacial sediments ($0.68 \pm 0.08 \mu\text{mol/mol}$; Fig. 2.8; Table 2.2) differs

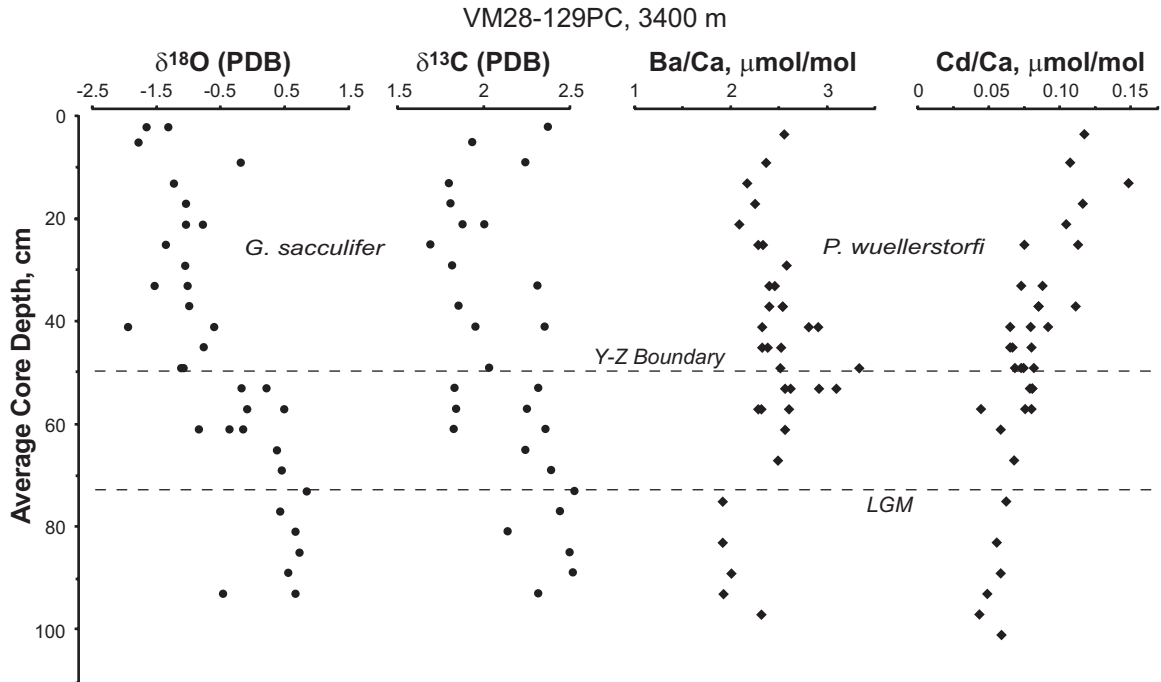


Figure 2.7. $\delta^{18}\text{O}$ and $\delta^{13}\text{C}$ from *Globigerinoides sacculifer*, and Ba/Ca and Cd/Ca from *Planulina wuellerstorfi* from Caribbean core VM28-129PC. See Table 2.5 for data summary. The Y-Z boundary is from Prell (1978).

Table 2.5. $\delta^{18}\text{O}$ and $\delta^{13}\text{C}$ in per mil from *Globigerinoides sacculifer* and Ba/Ca and Cd/Ca in $\mu\text{mol/mol}$ from *Planulina wuellerstorfi* from Caribbean core VM28-129PC.

VM28-129PC, 3400 m					
Core Depth (cm)	$\delta^{18}\text{O}$ (PDB) <i>G. sacculifer</i>	$\delta^{13}\text{C}$ (PDB) <i>G. sacculifer</i>	Core Depth (cm)	Ba/Ca <i>P. wuellerstorfi</i>	Cd/Ca <i>P. wuellerstorfi</i>
2	-1.66	2.37	3.5	2.56	0.117
2	-1.32	1.21	9	2.37	0.107
5	-1.79	1.93	13	2.17	0.149
9	-0.20	2.24	17	2.26	0.116
13	-1.24	1.79	21	2.09	0.104
17	-1.05	1.80	25	2.34	0.075
21	-0.78	2.00	25	2.29	0.113
21	-1.04	1.87	29	2.58	---
25	-1.36	1.69	33	2.40	0.073
29	-1.05	1.81	33	2.46	0.088
33	-1.54	1.19	37	2.55	0.085
33	-1.02	2.31	37	2.54	0.085
37	-0.99	1.85	37	2.40	0.111
41	-1.95	1.95	41	2.81	0.092
45	-0.77	1.26	41	2.91	0.079
41	-0.60	2.35	41	2.33	0.065
49	-1.08	2.03	45	2.38	0.067
49	-1.12	1.42	45	2.52	0.080
53	0.21	1.83	45	2.33	0.065
53	-0.18	2.31	49	---	0.082
57	-0.09	2.25	49	---	0.074
57	0.48	1.84	49	3.34	0.073
61	-0.16	2.35	49	2.52	0.068
61	-0.37	1.82	53	2.57	0.080
61	-0.84	1.28	53	2.92	---
65	0.37	2.24	53	3.10	0.081
69	0.44	2.39	53	2.62	0.079
73	0.84	2.53	57	2.29	0.044
77	0.42	2.44	57	2.61	0.080
81	0.65	2.13	57	2.32	0.076
85	0.73	2.50	61	2.56	0.058
89	0.54	2.51	67	2.49	0.068
93	0.66	2.31	75	1.92	0.062
93	-0.47	1.44	83	1.92	0.055
			89	2.01	0.059
			93	1.93	0.049
			97	2.32	0.043
			101	---	0.059

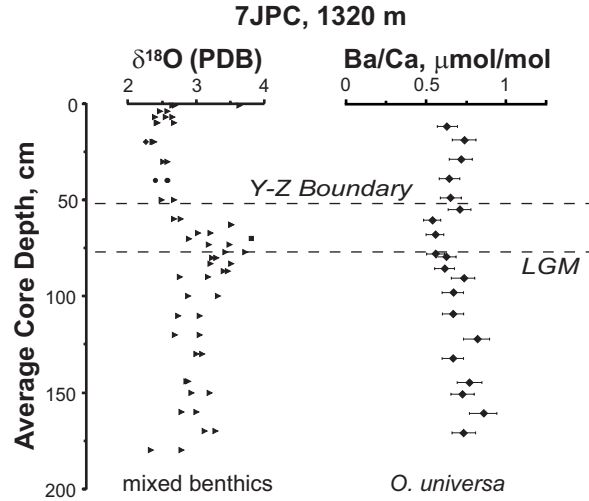


Figure 2.8. $\delta^{18}\text{O}$ from mixed benthic species (Slowey and Curry, 1995) and Ba/Ca in *Orbulina universa* from Bahaman core 7JPC. Maximum error bars are shown at 10%. See Table 2.2 for data summary. $\delta^{18}\text{O}$ is used to identify the LGM while the Y-Z boundary is based on the *Globorotalia menardii* complex (Appendix 2; Ericson and Wollin, 1956).

insignificantly from $0.62 \pm 0.08 \mu\text{mol/mol}$ Ba/Ca reported by Lea and Boyle (1991) between 0 and 12 ka BP in the northwest Atlantic. Therefore, changes in the barium inventory appear to be small and are not considered to have influenced foraminiferal Ba/Ca on the timescale of this investigation.

Figure 2.9 is a conceptual representation of circulation in a north-south section of the western Atlantic Ocean. Modern watermass circulation is based on the distribution of seawater barium in the present day western Atlantic Ocean (Chan et al., 1977). Reconstructed watermass circulation during the last deglaciation and the LGM is based on foraminiferal Ba/Ca, including data from Lea and Boyle (1990a, b). The rectangular box represents the region of this study, including thermocline and mid-depth waters of the Bahama banks and waters entering the Caribbean Sea.

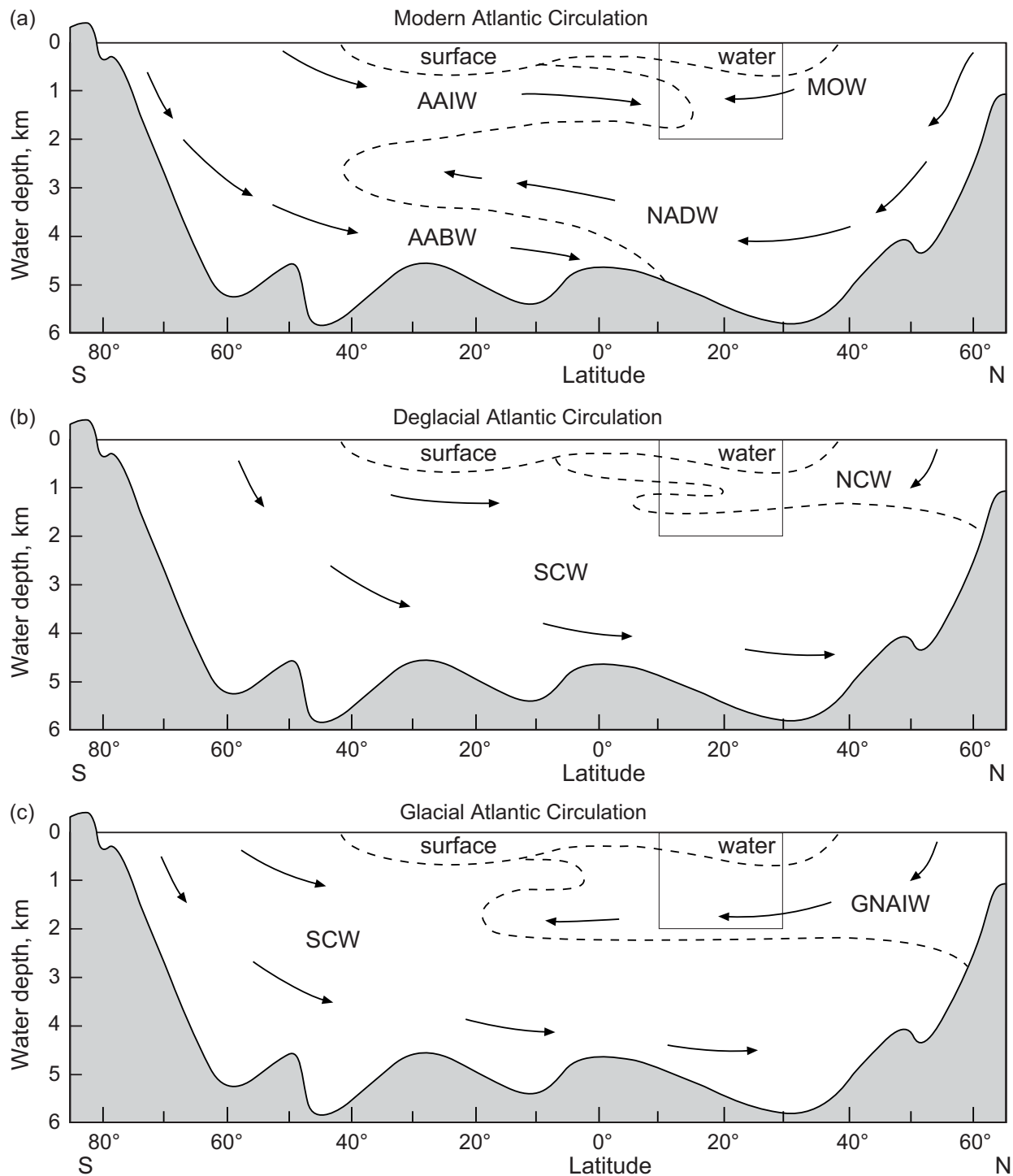


Figure 2.9. Conceptual representation of (a) modern, (b) deglacial, and (c) glacial Atlantic circulation based on foraminiferal Ba/Ca. The rectangular box includes thermocline and mid-depth waters of the Bahama banks and waters entering the Caribbean Sea. Watermasses identified are Antarctic Intermediate Water (AAIW), Mediterranean Overflow Water (MOW), North Atlantic Deep Water (NADW), Antarctic Bottom Water (AABW), Northern Component Water (NCW), Southern Component Water (SCW), and Glacial North Atlantic Intermediate Water (GNAIW).

2.4.1. The Last Glacial Maximum

2.4.1.1. Lower Thermocline Water

Previous work utilizing benthic foraminiferal Cd/Ca and $\delta^{13}\text{C}$ attributed decreased nutrients in the main thermocline during the LGM to an increase in ventilation rate and a southward shift of the thermocline outcrop areas (Slowey and Curry, 1992, 1995; Marchitto et al., 1998). In contrast to a 30 to 60% difference in the benthic $\delta^{13}\text{C}$ record (Slowey and Curry, 1995) and a 50% difference in the Cd/Ca record (Marchitto et al., 1998) during the LGM, foraminiferal Ba/Ca ratios at the base of the thermocline (800 to 1200 m) are depleted by less than 20% compared to Holocene values (Fig. 2.6). Differences in the present day concentration of lower thermocline waters from the Bahama Banks, at ~ 50 nmol/kg Ba (based on foraminiferal Ba/Ca), and the surface water at the north Atlantic isopycnal outcrop area, at ~ 40 nmol/kg Ba (Chan et al., 1977), are relatively small. Moreover, the regeneration of barium within the subtropical gyre is much slower than labile nutrients. For these reasons, an increase in ventilation rate during glacial time may have had little effect on the distribution of barium in the thermocline. Because, lower thermocline waters are at least partially influenced by deepwater circulation, this may also indicate that GNAIW was not as depleted in barium compared to cadmium depletion (Bertram et al., 1995).

2.4.1.2. Intermediate Water

GNAIW formed when the surface waters of the subarctic were unable to achieve the density required for deepwater formation and sank only to mid-depths (Fig. 2.9c) (Labeyrie et al., 1992). Because surface waters are depleted in barium, they are likely to produce a barium-poor watermass. During the LGM, the production of NADW ceased or was greatly reduced, while the production of GNAIW was enhanced and filled the North Atlantic basin above about

2000 m water depth (Boyle and Keigwin, 1987; Duplessy et al., 1988; Oppo and Fairbanks, 1990; Marchitto et al., 1998). Foraminiferal Ba/Ca at 1415 m paleo-depth is equivalent to Holocene values characteristic of upper NADW. Therefore, GNAIW may have a similar barium concentration as modern upper NADW.

Evidence of mid-depth nutrient depletion during the LGM due to the presence of GNAIW has also been shown in foraminiferal Ba/Ca, Cd/Ca, and $\delta^{13}\text{C}$ from Caribbean sediments (Boyle and Keigwin, 1987; Oppo and Fairbanks, 1987, 1990; Lea and Boyle, 1990b; deMenocal et al., 1992). Lea and Boyle (1990b) report a 20% depletion in foraminiferal Ba/Ca between the Holocene and the LGM in the Caribbean Basin. Data from Caribbean core VM28-129PC show consistently lower Ba/Ca ratios relative to those of the Holocene and deglacial time (Fig. 2.7). The glacial mean of $1.94 \pm 0.04 \mu\text{mol/mol}$ is identical to that observed in *P. wuellerstorfi* from Caribbean core KNR64-5PG (Lea and Boyle, 1990b). Cd/Ca in VM28-129PC also decreases with core depth reaching low values during the LGM (Fig. 2.7). These observations confirm the presence of GNAIW in the intermediate waters of the western Atlantic (Fig. 2.9c).

It has been suggested that depleted nutrients at mid-depth during glacial time and the subsequent rise in nutrients during deglacial time is due to the influence of Mediterranean Overflow Water (MOW) (Oppo and Fairbanks, 1987; Zahn et al., 1987). Waters entering the Caribbean Basin currently consist of 10% AAIW and 5% MOW (deMenocal et al., 1992). MOW is nutrient-poor and therefore enriched in $\delta^{13}\text{C}$ and depleted in cadmium, and theoretically provides a good source of nutrient-depleted intermediate depth water during glacial time. Lea and Boyle (1990b) rejected the presence of MOW in the Caribbean during glacial time based on evidence from foraminiferal Ba/Ca. Ba is enriched in MOW compared to Atlantic surface water

(Chan et al., 1977; Lea and Boyle 1990b). Therefore, the present study confirms that an increased influence of MOW during glacial time does not agree with foraminiferal Ba/Ca in the Caribbean. Additionally, as sea level was lower during the last glaciation, it is more likely that MOW was relatively restricted compared to today (Boyle and Keigwin, 1987; Duplessy et al., 1988). Based on the foraminiferal Ba/Ca data, MOW could not have been the source of depleted nutrients at mid-depth during glacial time. Therefore, depleted nutrients during glacial time is attributed to the influence of GNAIW and the decreased influence of AAIW and MOW that currently contribute 15% of the sill overflow water.

The Caribbean data set, however, should be treated with caution. Mn-carbonate overgrowths and Mn-oxide coatings contaminate samples by adding trace elements onto the foraminiferal test (Boyle, 1981, 1983). Despite rigorous cleaning of these samples, the Caribbean core contains significantly higher Mn/Ca than any other core in this study (Appendix 1). This potential source of contamination would explain the relatively high foraminiferal Ba/Ca values in the Holocene compared to adjacent Atlantic seawater. On the other hand, the consistently low Cd/Ca values obtained throughout the core do not seem to have been affected by manganese overgrowth contamination. Alternatively, elevated foraminiferal Ba/Ca in the Holocene may be due to postdepositional processes specific to the Caribbean Basin.

2.4.2. Deglaciation

Following the LGM, a significant deglacial nutrient enrichment can be seen along the Bahama Bank margins, increasing by as much as 41% at 1475 m paleo-depth (Fig. 2.6). Increased Ba/Ca during deglacial time at the base of the thermocline is indicative of a slowdown in thermohaline circulation. A slowdown could have been triggered by an increase in iceberg and meltwater discharge causing the production of GNAIW to diminish, thus resulting in

reduced ventilation of the mid-depth Atlantic (Venz et al., 1999; Rühlemann et al., 1999; Flower et al., 2000; Willamowski and Zahn, 2000). This is supported by Cd/Ca and ^{14}C records from deep-sea corals from the mid-depth western North Atlantic (1800 m) which also shows evidence of decreased ventilation during deglacial time (Adkins et al., 1998). In the absence of GNAIW, the mid-depth Atlantic was occupied by southern component water during deglacial time (Fig. 2.9b) (Venz et al., 1999; Flower et al., 2000; Willamowski and Zahn, 2000), increasing nutrients and barium. Foraminiferal Ba/Ca in the deep Caribbean increases by an average of 34% from the LGM, comparable to the enrichment at the Bahama Banks at 1475 m paleo-depth (Table 2.4). Further evidence of nutrient enrichment in the mid-depth North Atlantic during deglacial time has been reported as a Ba/Ca maximum of 2.77 $\mu\text{mol/mol}$ in *P. wuellerstorfi* at 43°N, 28°W (Lea and Boyle, 1990b) and in the Caribbean as a deglacial $\delta^{13}\text{C}$ minimum (Oppo and Fairbanks, 1987; Venz et al., 1999). A deglacial Ba/Ca maximum of 2.5 $\mu\text{mol/mol}$ in *P. wuellerstorfi* was also reported in the Gulf of Mexico (Buerkert, 1999).

A simple two endmember mixing model using northern and southern component watermasses can be used to calculate their relative contribution during the LGM and deglacial maximum. Glacial southern component water is enriched in barium by up to 22% and during deglacial time by around 9% compared to the Holocene (Lea, 1993, 1995), thus increasing the endmember concentration from 100 nmol/kg Ba (Fig. 2.1) to 122 and 109 nmol/kg respectively. As foraminiferal Ba/Ca ratios from 1535 to 1415 m water depth show little variation between Holocene and glacial time (Fig. 2.6), GNAIW is believed to be similar to NADW in barium concentration at 50 nmol/kg (Chan et al., 1977). During the LGM, the seawater barium concentration at 1415 m paleo-depth and for the deep Caribbean are calculated at 51.4 and 54.1 nmol/kg respectively using Eqn. 2.1. At 1063 m paleo-depth, the seawater barium concentration

is calculated at 42.6 nmol/kg for the base of the thermocline. These concentrations suggest that during the LGM, GNAIW was dominant in the Bahamas and in the Caribbean. During deglacial time, seawater barium concentrations rise to 72.2 nmol/kg at 1475 m paleo-depth and 72.7 nmol/kg in the deep Caribbean. At 1123 m paleo-depth, the seawater barium concentration is calculated at 58.1 nmol/kg. A two endmember mixing model indicates a 38% contribution from southern component water during deglacial time in the mid-depth North Atlantic to a water depth as shallow as 1475 m and a 14% contribution at 1123 m. These calculations show that the influence of southern component water extended to as shallow as 1123 m in the western North Atlantic when northern watermasses were unable to form due to the presence of meltwater in the surface ocean during deglacial time (Fig. 2.9b).

2.5. Conclusions

During the LGM, an increase in ventilation resulted in decreased nutrients within the thermocline layer (Slowey and Curry, 1992, 1995; Marchitto et al., 1998). Compared to the Holocene, foraminiferal Ba/Ca ratios from the Bahama Banks show less than 20% depletion of barium at the base of the main thermocline during the LGM. The glacial-interglacial change in foraminiferal Ba/Ca is smaller than in $\delta^{13}\text{C}$ and Cd/Ca. Increased ventilation rate has less effect on barium distribution because the difference in concentration between surface seawater and the lower thermocline is relatively small. Additionally, as lower thermocline waters are at least partially influenced by thermohaline circulation, this provides evidence that GNAIW may not be as depleted in barium as cadmium. Foraminiferal Ba/Ca further supports that during the LGM, NADW was replaced by GNAIW in the intermediate depth North Atlantic. Foraminiferal Ba/Ca from the Bahamas at 1415 m water depth is similar to Holocene values, which implies that GNAIW and upper NADW have similar barium concentrations. Nutrient depletion, however, is

evident in the deeper intermediate water, as shown by the benthic Ba/Ca and Cd/Ca record from the Caribbean Sea. These results are consistent with previously observed changes in the nutrient distribution of the glacial Atlantic.

Barium enrichment is observed during deglaciation in the basal thermocline and intermediate waters. Increased iceberg and meltwater discharge may have caused the production of GNAIW to cease. Consequently, GNAIW was replaced by southern component water in the mid-depth North Atlantic. A mixing model based on benthic Ba/Ca values indicates a 38% contribution from southern component water during deglacial time to a water depth as shallow as 1475 m and a 14% contribution at 1123 m. Therefore, foraminiferal Ba/Ca provides evidence that the influence of southern component water increased in the mid-depth North Atlantic when northern watermasses were unable to form due to the presence of meltwater in the surface ocean during deglacial time.

2.6. References

- Adkins J.F., Cheng H., Boyle E.A., Druffel E.R.M., and Edwards R.L. (1998) Deep-sea coral evidence for rapid change in ventilation of the deep North Atlantic 15,400 years ago. *Science* **280**, 725-728.
- Bertram C.J., Elderfield H., Shackleton N.J., and MacDonald J.A. (1995) Cadmium/calcium and carbon isotope reconstructions of the glacial northeast Atlantic Ocean. *Paleoceanography* **10**, 563-578.
- Bishop J.K.B. (1988) The barite-opal-organic carbon association in oceanic particulate matter. *Nature* **332**, 341-343.
- Boyle E.A. (1981) Cadmium, zinc, copper, and barium in foraminifera tests. *Earth and Planetary Science Letters* **53**, 11-35.
- Boyle E.A. (1983) Manganese carbonate overgrowths on foraminifera tests. *Geochimica et Cosmochimica Acta* **47**, 1815-1819.
- Boyle E.A. (1988) Cadmium: Chemical tracer of deepwater paleoceanography. *Paleoceanography* **3**, 471-489.

- Boyle E.A. and Keigwin L.D. (1982) Deep circulation of the North Atlantic over the last 200,000 years: Geochemical evidence. *Science* **218**, 784-787.
- Boyle E.A. and Keigwin L.D. (1985) Comparison of Atlantic and Pacific paleochemical records for the last 215,000 years: Changes in deep ocean circulation and chemical inventories. *Earth and Planetary Science Letters* **76**, 135-150.
- Boyle E.A. and Keigwin L.D. (1987) North Atlantic thermohaline circulation during the past 20,000 years linked to high-latitude surface temperature. *Nature* **330**, 35-40.
- Boyle E.A., Sclater F., and Edmond J.M. (1976) On the marine geochemistry of cadmium. *Nature* **263**, 42-44.
- Broecker W.S. and Peng T.-H. (1982) *Tracers in the Sea*. Eldigio Press.
- Broecker W.S., Ewing M., and Heezen B.C. (1960) Evidence for an abrupt change in climate close to 11,000 years ago. *American Journal of Science* **258**, 429-448.
- Buerkert T.P. (1999) Barium in water and foraminiferal shells: Indicators of oceanographic conditions in the Gulf of Mexico since the Late Pleistocene. Ph.D. dissertation, Louisiana State University.
- Chan L.-H., Edmond J.M., Stallard R.F., Broecker W.S., Chung Y.C., Weiss R.F., and Ku T.L. (1976) Radium and barium at GEOSECS stations in the Atlantic and Pacific. *Earth and Planetary Science Letters* **32**, 259-267.
- Chan L.-H., Drummond D., Edmond J.M., and Grant B. (1977) On the barium data from the GEOSECS expedition. *Deep-Sea Research* **24**, 613-649.
- Curry W.B., Duplessy J.-C., Labeyrie L.D., and Shackleton N.J. (1988) Changes in the distribution of $\delta^{13}\text{C}$ of deep water ΣCO_2 between the last glaciation and the Holocene. *Paleoceanography* **3**, 317-341.
- deMenocal P.B., Oppo D.W., Fairbanks R.G., and Prell W.L. (1992) Pleistocene $\delta^{13}\text{C}$ variability of North Atlantic Intermediate Water. *Paleoceanography* **7**, 229-250.
- Duplessy J.-C., Shackleton N.J., Fairbanks R.G., Labeyrie L., Oppo D.W., and Kallel N. (1988) Deepwater source variations during the last climatic cycle and their impact on the global deepwater circulation. *Paleoceanography* **3**, 343-360.
- Dehairs F., Chesselet R., and Jedwab J. (1980) Discrete suspended particles of barite and the barium cycle in the open ocean. *Earth and Planetary Science Letters* **49**, 529-550.
- Ericson D.B. and Wollin G. (1956) Micropaleontological and isotopic determinations of Pleistocene climates. *Micropaleontology* **2**, 257-270.

- Ericson D.B. and Wollin G. (1968) Pleistocene climates and chronology in deep-sea sediments. *Science* **162**, 1227-1234.
- Fairbanks R.G. (1989) A 17,000-year glacio-eustatic sea level record: Influence of glacial melting rates on the Younger Dryas event and deep-ocean circulation. *Nature* **342**, 637-642.
- Flower B.P., Oppo D.W., McManus J.F., Venz K.A., Hodell D.A., and Cullen J.L. (2000) North Atlantic intermediate to deep water circulation and chemical stratification during the past 1 Myr. *Paleoceanography* **15**, 388-403.
- Haddad G.A. and Droxler A.W. (1996) Metastable CaCO₃ dissolution at intermediate water depths of the Caribbean and western North Atlantic: Implications for intermediate water circulation during the past 200,000 years. *Paleoceanography* **11**, 701-716.
- Labeyrie L.D., Duplessy J.-C., Duprat J., Juillet-Leclerc A., Moyes J., Michel E., Kallel N., and Shackleton N.J. (1992) Changes in the vertical structure of the North Atlantic Ocean between glacial and modern times. *Quaternary Science Reviews* **11**, 401-413.
- Lea D.W. (1993) Constraints on the alkalinity and circulation of glacial Circumpolar Deep Water from benthic foraminiferal barium. *Global Biogeochemical Cycles* **7**, 695-710.
- Lea D.W. (1995) A trace metal perspective on the evolution of Antarctic Circumpolar Deep Water chemistry. *Paleoceanography* **10**, 733-747.
- Lea D.W. and Boyle E.A. (1989) Barium content of benthic foraminifera controlled by bottom-water composition. *Nature* **338**, 751-753.
- Lea D.W. and Boyle E.A. (1990a) A 210,000-year record of barium variability in the deep northwest Atlantic Ocean. *Nature* **347**, 269-272.
- Lea D.W. and Boyle E.A. (1990b) Foraminiferal reconstruction of barium distributions in water masses of the glacial oceans. *Paleoceanography* **5**, 719-742.
- Lea D.W. and Boyle E.A. (1991) Barium in planktonic foraminifera. *Geochimica et Cosmochimica Acta* **55**, 3321-3331.
- Lea D.W. and Boyle E.A. (1993) Determination of carbonate-bound barium in foraminifera and corals by isotope dilution plasma-mass spectrometry. *Chemical Geology* **103**, 73-84.
- Lea D.W. and Spero H.J. (1992) Experimental determination of barium uptake in shells of the planktonic foraminifera *Orbulina universa* at 22°C. *Geochimica et Cosmochimica Acta* **56**, 2673-2680.
- Lea D.W. and Spero H.J. (1994) Assessing the reliability of paleochemical tracers: Barium uptake in the shells of planktonic foraminifera. *Paleoceanography* **9**, 445-452.

- Marchitto T.M., Curry W.B., and Oppo D.W. (1998) Millennial-scale changes in North Atlantic circulation since the last glaciation. *Nature* **393**, 557-561.
- Martin P.A. and Lea D.W. (1998) Comparison of water mass changes in the deep tropical Atlantic derived from Cd/Ca and carbon isotope records: Implications for changing Ba composition of deep Atlantic water masses. *Paleoceanography* **13**, 572-585.
- McCorkle D.C., Martin P.A., Lea D.W., and Klinkhammer G.P. (1995) Evidence of a dissolution effect on benthic foraminiferal shell chemistry: $\delta^{13}\text{C}$, Cd/Ca, Ba/Ca, and Sr/Ca results from the Ontong Java Plateau. *Paleoceanography* **10**, 699-714.
- McIntyre K., Ravelo A.C., and Delaney M.L. (1999) North Atlantic Intermediate Water in the Pliocene to early Pleistocene. *Paleoceanography* **14**, 324-335.
- Oppo D.W. and Fairbanks R.G. (1987) Variability in the deep and intermediate water circulation of the Atlantic Ocean during the past 25,000 years: Northern Hemisphere modulation of the Southern Ocean. *Earth and Planetary Science Letters* **86**, 1-15.
- Oppo D.W. and Fairbanks R.G. (1990) Atlantic Ocean thermohaline circulation of the last 150,000 years: Relationship to climate and atmospheric CO_2 . *Paleoceanography* **5**, 277-288.
- Oppo D.W. and Lehman S.J. (1993) Mid-depth circulation of the subpolar North Atlantic during the last glacial maximum. *Science* **259**, 1148-1152.
- Paytan A. and Kastner M. (1996) Benthic Ba fluxes in the central equatorial Pacific, implications for the oceanic Ba cycle. *Earth and Planetary Science Letters* **142**, 439-450.
- Prell W.L. (1978) Upper Quaternary sediments of the Colombia Basin: Spatial and stratigraphic variation. *Geological Society of America Bulletin* **89**, 1241-1255.
- Rosenthal Y., Boyle E.A., and Labeyrie L. (1997) Last glacial maximum paleochemistry and deepwater circulation in the Southern Ocean: Evidence from foraminiferal cadmium. *Paleoceanography* **12**, 787-796.
- Rosenthal Y., Field M.P., and Sherrell R.M. (1999) Precise determination of element/calcium ratios in calcareous samples using sector field inductively coupled plasma mass spectrometry. *Analytical Chemistry* **71**, 3248-3253.
- Rühlemann C., Mulitza S., Müller P.J., Wefer G., and Zahn R. (1999) Warming of the tropical Atlantic Ocean and slowdown of thermohaline circulation during the last deglaciation. *Nature* **402**, 511-514.

- Sarnthein M., Winn K., Jung S.J.A., Duplessy J.-C., Labeyrie L., Erlenkeuser H., and Ganssen G. (1994) Changes in East Atlantic deepwater circulation over the last 30,000 years: Eight time slice reconstructions. *Paleoceanography* **9**, 209-267.
- Slowey N.C. and Curry W.B. (1992) Enhanced ventilation of the North Atlantic subtropical gyre thermocline during the last glaciation. *Nature* **358**, 665-668.
- Slowey N.C. and Curry W.B. (1995) Glacial-interglacial differences in circulation and carbon cycling within the upper western North Atlantic. *Paleoceanography* **10**, 715-732.
- Venz K.A., Hodell D.A., Stanton C., and Warnke D.A. (1999) A 1.0 myr record of Glacial North Atlantic Intermediate Water variability from ODP site 982 in the northeast Atlantic. *Paleoceanography* **14**, 42-52.
- Willamowski C. and Zahn R. (2000) Upper ocean circulation in the glacial North Atlantic from benthic foraminiferal isotope and trace element fingerprinting. *Paleoceanography* **15**, 515-527.
- Weihaupt J.G. (1979) *Exploration of the Oceans*. Macmillan Publishing Company.
- Wüst G. (1963) On the stratification and the circulation in the cold water sphere of Antillean-Caribbean basins. *Deep Sea Research* **16**, 165-187.
- Zahn R., Sarnthein M., and Erlenkeuser H. (1987) Benthic isotope evidence for changes of the Mediterranean outflow during the late Quaternary. *Paleoceanography* **2**, 543-559.

CHAPTER 3. BA/CA IN NEOGLOBOQUADRINA PACHYDERMA AS AN INDICATOR OF MELTWATER DISCHARGE INTO THE WESTERN ARCTIC OCEAN

3.1. Introduction

During the last deglaciation, the high flux of meltwater from the Laurentide Ice Sheet may have had a significant effect on ocean circulation and climate change by interrupting the formation of North Atlantic Deep Water (Broecker et al., 1985; Boyle and Keigwin, 1987). There were five major routes of meltwater runoff from the Laurentide Ice Sheet: the Mississippi River, the Hudson River, the St. Lawrence River, the Hudson Strait, and the Arctic Ocean (Teller, 1990; Clark et al., 2001). The abrupt redirection of meltwater runoff as ice margins retreated is believed to have caused changes in thermohaline circulation, particularly when freshwater flow was increased through the eastern outlets near sites of deepwater formation in the North Atlantic (Clark et al., 2001). The resulting reduction in surface water salinity inhibited deepwater formation, which in turn reduced heat transport and caused large-scale cooling (Broecker et al., 1985). The onset of the Younger Dryas cold interval around 11 ¹⁴C ka BP, is hypothesized to have been caused by the redirection of meltwater from the Mississippi River to the St. Lawrence River (Broecker et al., 1989). Clark et al. (2001) suggested a mechanism for the observed climatic variability during the last glaciation where thermohaline circulation was suppressed with increased meltwater input through the eastern outlets, but was enhanced when meltwater was diverted to the south through the Mississippi River. While the role of meltwater runoff to the Arctic Ocean in the global climate system is not yet fully understood, the importance of a freshwater export and its potential impact on deepwater formation is recognized (e.g.; Aagaard and Carmack, 1989; Andrews et al., 1993).

Although the growth and decay of the Laurentide Ice Sheet is well documented, the extent of ice sheets in the Eurasian Arctic during the last glacial maximum, including the chronology of their deglaciation, is controversial (Sher, 1995; Svendsen et al., 1999; Felzer, 2001). Glacial extent reported within the literature ranges from extensive ice sheet coverage (Grosswald, 1998; Grosswald and Hughes, 2002) to restricted glaciation that is limited to localized ice caps on Arctic islands (Velichko et al., 1997). In fact, Grosswald (1998) and Grosswald and Hughes (2002) report evidence for the continuous glaciation of Arctic Russia, including the formation of large proglacial lakes and an extensive meltwater drainage system. In contrast, Svendsen et al. (1999) concluded that during the LGM, much of the Russian Arctic remained ice free. Until a consensus is reached, it remains difficult to interpret a chronology of Eurasian Arctic deglacial meltwater activity or to assess its potential influence on thermohaline circulation.

Stable isotopes in foraminifera have long been used as tools for paleoceanographic reconstructions. Although low $\delta^{18}\text{O}$ deglacial meltwater events have been identified in the Arctic Ocean (Stein et al., 1994; Nørgaard-Pedersen et al., 1998; Poore et al., 1999a; Lubinski et al., 2001), knowledge concerning the history and timing of these events is limited. Interpretation and dating of meltwater events is complicated due to relatively low sediment accumulation rates in the Arctic Ocean (Darby et al., 1997). Traditionally, $\delta^{18}\text{O}$ in foraminifera has been used to document variations in salinity over time (e.g.; Leventer et al., 1982; Spero and Williams, 1990). However, the $\delta^{18}\text{O}$ record is equivocal because oxygen isotope composition in fossil shells is dependent on both the water composition (salinity) and temperature.

The distribution of barium in the global ocean has a general linear relationship with alkalinity and silica in that it is depleted in surface waters and regenerated at depth (Chan et al.,

1977; Lea and Boyle, 1989). The removal of barium from the surface water is attributed to biological processes in which barite (BaSO_4) is precipitated, although the mechanisms responsible are not fully understood (Dehairs et al., 1980; Bishop, 1988). The major sources of barium to the ocean are rivers (Martin and Meybeck, 1979) and hydrothermal vents (Edmond et al., 1979; Von Damm et al., 1985). Rivers are concentrated in barium compared to the depleted surface ocean. Moreover, the input of fluvial barium increases in the river-sea mixing zone as barium desorbs from the suspended load by ion exchange (e.g.; Hanor and Chan, 1977). For these reasons, high levels of barium in surface seawater are indicative of a continental origin.

Previous work on Ba/Ca in planktonic foraminifera has shown that foraminiferal barium incorporation occurs in direct proportion to seawater barium concentration and does not appear to vary with temperature or salinity (Lea and Boyle, 1991; Lea and Spero, 1992, 1994). The planktonic foraminifer *Neogloboquadrina pachyderma* sinstral is abundant in the cold polar regions and calcifies in the upper 50 m of the surface water within the Canada Basin (Bauch et al., 1997). As such, the barium content of this species reflects changes in the amount of continental runoff to the surface ocean. This investigation uses barium in the planktonic foraminifer *N. pachyderma* sin. as an independent meltwater proxy to estimate salinity changes in the surface Arctic Ocean over time.

3.2. Materials and Methods

The Lomonosov Ridge divides the Arctic Ocean into two main basins, the Amerasian Basin in the west and the Eurasian Basin in the east (Fig. 3.1). The Beaufort Gyre dominates the circulation of the surface water of the western Amerasian Basin, which includes the Mendeleev Ridge. Samples were obtained at 1 cm intervals from box core 94B-17, taken from the

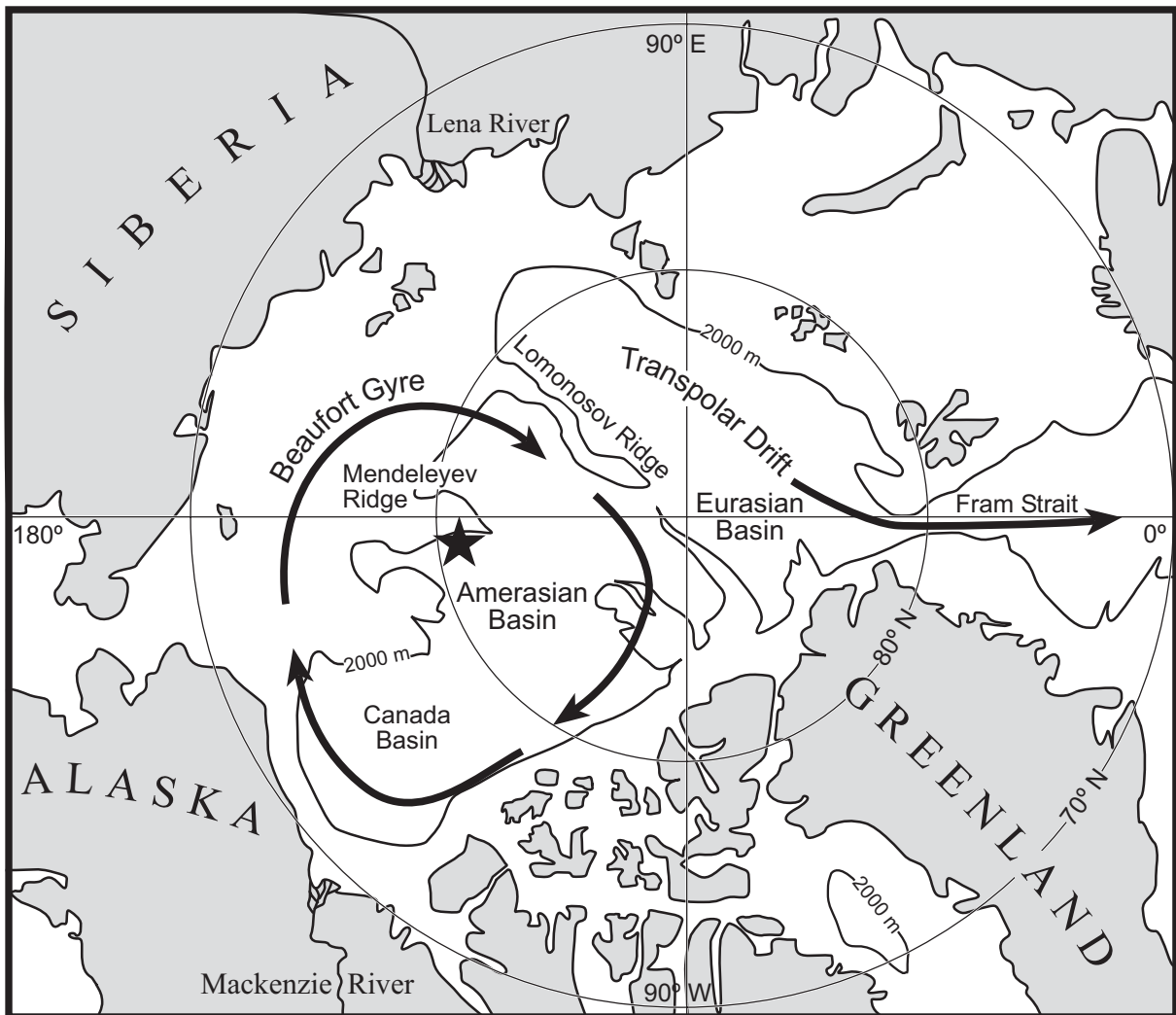


Figure 3.1. Location of box core 94B-17 (star) in the western Arctic Ocean at 81°15.91'N, 178°58.05'E, 2217 m water depth. The clockwise motion of the Beaufort gyre dominates surface water circulation in the western Arctic while the Transpolar Drift governs the surface flow of the eastern side through the Fram Strait.

Mendeleev Ridge at 81°15.91'N, 178°58.05'E in the western Arctic Ocean at 2217 m water depth (Fig. 3.1). Stable isotopic analyses of $\delta^{18}\text{O}$, by Finnigan MAT 252 mass spectrometry from *N. pachyderma* sin., were performed by Poore et al. (1999a, b). Radiocarbon ages were determined by accelerator mass spectrometry (AMS) from *N. pachyderma* sin. (Poore et al., 1999a, b). Sediments were picked for the planktonic foraminifer *N. pachyderma* sin. from a

>125 μm sieved fraction. A typical sample weighing 0.6 mg contained an average of 76 individuals. The *N. pachyderma* sin. tests were gently crushed and then purified following procedures modified from Lea and Boyle (1993). Samples were ultrasonically cleaned four times with distilled water and twice with methanol to remove detrital grains and fine clay particles. Metal oxide coatings were reduced in a solution consisting of anhydrous-hydrazine, citric-acid, and ammonium-hydroxide and organic matter was oxidized in a solution of hydrogen-peroxide and sodium-hydroxide. Sedimentary barite was dissolved in alkaline diethylenetriamine-pentaacetic acid (DTPA) and then removed by rinsing with ammonium hydroxide. Any remaining adsorbed metals were leached with 0.001 N nitric acid. All dilute nitric acids used in this study were prepared from SEASTAR™ high purity acid. The remaining shell material was then dissolved in 0.1 N nitric acid and simultaneously analyzed for barium and calcium with a ThermoQuest Finnigan Element 2 inductively coupled plasma mass spectrometer (ICP-MS) at the University of Southern Mississippi.

Element to calcium ratios were determined from intensity ratios with an external matrix matched standard using the method developed by Rosenthal et al. (1999). A multi-element standard was prepared from ICP-MS grade High-Purity Standards. This solution was standardized for barium by isotope dilution using a Finnigan MAT 262, thermal ionization mass spectrometer (TIMS) and procedures adapted from Chan et al. (1977). Calcium was standardized with a PerkinElmer Optima 3300DV inductively coupled plasma optical emission spectrometer (ICP-OES). Replicate analyses of dilute Atlantic seawater (FAT 85 Sta. 3, 1143 m) were performed to monitor the reproducibility and accuracy of the method. The precision of the seawater replicates was 1% for Ba/Ca, averaging $5.42 \pm 0.07 \mu\text{mol/mol Ba/Ca}$. This is within 5% accuracy of the $5.17 \pm 0.05 \mu\text{mol/mol Ba/Ca}$ reported for this seawater sample

(Klinkhammer and Chan, 1990). Core top samples of *N. pachyderma* sin. determined from intensity ratios using ICP-MS (Rosenthal et al., 1999) and isotopic dilution (ID) yield 1.47 ± 0.11 (1σ) $\mu\text{mol/mol}$ Ba/Ca (Table 3.1). Replicate analyses from 14.5 cm core depth yield an average of 2.27 ± 0.24 (1σ) $\mu\text{mol/mol}$ Ba/Ca. Therefore, the 1σ precision of the method for foraminiferal samples is estimated between 7 and 10%.

Table 3.1. Replicate analyses of Ba/Ca in *Neogloboquadrina pachyderma* sinistral from western Arctic Ocean box core 94B-17, 2217 m water depth determined from intensity ratios using ICP-MS (Rosenthal et al., 1999) and isotopic dilution (ID) using TIMS.

Core Depth (cm)	Ba/Ca <i>N. pachyderma</i> sin.	Method
0.5	1.48	ICP-MS
	1.35	ICP-MS
	1.57	ID-TIMS
Average	1.47 ± 0.11 (1σ)	
14.5	2.24	ICP-MS
	2.00	ICP-MS
	2.59	ID-TIMS
	2.25	ID-TIMS
Average	2.27 ± 0.24 (1σ)	

3.3. Results

3.3.1. Ba/Ca and $\delta^{18}\text{O}$

Ba/Ca in *N. pachyderma* sin., together with $\delta^{18}\text{O}$ determined by Poore et al. (1999a), are presented in Table 3.2 and their down-core distributions are shown in Fig. 3.2. A prominent $\delta^{18}\text{O}$ minimum occurs between 15.5 and 12.5 cm core depth, with a maximum difference of

1.7‰ at 15.5 cm and 1.5‰ at 12.5 cm, relative to the core top value. This $\delta^{18}\text{O}$ minimum broadly corresponds to a Ba/Ca maximum between 10.5 and 15.5 cm, with a maximum increase of 59% at 12.5 cm compared to the Ba/Ca of the surface sediments. A second $\delta^{18}\text{O}$ minimum is observed at 8.5 cm core depth, decreasing by 0.7‰, which corresponds to a Ba/Ca increase of 12% relative to the core top. There is generally a positive linear relationship between Ba/Ca and $\delta^{18}\text{O}$ (Fig. 3.3), indicating a common source for these two meltwater proxies. Therefore, two meltwater discharge events are recognized in this core, one at 12.5 cm and the other around 8.5 cm core depth.

Radiocarbon chronology is based on AMS ^{14}C dating of *N. pachyderma* sin. assuming a 440 yr reservoir age (Poore et al., 1999a, b). AMS ^{14}C dates are shown in Fig. 3.2. The last glacial maximum is extremely condensed or may be entirely absent in this core because thick and continuous sea ice cover inhibited sedimentation during that period. Sedimentation rates increased during deglacial time as seen by the expansion of the ^{14}C ages, all of which are in stratigraphic order (Fig. 3.2). Radiocarbon chronology, interpolated assuming a constant sedimentation rate between measured dates (Table 3.2), indicates that the first meltwater event occurred between 12.4 ka and 11.3 ^{14}C ka BP, reaching a maximum at 11.8 ka ^{14}C BP, while the second meltwater event occurred around 9.4 ^{14}C ka BP (Fig. 3.4). As discussed by Poore et al. (1999a), these two meltwater events coincide with rapid sea level rise associated with mwp-IA (12 ka) and mwp-IB (9.5 ka) determined from the Barbados coral record by Fairbanks (1989).

Table 3.2. Data summary for western Arctic Ocean box core 94B-17, 2217 m water depth from *Neogloboquadrina pachyderma* sinistral. AMS ^{14}C dates are radiocarbon ages with reservoir correction of 440 years, extrapolated from data reported in Poore et al. (1999a, b). Ba/Ca was analyzed by ICP-MS using intensity ratios (Rosenthal et al., 1999). Ba_{mw} was calculated with Eqn. 3.5 and Ba_{fw} with Eqn. 3.6. $\delta^{18}\text{O}_{\text{mw}}$ SMOW was calculated with Eqn. 3.1 and Eqn. 3.2. Stable isotopic analyses from Poore et al. (1999a, b).

Core Depth (cm)	Corrected ^{14}C Age (yr)	Ba/Ca ($\mu\text{mol/mol}$)	Ba_{mw} (nmol/l)	Ba_{fw} (nmol/l)	$\delta^{18}\text{O}_{\text{c}}$ (PDB)	$\delta^{18}\text{O}_{\text{mw}}$ (SMOW)
0.5	0	1.42	63	415	1.51	-3.01
1.5	1342	1.33	59	388	1.77	-2.76
2.5	2684	1.26	56	354	1.90	-2.62
3.5	4026	1.32	58	335	1.49	-3.03
4.5	5368	1.37	61	445	1.86	-2.66
5.5	6710	1.45	64	487	1.76	-2.77
6.5	7618	1.42	63	444	1.67	-2.86
7.5	8526	1.55	68	447	1.16	-3.36
8.5	9434	1.59	69	417	0.80	-3.72
9.5	10342	1.86	81	624	1.06	-3.47
10.5	11250	2.22	96	764	0.75	-3.78
11.5	11530	2.18	95	751	0.76	-3.76
12.5	11810	2.26	96	636	0.05	-4.47
13.5	12008	2.21	94	646	0.23	-4.29
14.5	12205	2.12	90	556	-0.06	-4.58
15.5	12403	2.11	89	533	-0.18	-4.70
16.5	12600	1.98	85	594	0.57	-3.95
17.5	16690	1.84	80	559	0.78	-3.74
18.5	20780	1.53	68	527	1.63	-2.89
19.5	24870	1.45	63	352	0.96	-3.56
20.5	28960	1.45	63	321	0.68	-3.85

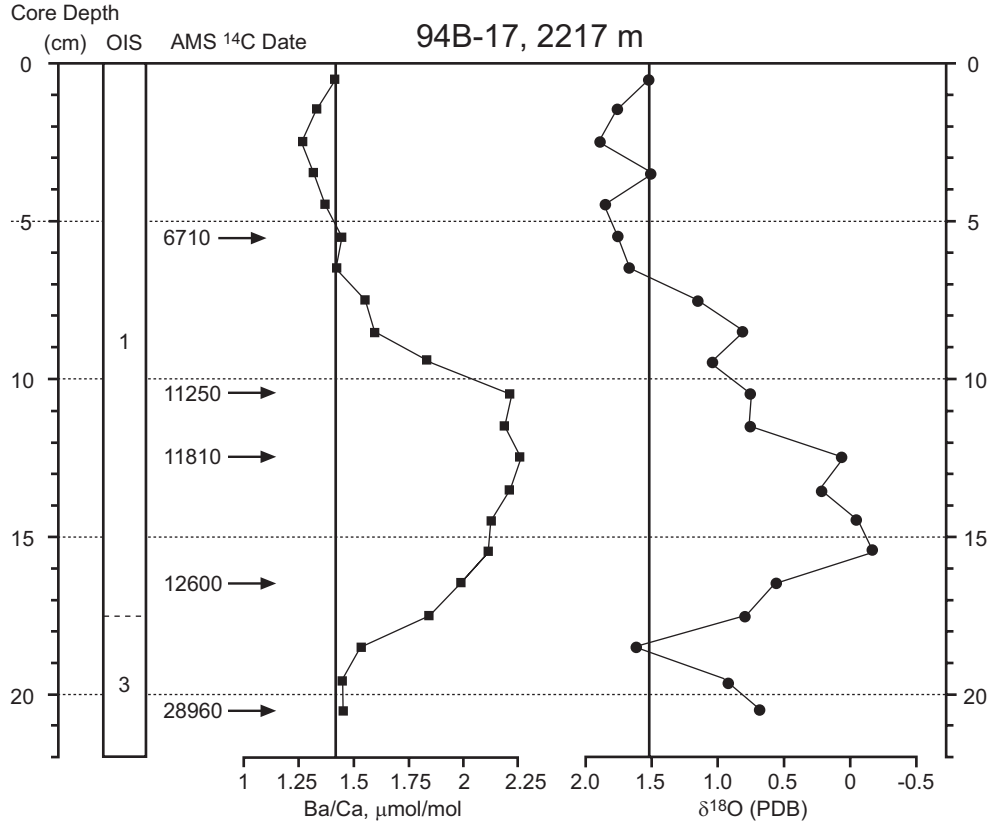


Figure 3.2. Average core depth versus Ba/Ca and $\delta^{18}\text{O}$ PDB from *Neogloboquadrina pachyderma* sinistral from the western Arctic Ocean. Vertical lines represent core top averages. Oxygen isotope stages (OIS) were determined from AMS ^{14}C dates. OIS 2, which includes the last glacial maximum, is extremely condensed or is absent in this core. Stable isotopic analyses and AMS ^{14}C dates from Poore et al. (1999a, b).

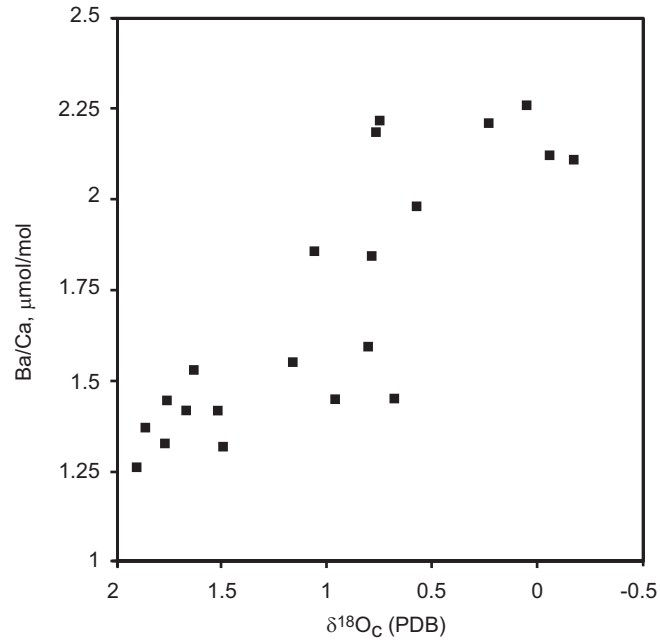


Figure 3.3. The relationship between Ba/Ca and $\delta^{18}\text{O}$ PDB from *Neogloboquadrina pachyderma* sinistral in western Arctic Ocean box core 94B-17, 2217 m water depth.

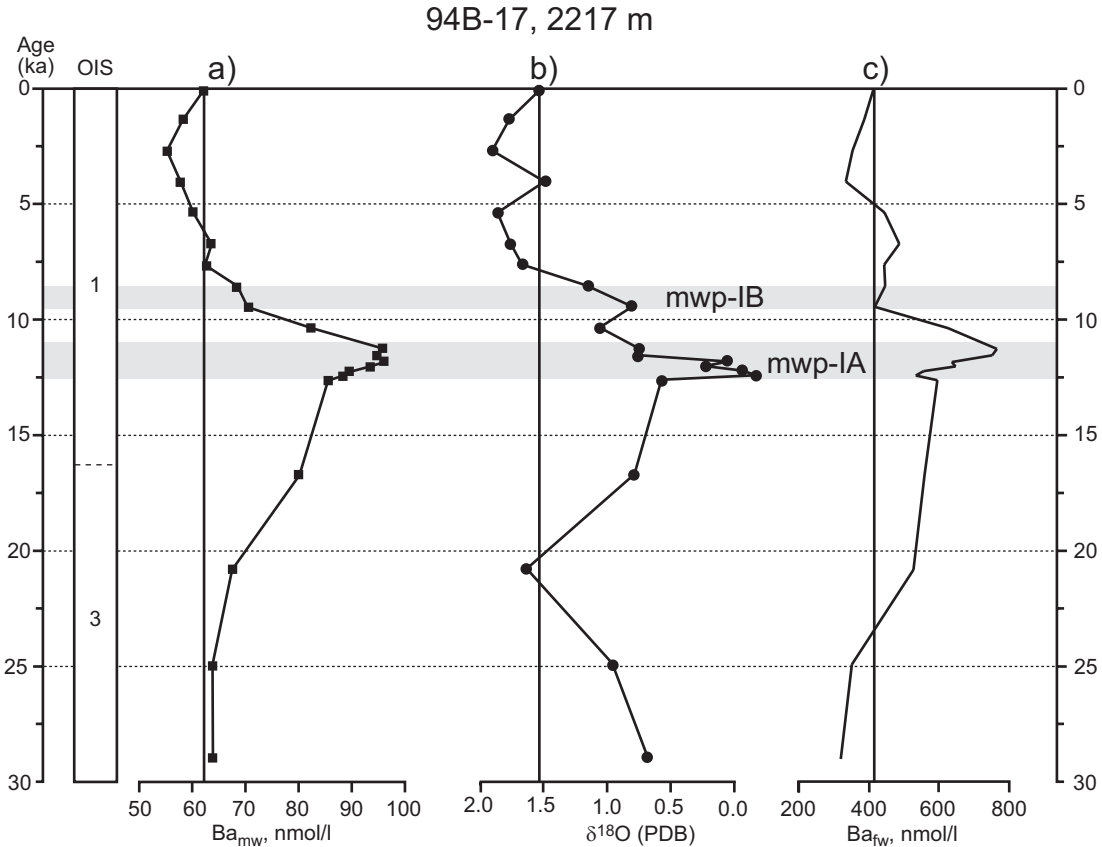


Figure 3.4. Age, ka BP determined by AMS ^{14}C dates assuming a constant sedimentation rate versus (a) Ba_{mw} , (b) $\delta^{18}\text{O}$ PDB, and (c) Ba_{fw} from *Neogloboquadrina pachyderma* sinistral from the western Arctic Ocean. Oxygen isotope stages (OIS) were determined from AMS ^{14}C dates. OIS 2, which includes the last glacial maximum, is extremely condensed or is absent in this core. Stable isotopic analyses and AMS ^{14}C dates from Poore et al. (1999a, b).

3.3.2. Reconstruction of Meltwater Input Using $\delta^{18}\text{O}$

In this study, oxygen isotopic composition of the mixed surface water (δ_{mw}) is calculated using Eqn. 3.1. This equation was derived in accordance with O'Neil et al. (1969) using $\delta^{18}\text{O}$ derived from seawater and the planktonic foraminifer *N. pachyderma* sin. at ambient seawater temperature (T) in the Arctic Ocean (Aksu and Vilks, 1988; Bauch et al., 1997; Volkmann and Mensch, 2001). In this equation, the term δ_c is the equilibrium oxygen isotope composition of *N. pachyderma* calcite ($\delta^{18}\text{O}_c$ PDB). As the surface waters of the ice covered Arctic Ocean (low

salinity mixed layer and the halocline) are continually near freezing, any fluctuation in temperature should be minor and is considered negligible. Therefore, a constant temperature just above freezing is assumed for the upper 50 m at -1.6 °C based on the average surface salinity of 32.5‰ at the western edge of the Mendeleev Ridge (Spielhagen and Erlenkeuser, 1994; Guay and Falkner, 1997). Equation 3.2 was used to convert δ_{mw} calculated in Eqn. 3.1 to $\delta^{18}\text{O}$ of mixed surface water ($\delta^{18}\text{O}_{mw}$ SMOW) in accordance with Bemis et al. (1998). The calculated $\delta^{18}\text{O}_{mw}$ with time is presented in Table 3.2.

$$T (\text{°C}) = 16.9 - 4.38 (\delta_c - \delta_{mw}) + 0.1 (\delta_c - \delta_{mw})^2 \quad (\text{Eqn. 3.1})$$

$$\delta^{18}\text{O}_{mw} (\text{SMOW}) = (\delta_{mw} + 0.2) / 0.9998 \quad (\text{Eqn. 3.2})$$

The modern relationship between $\delta^{18}\text{O}_c$ values in living *N. pachyderma* sin. and surface salinity demonstrates that oxygen isotopes can be used as a proxy for paleosalinity (Volkman and Mensch, 2001). However, this relationship may be offset by the formation of sea ice (Spielhagen and Erlenkeuser, 1994; Bauch et al., 1997). This is because sea ice formation does not significantly change the $\delta^{18}\text{O}$ composition of surface water whereas the brine that remains after its creation will affect the salinity considerably. The relationship between salinity in parts per thousand (S) and $\delta^{18}\text{O}_{mw}$ can be quantified according to Eqn. 3.3, which was generated using -3.01‰ $\delta^{18}\text{O}_{mw}$ SMOW from the calculated core top δ_{mw} (Table 3.2) and an average salinity of 32.5‰ (Guay and Falkner, 1997), assuming no net sea ice formation during the deglacial period. Equation 3.3 uses -42‰ (SMOW) as the $\delta^{18}\text{O}$ value for the glacial ice of the Laurentide Ice Sheet (Fairbanks, 1989).

$$\delta^{18}\text{O}_{mw} (\text{SMOW}) = 1.2 * S - 42 \quad (\text{Eqn. 3.3})$$

Based on the oxygen isotope data, salinity increases from 31.3‰ at 11.8 ka and 31.9‰ at 9.4 ¹⁴C ka BP to 32.5‰ in the present day (Eqn. 3.3). Assuming the undiluted Arctic surface seawater has a salinity of 34.5 ‰, much like the lower halocline water in the western Arctic (Guay and Faulkner, 1997), the fraction of fresh or meltwater (f) mixing with Arctic surface seawater can be estimated using Eqn. 3.4.

$$f = 1 - \left(\frac{S}{34.5} \right) \quad (\text{Eqn. 3.4})$$

3.3.3. Reconstruction of Surface Ba

The barium content of mixed surface water ($\text{Ba}/\text{Ca}_{\text{mw}}$) and the Ba/Ca of foraminifera ($\text{Ba}/\text{Ca}_{\text{foram}}$) are related through a distribution coefficient (D_{Ba}) as shown in Eqn. 3.5. Using the core top average of Ba/Ca for *N. pachyderma* sin. (1.47 ± 0.11) and the Ba/Ca of modern Arctic surface water, which corresponds to 65 nmol/l Ba (Guay and Falkner, 1997, 1998), and 9.8 mmol/l Ca at 32.5‰ salinity (Bruland, 1983), D_{Ba} for *N. pachyderma* sin. is estimated to be 0.22 ± 0.02 . Because calcium is largely conservative in the ocean and has a residence time greater than 1 Ma (Broecker and Peng, 1982), the modern value of calcium, normalized to the corresponding salinity estimated in Eqn. 3.3, can be used to calculate the concentration of barium in the mixed surface water (Ba_{mw}) through time based on foraminiferal Ba/Ca (Table 3.2).

$$D_{Ba} = \frac{(Ba / Ca)_{foram}}{(Ba / Ca)_{mw}} \quad (\text{Eqn. 3.5})$$

3.3.4. Reconstruction of Meltwater Input Using Ba

The concentration of barium in deglacial meltwater $(Ba)_{fw}$ is determined from Eqn. 3.6 and summarized in Table 3.2. The barium to calcium ratio in mixed surface waters over time $(Ba/Ca)_{mw}$ is calculated using Eqn. 3.5. The endmember barium concentration in Arctic surface water $(Ba)_{sw}$ at 34.5‰ salinity is estimated to be 41.4 nmol/l, based on concentrations measured at GEOSECS Station 17 in the Greenland Sea (Chan et al., 1977). This value is also similar to those observed in the surface mixed layer north of the Barents Sea (Guay and Falkner, 1997). The meltwater calcium concentration $(Ca)_{fw}$ is assumed to be 0.9 mmol/l, based on the modern value for freshwater runoff from the Mackenzie River (Reeder et al., 1972). The fraction of meltwater input (f) is calculated using Eqn. 3.4. Figure 3.4c depicts the presence of a high-barium source water occurring between 12.0 ka and 11.3 ^{14}C ka BP, increasing by a total of 54% compared to the present day freshwater value derived from the surface sediment, while the barium concentration of the meltwater endmember at 9.4 ^{14}C ka BP is comparable to Holocene values.

$$\left(\frac{Ba}{Ca} \right)_{mw} = \frac{f(Ba)_{fw} + (1-f)(Ba)_{sw}}{f(Ca)_{fw} + (1-f)(Ca)_{sw}} \quad (\text{Eqn. 3.6})$$

3.4. Discussion

The modern Arctic Ocean receives roughly 10% (3300 km³/yr) of the world's fluvial discharge but represents only about 5% of the total surface area and 1.5% of the total volume of the global ocean (Aagaard and Carmack, 1989). The disproportionate amount of fluvial discharge contributes to salinity-dominated stratification in the water column, with perennial sea ice covering a low-salinity mixed surface layer and a near freezing halocline overlying a warm saline Atlantic layer. The current mean residence time of fluvial waters within the halocline is estimated to be between 11 to 14 years (Bauch et al., 1995). There is a net export of freshwater from the Arctic Ocean through the Fram Strait and the Canadian Archipelago, which affects water column stability and deepwater formation in the North Atlantic (Aagaard and Carmack, 1989). While only a small salinity gradient is necessary for deepwater formation, increased stratification suppresses convection. Consequently, an increased export of meltwater during deglacial time would have hindered deepwater formation.

The barium concentrations of Eurasian rivers that flow into the Arctic Ocean are reported to be 24 to 120 nmol/l, while the values for the Mackenzie River are 410 to 574 nmol/l (Guay and Falkner, 1998). The effective fluvial endmember for dissolved barium concentration in the Mackenzie River is estimated at 520 nmol/l and at 130 nmol/l in the Lena River, which dominates Eurasian sourced fluvial discharge in the western Arctic Ocean (Guay and Falkner, 1998). The latter values include non-conservative behavior in the estuary as barium is desorbed from suspended clays at low to intermediate salinities (Hanor and Chan, 1977). The calculated modern barium concentration in the freshwater endmember (Table 3.2 and Fig. 3.4c) falls within the range of the dissolved barium content of the present day Mackenzie River. Elevated barium concentrations of 65 to 70 nmol/l are currently observed in surface water over the Mendeleev

Ridge region (Guay and Falkner, 1997). Therefore, the Mackenzie River is considered to be the source of high-barium concentrations, transported by the clockwise circulation of the Beaufort Gyre (Fig. 3.1) to the western Amerasian Basin (Guay and Falkner, 1998).

The high-barium concentrations found in the modern Mackenzie River system reflect the weathering of the bedrock characteristic to the drainage basin (Guay and Falkner, 1997, 1998), which includes marine sedimentary rocks that may be high in biogenic barium (Collier and Edmond, 1984; Bishop, 1988; Dymond et al., 1992). The high concentration of barium released between 12 ka and 11.3 ^{14}C ka BP exceeds the current Mackenzie River endmember value of 520 nmol/l Ba. This may be due to increased weathering of the bedrock during glaciation (e.g.; Holland, 1978; Blum and Erel, 1995; Mitchell et al., 2001) and may in addition include the weathering of other barium-rich rock types in the expanded drainage basin during this time interval. Furthermore, increased erosion with higher meltwater flux during deglacial time would likely increase the amount of river borne clays, effectively increasing the amount of barium desorbed in the estuary environment.

Reconstructed history of ice sheet retreat and the evolution of the Mackenzie River drainage basin can be directly correlated to variations in surface water barium over time. The regional recession of the Laurentide Ice Sheet Mackenzie Lobe began as early as 17 ^{14}C ka BP or around 16.2 ka to 14.4 ^{14}C ka BP (Dyke et al., 2002), allowing meltwater to drain into the Beaufort Sea. The discharge would gradually increase the amount of barium in the surface water (Fig. 3.4). By 13 ^{14}C ka BP, deglaciation became more rapid, creating the drainage route that is today the Mackenzie River (Lemmen et al., 1994; Duk-Rodkin and Hughes, 1995). Further ice retreat between 11.8 ka and 11 ^{14}C ka BP (Teller, 1990; Andrews et al., 1993) caused the Mackenzie River drainage basin to expand significantly (Lemmen et al., 1994; Duk-Rodkin and

Hughes, 1995). Evidence of the resulting increase in meltwater discharge through the Mackenzie River is seen by maximum barium concentrations and minimum $\delta^{18}\text{O}$ during this interval. This increase in meltwater discharge may have led to an increased export of meltwater from the Arctic Ocean to the North Atlantic, transported by the Transpolar Drift through the Fram Strait (Fig. 3.1). This is significant in that the subsequent freshening of the North Atlantic surface water may have inhibited deepwater formation and contributed to the onset of the Younger Dryas beginning around 11 ^{14}C ka BP (Broecker et al., 1985).

The meltwater event at 9.4 ^{14}C ka BP is characterized by a $\delta^{18}\text{O}$ minimum but lacks a distinct barium maximum (Fig. 3.4). The high freshwater flux associated with this event is less enriched in barium compared to the meltwater around 11.8 ^{14}C ka BP, but is still comparable to the high-barium concentration of the present day Mackenzie River. The $\delta^{18}\text{O}$ minimum around 9.4 ^{14}C ka BP may be the result of a paleoflood through the Clearwater spillway connecting glacial Lake Agassiz to the Mackenzie River via glacial Lake McConnell (Smith and Fisher, 1993; Fisher and Smith, 1994). The rapid discharge of a more pure meltwater source is consistent with a greater change in $\delta^{18}\text{O}$ and the lack a second barium maximum. However, there is some question as to the timing of this event. Smith and Fisher (1993) report four ^{14}C analyses, three from wood and one from peat taken from flood gravel at the distal end of the spillway that indicate an average age of 9.9 ^{14}C ka BP. Anderson and Lewis (1992) report a bulk sample age of 11.1 ^{14}C ka BP taken from a scour lake at the head of the spillway. If the younger age of 9.9 ^{14}C ka BP is correct, then this flooding event may correspond to the ^{18}O minimum associated with mwp-IB (Fig. 3.4b). If the older bulk sample age of 11.1 ^{14}C ka BP is correct, the timing would correspond to the maximum barium peak associated with mwp-IA. However, until further studies are done, the precise timing and magnitude of this flooding remains

uncertain. Barium concentrations return to modern values after 8.5 ^{14}C ka BP (Fig. 3.4), which corresponds to the termination of Laurentide Ice Sheet meltwater contribution to the Mackenzie River drainage basin (Lemmen et al., 1994).

3.5. Conclusions

Ba/Ca in the planktonic foraminifer *N. pachyderma* sin. can be used as a new proxy for meltwater discharge. The Ba/Ca in *N. pachyderma* sin. reflects the trace element concentration of the seawater in which they grew with an apparent distribution coefficient of 0.22 ± 0.02 . Two deglacial meltwater events are identified by high foraminiferal Ba/Ca and corresponding low $\delta^{18}\text{O}$. These two meltwater events coincide with rapid sea level rise associated with mwp-IB (9.5 ka) and mwp-IA (12 ka). The high concentrations calculated for barium in the surface water during deglacial time are indicative of a continental source. The calculated concentration of barium released between 12 ka and 11.3 ^{14}C ka BP exceeds the current Mackenzie River endmember value. This may be due to increased weathering of the bedrock during glaciation, which may have led to an increase in river borne clays, eroded during high meltwater discharge. This in turn increased the amount of barium desorbed in the estuarine environment. Reconstruction of the meltwater endmember during mwp-IB yields a concentration that is equivalent to the modern Mackenzie River value.

The reconstruction of surface water barium concentrations can be directly correlated to the ice sheet retreat and evolution of the Mackenzie River drainage basin. The oldest meltwater event (12 ka to 11.3 ^{14}C ka BP) occurred as the result of the expansion of the Mackenzie River drainage basin due to retreating ice. The subsequent increase in the export of freshwater from the Arctic Ocean may have led to the freshening of North Atlantic surface waters and contributed to the onset of the Younger Dryas. Although there is some question regarding the timing and

magnitude, a second meltwater event (9.4 ^{14}C ka BP) may be the result of glacial Lake Agassiz flooding through the Clearwater spillway to the Mackenzie River.

3.6. References

- Aagaard K. and Carmark E.C. (1989) The role of sea ice and other fresh water in the Arctic circulation. *Journal of Geophysical Research* **94**, 14485-14498.
- Aksu A.E. and Vilks G. (1988) Stable isotopes in planktonic and benthic foraminifera from the Arctic Ocean surface sediments. *Canadian Journal of Earth Science* **25**, 701-709.
- Anderson T.W. and Lewis C.F.M (1992) Evidence for ice margin retreat and proglacial lake [Agassiz?] drainage by about 11 ka, Clearwater Spillway area, Saskatchewan. Current Research, Part B, Geological Survey of Canada Paper 92-1B, 7-11.
- Andrews J.T., Dyke A.S., Tedesco K., and White J.W. (1993) Meltwater along the Arctic margin of the Laurentide ice sheet (8-12 ka): Stable isotopic evidence and implications for past salinity anomalies. *Geology* **21**, 881-884.
- Bauch D., Carstens J., and Wefer G. (1997) Oxygen isotope composition of living *Neogloboquadrina pachyderma* (sin.) in the Arctic Ocean. *Earth and Planetary Science Letters* **146**, 47-58.
- Bauch D., Schlosser P., and Fairbanks R.G. (1995) Freshwater balance and sources of deep and bottom waters in the Arctic Ocean inferred from the distribution of H_2^{18}O . *Progress in Oceanography* **35**, 53-80.
- Bemis B.E., Spero H.J., Bijma J., and Lea D.W. (1998) Reevaluation of the oxygen isotopic composition of planktonic foraminifera: Experimental results and revised paleotemperature equations. *Paleoceanography* **13**, 150-160.
- Bishop J.K.B. (1988) The barite-opal-organic carbon association in oceanic particulate matter. *Nature* **332**, 341-343.
- Blum J.D. and Erel Y. (1995) A silicate weathering mechanism linking increases in marine $^{87}\text{Sr}/^{86}\text{Sr}$ with global glaciation. *Nature* **373**, 415-418.
- Boyle E.A. and Keigwin L.D. (1987) North Atlantic thermohaline circulation during the past 20,000 years linked to high-latitude surface temperature. *Nature* **330**, 35-40.
- Broecker W.S., Kennett J.P., Flower B.P., Teller J.T., Trumbore S., Bonani G., and Wolfli W. (1989) Routing of meltwater from the Laurentide Ice Sheet during the Younger Dryas cold episode. *Nature* **341**, 318-321.
- Broecker W.S. and Peng T.-H. (1982) *Tracers in the Sea*. Eldigio Press.

- Broecker W.S., Peteet D.M., and Rind D. (1985) Does the ocean-atmosphere system have more than one stable mode of operation? *Nature* **315**, 21-26.
- Bruland K.W. (1983) Trace elements in sea-water. In: *Chemical Oceanography* vol. 8 (Eds. J.P. Riley and R. Chester). Academic Press.
- Chan L.-H., Drummond D., Edmond J.M., and Grant B. (1977) On the barium data from the Atlantic GEOSECS expedition. *Deep-Sea Research* **24**, 613-649.
- Clark P.U., Marshall S.J., Clarke G.K.C., Hostetler S.W., Licciardi J.M., and Teller J.T. (2001) Freshwater forcing of abrupt climate change during the last glaciation. *Science* **293**, 283-287.
- Collier R.W. and Edmond J. (1984) The trace element geochemistry of marine biogenic particulate matter. *Progress in Oceanography* **13**, 113-199.
- Darby D.A., Bischof J.F., and Jones G.A. (1997) Radiocarbon chronology of depositional regimes in the western Arctic Ocean. *Deep-Sea Research II* **44**, 1745-1757.
- Dehairs F., Chesselet R., and Jedwab J. (1980) Discrete suspended particles of barite and the barium cycle in the open ocean. *Earth Planetary Science Letters* **49**, 529-550.
- Duk-Rodkin A. and Hughes O.L. (1995) Quaternary geology of the northeastern part of the central Mackenzie Valley corridor, District of Mackenzie, Northwest Territories. *Geological Survey of Canada, Bulletin* 458.
- Dyke A.S., Andrews J.T., Clark P.U., England J.H., Miller G.H., Shaw J., and Veillette J.J. (2002) The Laurentide and Innuitian ice sheets during the last glacial maximum. *Quaternary Science Reviews* **21**, 9-31.
- Dymond J., Suess E., and Lyle M. (1992) Barium in deep-sea sediment: a geochemical proxy for paleoproductivity. *Paleoceanography* **7**, 163-181.
- Edmond J.M., Measures C., McDuff R.E., Chan L.-H., Collier R., Grant B., Gordon L.I., and Corliss J.B. (1979) Ridge crest hydrothermal activity and the balance of the major and minor elements in the ocean: The Galapagos data. *Earth Planetary Science Letters* **46**, 1-18.
- Fairbanks R.G. (1989) A 17,000-year glacio-eustatic sea level record: Influence of glacial melting rates on the Younger Dryas event and deep-ocean circulation. *Nature* **342**, 637-642.
- Felzer B. (2001) Climate impacts of an ice sheet in East Siberia during the last glacial maximum. *Quaternary Science Reviews* **20**, 437-447.

- Fisher T.G. and Smith D.G. (1994) Glacial Lake Agassiz: It's northwest maximum extent and outlet in Saskatchewan (Emerson Phase). *Quaternary Science Reviews* **13**, 845-858.
- Grosswald M.G. (1998) Late-Weichselian ice sheets in Arctic and Pacific Siberia. *Quaternary International* **45/46**, 3-18.
- Grosswald M.G. and Hughes T.J. (2002) The Russian component of an Arctic ice sheet during the last glacial maximum. *Quaternary Science Reviews* **21**, 121-146.
- Guay C.K. and Falkner K.K. (1997) Barium as a tracer of Arctic halocline and river waters. *Deep-Sea Research II* **44**, 1543-1569.
- Guay C.K. and Falkner K.K. (1998) A survey of dissolved barium in the estuaries of major Arctic rivers and adjacent seas. *Continental Shelf Research* **18**, 859-882.
- Hanor J.S. and Chan L.-H. (1977) Non-conservative behavior of barium during mixing of Mississippi River and Gulf of Mexico waters. *Earth Planetary Science Letters* **37**, 242-250.
- Holland H.D. (1978) *The chemistry of the atmosphere and oceans*. John Wiley and Sons. 351 pp.
- Klinkhammer G. P. and Chan L.-H. (1990) Determination of barium in marine waters by isotope dilution inductively coupled plasma mass spectrometry. *Analytica Chimica Acta* **232**, 323-329.
- Lea D.W. and Boyle E.A. (1989) Barium content of benthic foraminifera controlled by bottom-water composition. *Nature* **338**, 751-753.
- Lea D.W. and Boyle E.A. (1991) Barium in planktonic foraminifera. *Geochimica et Cosmochimica Acta* **55**, 3321-3331.
- Lea D.W. and Boyle E.A. (1993) Determination of carbonate-bound barium in foraminifera and corals by isotope dilution plasma-mass spectrometry. *Chemical Geology* **103**, 73-84.
- Lea D.W. and Spero H.J. (1992) Experimental determination of barium uptake in shells of the planktonic foraminifera *Orbulina universa* at 22°C. *Geochimica et Cosmochimica Acta* **56**, 2673-2680.
- Lea D.W. and Spero H.J. (1994) Assessing the reliability of paleochemical tracers: Barium uptake in the shells of planktonic foraminifera. *Paleoceanography* **9**, 445-452.
- Lemmen D.S., Duk-Rodkin A., and Bednarski J.M. (1994) Late glacial drainage systems along the northwestern margin of the Laurentide ice sheet. *Quaternary Science Reviews* **13**, 805-828.

- Leventer A., Williams D.F., and Kennett J.P. (1982) Dynamics of the Laurentide ice sheet during the last deglaciation: Evidence from the Gulf of Mexico. *Earth and Planetary Science Letters* **59**, 11-17.
- Lubinski D.J., Polyak L., and Forman S.L. (2001) Freshwater and Atlantic water inflows to the deep northern Barents and Kara seas since ca 13 ¹⁴C ka: Foraminifera and stable isotopes. *Quaternary Science Reviews* **20**, 1851-1879.
- Martin J.M. and Meybeck M. (1979) Elemental mass-balance of material carried by major world rivers. *Marine Chemistry* **7**, 173-206.
- Mitchell A., Brown G.H., and Fuge R. (2001) Minor and trace element export from a glacierized Alpine headwater catchment (Haut Glacier d'Arolla, Switzerland). *Hydrological Processes* **15**, 3499-3524.
- Nørgaard-Pedersen N., Spielhagen R.F., Thiede J., and Kassens H. (1998) Central Arctic surface ocean environment during the past 80,000 years. *Paleoceanography* **13**, 193-204.
- O'Neil J.R., Clayton R.N., and Mayeda T.K. (1969) Oxygen isotope fractionation in divalent metal carbonates. *Journal of Chemical Physics* **51**, 5547-5558.
- Poore R.Z., Osterman L., Curry W.B., and Phillips R.L. (1999a) Late Pleistocene and Holocene meltwater events in the western Arctic Ocean. *Geology* **27**, 759-762.
- Poore R.Z., Ostermann D.R., and McGeehin J. (1999b) Stable isotope data and AMS ¹⁴C dates from Arctic Ocean section 1994 surface sediment transect and box core samples from the Mendeleev Ridge area. USGS Open-File Report 99-48, p. 17.
- Reeder S.W., Hitchon B., and Levinson A.A. (1972) Hydrogeochemistry of the surface waters of the Mackenzie River drainage basin, Canada-I. Factors controlling inorganic composition. *Geochimica et Cosmochimica Acta* **36**, 825-865.
- Rosenthal Y., Field M.P., and Sherrell R.M. (1999) Precise determination of element/calcium ratios in calcareous samples using sector field inductively coupled plasma mass spectrometry. *Analytical Chemistry* **71**, 3248-3253.
- Sher A. (1995) Is there any real evidence for a huge ice sheet in East Siberia? *Quaternary International* **28**, 39-40.
- Smith D.G. and Fisher T.G. (1993) Glacial Lake Agassiz: The northwestern outlet and paleoflood. *Geology* **21**, 9-12.
- Spero H.J. and Williams D.F. (1990) Evidence for seasonal low-salinity surface waters in the Gulf of Mexico over the last 16000 years. *Paleoceanography* **5**, 963-975.

- Spielhagen R.F. and Erlenkeuser H. (1994) Stable oxygen and carbon isotopes in planktonic foraminifers from Arctic Ocean surface sediments: Reflection of the low salinity surface water layer. *Marine Geology* **119**, 227-250.
- Stein R., Seung-II N., Schubert C., Vogt C., Fütterer D., and Heinemeier J. (1994) The last deglaciation event in the eastern central Arctic Ocean. *Science* **264**, 692-696.
- Svendsen J.I., Astakhov V.I., Bolshiyarov D. et al., (1999) Maximum extent of the Eurasian ice sheets in the Barents and Kara Sea region during the Weichselian. *Boreas* **28**, 234-242.
- Teller J.T. (1990) Meltwater and precipitation runoff to the North Atlantic, Arctic and Gulf of Mexico from the Laurentide Ice Sheet and adjacent regions during the Younger Dryas. *Paleoceanography* **5**, 897-905.
- Velichko A.A., Kononov Y.M., and Faustova M.A. (1997) The last glaciation of Earth: Size and volume of ice-sheets. *Quaternary International* **41/42**, 43-51.
- Volkman R. and Mensch M. (2001) Stable isotope composition ($\delta^{18}\text{O}$, $\delta^{13}\text{C}$) of living planktonic foraminifers in the outer Laptev Sea and the Fram Strait. *Marine Micropaleontology* **42**, 163-188.
- Von Damm K.L., Edmond J.M., Grant B., Measures C.I., Walden B., and Weiss R.F. (1985) Chemistry of submarine hydrothermal solutions at 21°N, East Pacific Rise. *Geochimica et Cosmochimica Acta* **49**, 2197-2220.

CHAPTER 4. LI/CA IN MULTIPLE SPECIES OF BENTHIC AND PLANKTONIC FORAMINIFERA: THERMOCLINE, LATITUDINAL, AND GLACIAL-INTERGLACIAL VARIATION

4.1. Introduction

Lithium has a constant concentration (26 μM) and isotopic composition (-32‰ $\delta^6\text{Li}$) throughout the world's oceans (Chan and Edmond, 1988). The major sources of lithium to the ocean are from rivers and hydrothermal interaction with oceanic crust (Stoffyn-Egli and Mackenzie, 1984). Therefore, changes in the lithium concentration of the ocean should reflect changes in hydrothermal input and continental weathering over geologic time, provided the removal rate constants do not vary (Delaney et al., 1985). Foraminiferal Li/Ca has the potential to be used as a proxy for changes in the lithium concentration of seawater because calcareous foraminifera secrete a test from the surrounding water in which they live, incorporating lithium as a trace element. Lithium and calcium exhibit conservative behavior in the ocean. Lithium has an oceanic residence time around 1.5 Ma (Huh et al., 1998) and calcium around 1 Ma (Broecker and Peng, 1982). With such long residence times, the Li/Ca ratio in seawater is not expected to have changed over glacial-interglacial timescales. This notion is supported by preliminary data from foraminiferal $\delta^6\text{Li}$ (Chapter 5).

To date, the use of foraminiferal Li/Ca as a paleoceanographic proxy has been limited. Pioneering work by Delaney et al. (1985) indicated that foraminiferal Li/Ca is directly related to the Li/Ca ratio of the seawater in which these organisms grow. Delaney et al. (1985) also investigated the effect of temperature on foraminiferal lithium incorporation through laboratory culture and examination of core top and sediment trap samples. Laboratory culture of *Globigerinoides sacculifer* in natural seawater yields 15.4 ± 5.7 $\mu\text{mol/mol}$ at 30°C and 14.9 ± 1.0 $\mu\text{mol/mol}$ at 20°C . However, only one measurement for *Orbulina universa* at 30°C (11.7

$\mu\text{mol/mol}$) and two at 20°C (14.4 and $11.5 \mu\text{mol/mol}$) were made. Core top and sediment trap samples show a varied relationship between Li/Ca and temperature. Therefore, the influence of temperature on foraminiferal lithium incorporation seems complex and may be subject to other temperature dependent variables such as growth rate (Delaney et al., 1985). Subsequent work by Delaney and Boyle (1986) used the lithium content of mixed planktonic foraminiferal species to investigate changes in hydrothermal input over the last 116 Ma. The results of this study indicate that hydrothermal fluxes have not varied from the present by more than 30 to 40%. This estimation is based on the assumption that the dominant influence on foraminiferal lithium incorporation was seawater composition and that the removal constants for lithium sinks have remained unchanged.

The present study further investigates the usefulness of foraminiferal Li/Ca as a paleoceanographic proxy. In particular, measurements of Li/Ca ratios in single species of benthic and planktonic foraminifera were carried out to investigate the factors influencing lithium incorporation into foraminiferal tests. Several factors are evaluated including temperature, pressure, dissolution, vital effects, and shell mass.

4.1.1. Sediment Samples and Oceanographic Setting

Sediment cores and surface sediment samples used for this study are listed in Table 4.1. The distribution of sampling sites is shown on the map in Fig. 4.1. The sediment materials include the following: (1) Giant gravity cores and jumbo piston cores recovered from the Bahama Banks between 423 to 1535 m water depths. This depth interval intersects the thermocline of the subtropical gyre and the upper North Atlantic Deep Water (Slowey and Curry, 1995). Bottom water temperatures in this area range between 16.5 and 4°C , whereas surface

Table 4.1. Dredge and sediment cores; jumbo piston core (JPC), piston core (PC), giant gravity core (GGC), giant piston core (GPC), box core (BC).

Core	Latitude, °N	Longitude, °W	Water Depth (m)
<i>Bahama banks:</i>			
OC205-2-149JPC	26.26	77.67	423
OC205-2-108GGC	25.98	78.18	743
OC205-2-103GGC	26.07	78.06	965
OC205-2-100GGC	26.06	78.03	1057
OC205-2-97JPC	25.94	77.85	1183
OC205-2-7JPC	26.14	77.74	1320
OC205-2-117JPC	26.03	77.88	1535
<i>North Atlantic:</i>			
CHN75-2-43-33PC	12.18	59.05	2173
CHN75-2-29-19PC	12.97	44.57	3266
AII42-1-17-16PC	19.56	46.13	2471
CHN61-10-175PC	27.88	45.18	3690
KNR31-3-1-1GPC	36.45	32.00	2829
CHN43-1-102-28PC	45.5	27.83	3012
AII94-2-91-16PC	57.49	26.77	2708
KNR54-6-100-27BC	63	14.20	1526
<i>Caribbean:</i>			
VM28-129PC	11.12	80.40	3400
<i>Sierra Leone Rise:</i>			
EN066-1-42GGC	5.17	21.03	2666
EN066-1-20GGC	5.08	20.99	2756
EN066-1-10GGC	6.64	21.90	3527
EN066-1-11GGC	6.02	21.90	3695
EN066-1-21GGC	4.23	20.63	3792
EN066-1-36GGC	4.31	20.21	4095
EN066-1-24GGC	3.85	20.37	4518
EN066-1-26GGC	3.09	20.02	4745
EN066-1-33GGC	2.64	19.75	4848
EN066-1-29GGC	2.46	19.76	5105
<i>Indian Ocean:</i>			
KNR162-13-D7	Latitude, °S 24.50	Longitude, °E 69.92	2255

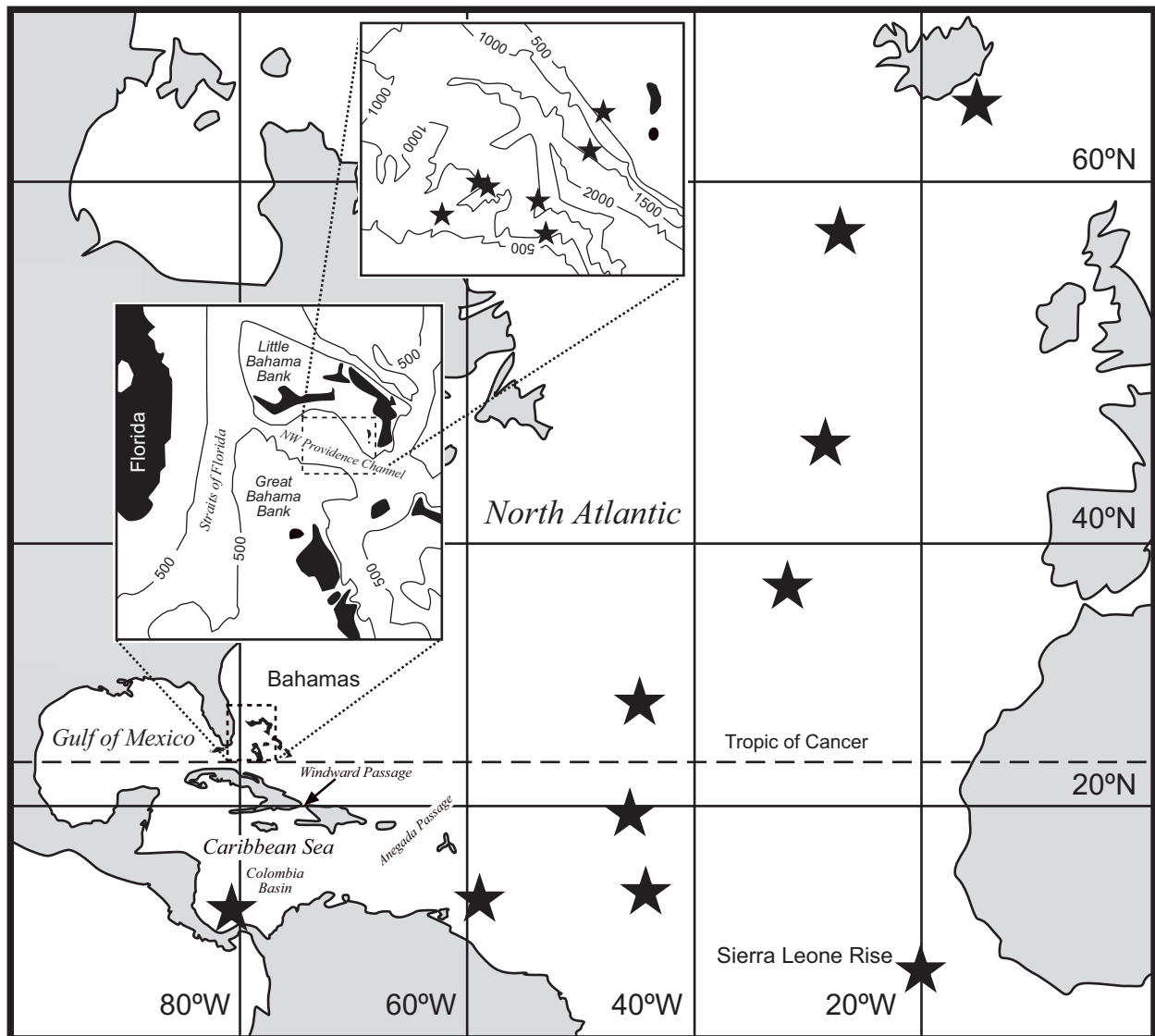


Figure 4.1. Map showing locations of sampling sites (stars) from three sets of cores: (1) the Northwest Providence Channel of the Bahama Banks between 423 to 1535 m water depths. (2) Holocene and core top sediments transecting the mid-depth North Atlantic (1526 to 3690 m) from 12 to 63°N latitude. (3) Surface sediments recovered from the Sierra Leone Rise between 2666 to 5105 m water depths, and one core from the Colombia Basin of the Caribbean Sea from 3400 m water depth. See Table 4.1 for core descriptions.

water temperature is about 26°C (Slowey and Curry, 1995). Down-core sediments, including oxygen isotope stages 1, 2, and 3, are used to characterize glacial-interglacial variation in planktonic and benthic foraminifera. Holocene and core top sediments are used to estimate changes along the Bahama Bank margins. (2) A suite of Holocene and core top sediments

transecting the mid-depth North Atlantic (1526 to 3690 m water depth) from 12 to 63°N latitude. The total range in surface water temperature for this transect is approximately 12 to 17°C (Levitus and Boyer, 1994). (3) Surface sediments recovered from the deep submarine Sierra Leone Rise between 2684 to 5104 m water depths, reaching below the eastern Atlantic lysocline at 4800 m (Rosenthal et al., 2000). Variations in planktonic shell chemistry are dominated by postdepositional dissolution at this site, increasing with increasing water depth (Rosenthal et al., 2000). (4) Core VM28-129PC from the Columbia Basin of the Caribbean Sea from 3400 m water depth (Prell, 1978). The deep water of the Caribbean Sea reflects the intermediate waters (1700 – 1800 m) of the North Atlantic that flow over the sills into the basin (Wüst, 1963). The bottom water temperature in the Columbia Basin is 4°C (Wüst, 1963), which is the same as the bottom water temperature in the Bahama Banks at 1500 m (Slowey and Curry, 1995). This core is used to estimate the effect of increased water depth. (5) A dredge taken from the tropical Indian Ocean at 2255 m water depth. Surface sediments from this core were included to provide a comparison of planktonic foraminifera from different ocean basins.

4.2. Methods

4.2.1. Sample Preparation and Analysis

Down-core samples from the Bahaman cores were typically taken every 3 to 5 cm from sediments representing deglacial and glacial time and otherwise at 10 cm intervals. Down-core samples from the Caribbean core were taken in 3 to 4 cm intervals. All sediment samples were disaggregated in distilled water on a shaker table and then wet-sieved through a 150 µm polypropylene mesh. The coarse fraction remaining in the sieve was then dried in an oven for 30 minutes to an hour at 55 to 60°C. Sediments were picked for planktonic (*Orbulina universa*, *Globigerinoides ruber*, and *Globigerinoides sacculifer*) and benthic foraminifera including

Planulina wuellerstorfi (synonymous with *Cibicidoides wuellerstorfi*), *Planulina rugosus*, *Cibicidoides cicatricosus*, *Cibicidoides incrassatus* (synonymous with *Cibicidoides corpulentus*), *Cibicidoides pachyderma* (synonymous with *Cibicidoides floridanus*), *Cibicidoides robertsonianus*, and *Hoeglandina elegans*. A typical sample weighing 0.5 mg contained an average of 4 to 25 individuals. Foraminiferal tests were gently crushed and then purified following modified procedures from Lea and Boyle (1993). Samples were ultrasonically cleaned four times with distilled water and twice with methanol to remove detrital grains and fine clay particles. Metal oxide coatings were reduced in a solution consisting of anhydrous-hydrazine, citric-acid, and ammonium-hydroxide and organic matter was oxidized in a solution of hydrogen-peroxide and sodium-hydroxide. Sedimentary barite (BaSO_4) was dissolved in alkaline diethylenetriamine-pentaacetic acid (DTPA) and then removed by rinsing with ammonium hydroxide. Any remaining adsorbed metals were leached with 0.001 N nitric acid. All dilute nitric acids used in this study were prepared from SEASTAR™ high purity acid. The remaining shell material was then dissolved in 0.1 N nitric acid for elemental analysis. Solutions of cleaned *G. sacculifer* from surface sediments of the Sierra Leone Rise were generously provided by Y. Rosenthal. The preparation of these solutions is described in Rosenthal et al. (2000). The cleaning procedures for these samples did not include a reductive step or removal of sedimentary barite.

Sample solutions were simultaneously analyzed for lithium, magnesium, strontium, manganese, and calcium with a ThermoQuest Finnigan Element 2 inductively coupled plasma mass spectrometer (ICP-MS) at the University of Southern Mississippi according to the method of Rosenthal et al. (1999). In this technique, element to calcium ratios were determined from intensity ratios of appropriate isotopes using an external matrix matched standard. The multi-

element standard was prepared with ICP-MS grade High-Purity Standards. This solution was standardized for lithium by isotope dilution using a Finnigan MAT 262, thermal ionization mass spectrometer (TIMS) and procedures developed by You and Chan (1996). Magnesium, strontium, and manganese were standardized by the standard additions method using ICP-MS, and calcium with a PerkinElmer Optima 3300DV inductively coupled plasma optical emission spectrometer (ICP-OES). Replicate analyses of dilute seawater were performed to monitor the reproducibility and accuracy of the method. The long-term precision of the seawater Li/Ca replicates was $2368 \pm 3.9\%$, which is within 3% accuracy of the Li/Ca analyzed in seawater at $2443 \pm 1.2\%$ using a flame emission technique (Chapter 5). Precision was about 3.5% for Li/Ca, 3.7% for Sr/Ca, and 7.4% for Mg/Ca in replicate analyses of *O. universa* (Table 4.2).

Some data were rejected from this study based on several criteria. Foraminiferal Mn/Ca was analyzed to monitor the effectiveness of the cleaning procedures (Appendix 1). Mn-carbonate overgrowths and Mn-oxide coatings contain a variety of other elements and therefore, must be removed before chemical analyses (Boyle, 1981, 1983). Samples with Mn/Ca ratios above 90 $\mu\text{mol/mol}$ are considered to be contaminated and were eliminated from this study. However, Li/Ca samples with Mn/Ca ratios above 90 $\mu\text{mol/mol}$ were retained if foraminiferal Li/Ca was reproducible within 0.6 $\mu\text{mol/mol}$. In addition, as the cleaning procedures were quite rigorous, some amount of shell material was inevitably lost. Cleaned sample with excessively low yields were rejected from the data set as well as samples that were obviously contaminated with sedimentary barite ($> 4 \mu\text{mol/mol Ba/Ca}$).

Table 4.2. Replicate analyses of Li/Ca, Mg/Ca, and Sr/Ca in *Orbulina universa* from core top sediments from Bahaman core OC205-2-97JPC and Indian Ocean Dredge KNR162-13-D7.

<i>O. universa</i>		
Li/Ca ($\mu\text{mol/mol}$)	Mg/Ca (mmol/mol)	Sr/Ca (mmol/mol)
OC205-2-97JPC		
10.5	9.2	1.31
10.1	8.9	1.40
10.4	7.1	1.28
10.8	9.3	1.44
10.8	9.3	1.32
10.6	7.6	1.29
Average		
10.5 \pm 0.3	8.6 \pm 1.0	1.34 \pm 0.06
KNR162-13-D7		
10.5	5.1	1.33
9.9	5.5	1.30
10.9	5.5	1.33
10.0	5.4	1.34
Average		
10.3 \pm 0.5	5.4 \pm 0.2	1.33 \pm 0.2

4.2.2. Chronology

The Y-Z boundary is a biostratigraphic designation defined by the first consistent appearance of the *Globorotalia menardii* complex and represents the Pleistocene/Holocene boundary (Ericson and Wollin, 1956). Core sediments from a >150 μm sieved fraction were dried, weighed, and then picked for the *G. menardii* complex. The frequency of the *G. menardii* complex was then calculated by dividing the number of individuals by the weight of the sample (Appendix 2). The radiocarbon age of the Y-Z boundary in the Gulf of Mexico, Caribbean Sea, and in the Bahamas is 11,000 \pm 500 yr BP (Ericson and Wollin, 1956; Broecker et al., 1960; Ericson and Wollin 1968). The Y-Z boundary for Caribbean core VM28-129PC was determined by Prell (1978) based on the carbonate and coarse fraction contents. Corrected radiocarbon ages

from *G. sacculifer* analyzed by accelerator mass spectrometry (AMS) were reported for 100GGC by Slowey and Curry (1995) and for 103GGC by Marchitto et al. (1998), assuming a 400 year reservoir age.

Stable isotopic measurements on *G. sacculifer* were made for Caribbean core V28-129PC at the Woods Hole Oceanographic Institution using a Finnigan MAT 252 mass spectrometer with a Kiel device. Stable isotopic analyses on the Bahaman cores, also using a Finnigan MAT 252 mass spectrometer, were performed on several species of benthic foraminifera and are reported by Slowey and Curry (1995). According to the oxygen isotope records, Caribbean core V28-129PC includes Holocene and last glacial maximum (LGM) sediments whereas the cores taken from the Bahama Banks include the Holocene and the LGM, with some cores extending into oxygen isotope stage 3 (Fig. 4.2). The LGM is defined in the Bahaman cores by the oxygen isotope record and in Caribbean core V28-129PC by percent carbonate and coarse-fraction (Prell, 1978) in addition to the oxygen isotope data.

4.3. Results

4.3.1. Down-core Variation in Bahamas and Caribbean

Given the current understanding of lithium behavior in the ocean, Li/Ca in foraminiferal tests is not expected to change over glacial-interglacial timescales. However, Li/Ca in *P. wuellerstorfi* and *O. universa* varies consistently with glacial-interglacial benthic foraminiferal $\delta^{18}\text{O}$ in each of the cores analyzed in this study (Fig. 4.2; Table 4.3). Based on the oxygen isotope record, it is unclear if Bahaman core 149JPC, 423 m includes the LGM. However, the maximum Li/Ca value for planktonic *O. universa*, coincident with a $\delta^{18}\text{O}$ maximum, is 16.0 $\mu\text{mol/mol}$, decreasing to $10.7 \pm 0.2 \mu\text{mol/mol}$ during the Holocene (Fig. 4.2a). Li/Ca for

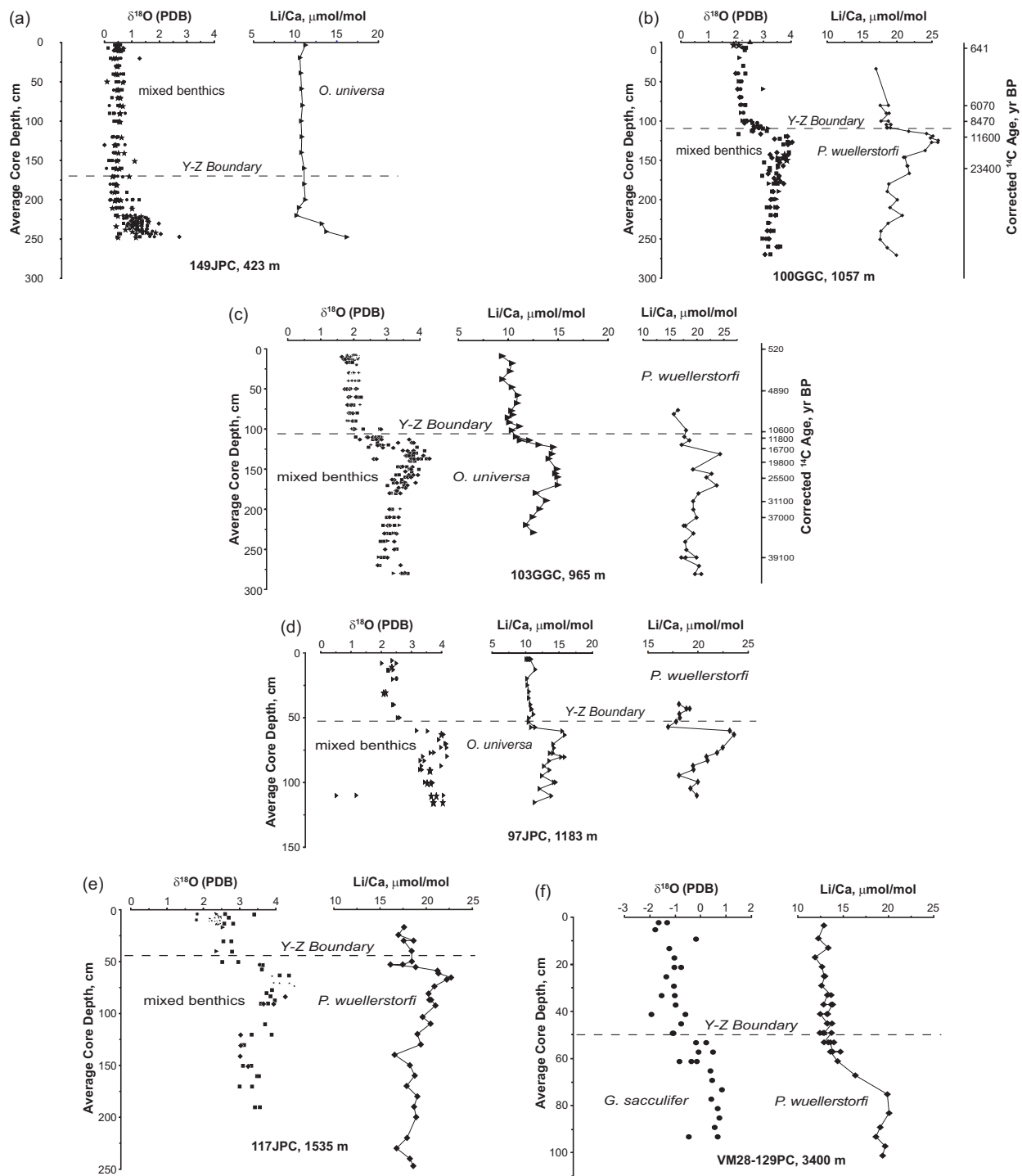


Figure 4.2. Down-core $\delta^{18}\text{O}$ from individual mixed benthic species (Slowey and Curry, 1995) and Li/Ca from *Orbulina universa* and *Planulina wuellerstorfi* from Bahama Bank cores: (a) 149JPC, (b) 100GGC, (c) 103GGC, (d) 97JPC, and (e) 117JPC. Corrected AMS ages from *Globigerinoides sacculifer* assume a 400 year reservoir age (Slowey and Curry, 1995; Marchitto et al., 1998). The Y-Z boundary is based on the *Globorotalia menardii* complex (Appendix 2; Ericson and Wollin 1956). (f) $\delta^{18}\text{O}$ from Caribbean core VM28-129PC from *Globigerinoides sacculifer* and Li/Ca from *Planulina wuellerstorfi*. The Y-Z boundary is from Prell (1978). See Table 4.3 for data summary.

Table 4.3. Li/Ca in *Orbulina universa* and *Planulina wuellerstorfi* from Bahama Bank cores 149JPC, 100GGC, 103GGC, 97JPC, and 117JPC and from Caribbean core VM28-129PC.

OC205-2-149JPC, 423 m		OC205-2-100GGC, 1057 m		OC205-2-103GGC, 965 m		
Average Core Depth (cm)	Li/Ca ($\mu\text{mol/mol}$)	Average Core Depth (cm)	Li/Ca ($\mu\text{mol/mol}$)	Average Core Depth (cm)	Li/Ca ($\mu\text{mol/mol}$)	Li/Ca ($\mu\text{mol/mol}$)
<i>O. universa</i>		<i>P. wuellerstorfi</i>		<i>O. universa</i>	<i>P. wuellerstorfi</i>	
3	11.1	43.5	16.6	8.5	9.3	---
19	10.4	90	18.3	17.5	10.3	---
38.5	10.5	90	17.1	27.5	10.1	---
58.5	10.6	100	17.9	37.5	9.4	---
79.5	10.7	100	18.3	47.5	10.3	---
99.5	10.5	110	17.2	57.5	10.9	---
119.5	10.6	110	18.3	67.5	10.8	---
139.5	10.6	114.5	18.6	77	10.3	16.5
159.5	10.9	114.5	18.0	82	10.4	15.6
179.5	10.9	118.5	18.1	85.5	9.9	---
199.5	11.0	118.5	18.2	91.5	10.1	---
209.5	10.2	118.5	18.6	96.5	11.1	---
219.5	9.9	123	21.4	101.5	10.4	18.0
230	13.0	126	24.0	109.5	10.8	17.7
240	13.5	129	25.0	114	12.2	18.6
247	16.0	131.5	24.7	114	11.3	---
		134.5	25.9	119.5	13.2	17.1
		137	25.9	122.5	14.7	---
		137	25.1	131	14.6	24.3
		147.5	24.3	137	14.3	---
		156	21.3	150	15.1	19.2
		156	21.6	155.5	14.9	22.7
		167	21.1	160	15.0	21.8
		167	21.2	170	15.0	23.7
		176.5	21.3	180	12.8	20.3
		190	18.6	189.5	13.8	19.3
		199.5	18.4	200	13.1	19.3
		210	20.0	210	12.3	19.9
		220	19.0	220	11.6	17.8
		230	20.9	220	---	17.5
		230	20.9	229.5	12.3	19.4
		240	18.9	240	---	17.8
		250	17.9	250	---	18.0
		260.5	17.9	259.5	---	19.9
		271	19.0	259.5	---	17.9
		280.5	20.5	259.5	---	17.1
				270	---	20.4
				280	---	19.6
				280	---	20.8

Table 4.3 continued

OC205-2-97JPC, 1183 m			OC205-2-117JPC, 1535 m		VM28-129PC, 3400 m	
Average Core Depth (cm)	Li/Ca ($\mu\text{mol/mol}$)	Li/Ca ($\mu\text{mol/mol}$)	Average Core Depth (cm)	Li/Ca ($\mu\text{mol/mol}$)	Average Core Depth (cm)	Li/Ca ($\mu\text{mol/mol}$)
	<i>O. universa</i>	<i>P. wuellerstorfi</i>		<i>P. wuellerstorfi</i>		<i>P. wuellerstorfi</i>
4.5	10.5	---	17	17.7	3.5	12.7
4.5	10.1	---	24.5	17.0	9	12.1
4.5	10.4	---	30	18.6	13	13.2
4.5	10.8	---	30	17.4	17	11.9
4.5	10.8	---	40	18.2	21	12.7
4.5	10.6	---	50	18.2	25	12.8
12.5	11.5	---	53	17.1	25	13.0
19.5	10.2	---	53	15.8	29	12.7
24.5	10.3	---	55.5	18.4	33	13.8
29.5	10.5	---	59	20.5	33	13.1
34.5	10.5	---	61.5	20.6	37	13.6
39.5	10.7	18.1	65.5	21.9	37	13.0
43	10.8	18.9	67.5	21.4	37	14.1
43	10.9	19.2	74	20.1	41	13.5
47	11.2	18.1	81	19.5	41	13.5
50	10.5	18.2	87	19.6	41	12.4
53	10.4	17.8	87	19.7	45	13.7
57	11.5	17.0	92.5	20.2	45	13.5
57	10.8	---	103.5	19.1	45	13.4
60	15.5	23.2	110	19.6	49	13.1
63	15.9	23.6	120	18.4	49	12.9
70	14.1	---	130	19.0	49	12.5
73	14.2	22.5	140	16.3	49	13.6
77	14.1	21.9	150	18.0	53	13.5
77	13.6	---	160	18.7	53	13.0
80	15.8	20.8	170	17.9	53	14.0
80	15.3	---	180	19.2	53	13.4
83	13.5	21.0	190	19.0	57	13.7
87	12.7	19.5	200	19.3	57	13.8
90	13.6	19.6	220	17.9	57	14.7
94.5	12.4	18.1	230	16.7	61	14.3
99.5	14.2	20.0	240	18.1	67	16.3
99.5	14.5	---	247	18.2	75	19.8
104.5	12.1	19.2			83	20.0
110	13.9	19.9			89	19.1
					93	18.6
					97	19.6
					101	19.3

Table 4.3 continued

O. universa from 103GGC, 965 m is 14.8 ± 0.3 $\mu\text{mol/mol}$ during the LGM, decreasing to 10.3 ± 0.5 $\mu\text{mol/mol}$ during the Holocene (Fig. 4.2c), while 97JPC, 1183 m is 15.7 ± 0.3 $\mu\text{mol/mol}$, decreasing to 10.6 ± 0.4 $\mu\text{mol/mol}$ (Fig. 4.2d).

The benthic foraminifer *P. wuellerstorfi* is a deep-water species, and is therefore not present at 423 m water depth and is relatively scarce in the Holocene compared to glacial sediments. The average value for benthic *P. wuellerstorfi* during the LGM from Bahaman core 100GGC, 1057 m is 25.7 ± 0.4 , decreasing to 17.7 ± 0.7 $\mu\text{mol/mol}$ during the Holocene (Fig. 4.2b), 103GGC, 965 m is 24.3, decreasing to 16.7 ± 1.2 $\mu\text{mol/mol}$ (Fig. 4.2c), 97JPC, 1183 m is 23.4 ± 0.3 , decreasing to 18.5 ± 0.5 $\mu\text{mol/mol}$ (Fig. 4.2d), and 117JPC, 1535 m is 21.7 ± 0.3 , decreasing to 17.8 ± 0.6 $\mu\text{mol/mol}$ (Fig. 4.2e). The value for benthic *P. wuellerstorfi* during the LGM from Caribbean core VM28-129PC, 3400 m yields 20.0 $\mu\text{mol/mol}$, decreasing to 13.1 ± 0.6 $\mu\text{mol/mol}$ during the Holocene (Fig. 4.2f). LGM to Holocene ratios of foraminiferal Li/Ca can be seen in Table 4.4. Li/Ca ratios are analytically indistinguishable in Holocene samples of *O. universa* and *P. wuellerstorfi* despite differences in shell mass per individual test (Fig. 4.3; Table 4.5). As such, differences in shell mass do not appear to influence lithium incorporation in *P. wuellerstorfi* and *O. universa*.

4.3.2. Sierra Leone Rise

Down-slope Li/Ca in the planktonic foraminifer *G. sacculifer*, recovered from the deep submarine Sierra Leone Rise between 2684 and 5104 m water depth, gradually decreases by 9% with increasing water depth (Fig. 4.4; Table 4.6). The dissolution of these sediments increases with increasing water depth and extend below the eastern Atlantic lysocline at 4800 m

Table 4.4. Li/Ca in $\mu\text{mol/mol}$ and LGM to Holocene ratios in *Planulina wuellerstorfi* and *Orbulina universa* from the Bahama Banks (149JPC, 103GGC, 100GGC, 97JPC, 7JPC, 117JPC) and the Caribbean Sea (VM28-129PC).

Core	Li/Ca (Holocene)	Li/Ca (LGM)	LGM Holocene
<i>P. wuellerstorfi</i>			
103GGC, 965m	16.7 \pm 1.2	24.3	1.46
100GGC, 1057m	17.7 \pm 0.7	25.7 \pm 0.4	1.45
97JPC, 1183m	18.5 \pm 0.5	23.4 \pm 0.3	1.26
7JPC, 1320m	17.5 \pm 0.7	20.2	1.15
117JPC, 1535m	17.8 \pm 0.6	21.7 \pm 0.3	1.22
129PC, 3400m	13.1 \pm 0.6	20.0	1.53
<i>O. universa</i>			
149JPC, 423m	10.7 \pm 0.2	16.0	1.50
103GGC, 965m	10.3 \pm 0.5	14.8 \pm 0.3	1.44
97JPC, 1183m	10.6 \pm 0.4	15.7 \pm 0.3	1.47
7JPC, 1320m	10.9 \pm 0.5	15.0	1.37

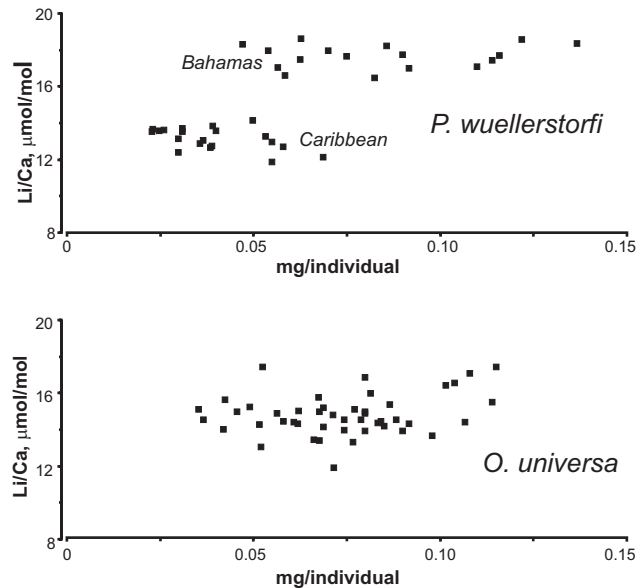


Figure 4.3. Holocene Li/Ca versus weight per individual from *Planulina wuellerstorfi* and *Orbulina universa*. See Table 4.5 for data summary.

Table 4.5. Holocene Li/Ca in $\mu\text{mol/mol}$ versus weight per individual from *Planulina wuellerstorfi* and *Orbulina universa*.

Weight (mg)	Number of individuals	mg per individual	Li/Ca <i>P. wuellerstorfi</i>	Weight (mg)	Number of individuals	mg per individual	Li/Ca <i>P. wuellerstorfi</i>
VM28-129PC				OC205-2-117JPC			
0.56	14	0.040	13.5	0.27	3	0.090	17.7
0.56	18	0.031	13.5	0.34	6	0.057	17.0
0.55	11	0.050	14.1	0.44	7	0.063	18.6
0.55	15	0.037	13.0	0.50	8	0.063	17.4
0.55	14	0.039	13.8	0.60	7	0.086	18.2
0.39	10	0.039	12.7				
0.66	12	0.055	13.0				
0.58	10	0.058	12.7	OC205-2-100GGC			
0.44	8	0.055	11.9	0.41	7	0.059	16.6
0.48	9	0.053	13.2	0.33	7	0.047	18.3
0.55	8	0.069	12.1	0.44	4	0.110	17.1
0.54	14	0.039	12.7	0.35	5	0.070	17.9
0.25	7	0.036	12.8	0.41	3	0.137	18.3
0.72	24	0.030	13.1				
0.62	25	0.025	13.6	OC205-2-7JPC			
0.18	6	0.030	12.4				
0.95	41	0.023	13.7	0.54	10	0.054	17.9
0.60	23	0.026	13.6	0.30	4	0.075	17.6
0.48	21	0.023	13.5	0.57	5	0.114	17.4
0.28	9	0.031	13.7	0.61	5	0.122	18.6
				0.33	4	0.083	16.5
				0.55	6	0.092	17.0
				0.58	5	0.116	17.7

Table 4.5 continued

Weight (mg)	Number of individuals	mg per individual	Li/Ca <i>O. universa</i>	Weight (mg)	Number of individuals	mg per individual	Li/Ca <i>O. universa</i>
	KNR31-3-1-1GPC				OC205-2-97JPC		
0.57	7	0.08	11.9	0.57	5	0.11	11.5
0.54	8	0.07	11.7	0.62	12	0.05	10.2
	AII94-2-91-16PC			0.62	10	0.06	10.3
0.52	10	0.05	9.0	0.53	6	0.09	10.5
0.67	11	0.06	10.3	0.63	8	0.08	10.5
0.53	15	0.04	11.1	0.57	8	0.07	10.7
	CHN61-10-175PC			0.56	7	0.08	10.8
0.69	6	0.12	13.4	0.61	9	0.07	10.9
0.54	5	0.11	13.0	0.54	11	0.05	11.2
	CHN43-1-102-28PC			0.52	7	0.07	10.5
0.52	5	0.10	12.5		OC205-2-103GGC		
0.61	6	0.10	12.4	0.61	9	0.07	9.3
0.56	7	0.08	12.8	0.64	6	0.11	10.3
	CHN75-2-29-19PC			0.51	6	0.09	10.1
0.49	5	0.10	9.6	0.53	8	0.07	9.4
0.52	6	0.09	11.3	0.50	6	0.08	10.3
	CHN75-2-43-33PC			0.64	8	0.08	10.9
0.69	9	0.08	9.2	0.62	11	0.06	10.8
0.56	9	0.06	11.0	0.55	6	0.09	10.3
	AII42-1-17-16PC			0.59	7	0.08	10.4
0.48	6	0.08	9.9	0.52	7	0.07	9.9
0.54	7	0.08	11.1	0.55	8	0.07	10.1
	KNR54-6-100-27BC			0.55	8	0.07	11.1
0.63	12	0.05	13.4	0.58	10	0.06	10.4
0.51	12	0.04	11.6		KNR162-13-D7		
				0.44	12	0.04	10.5
				0.54	6	0.09	9.9
				0.41	9	0.05	10.9
				0.63	15	0.04	10.0

Table 4.5 continued

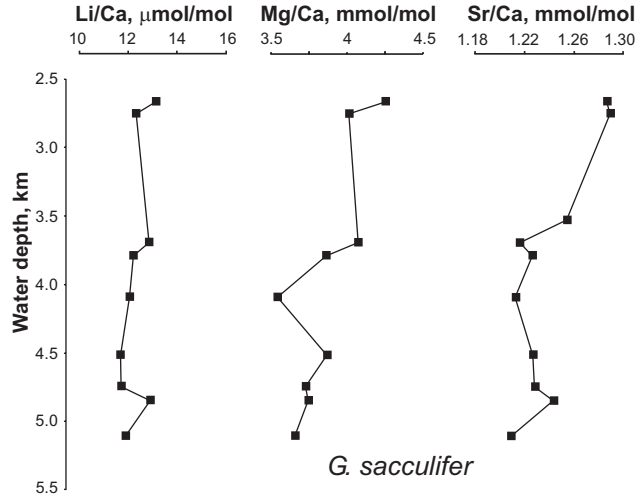


Figure 4.4. Li/Ca, Mg/Ca, and Sr/Ca in *Globigerinoides sacculifer* from the Sierra Leone Rise between 2666 to 5105 m water depths. See Table 4.6 for data summary.

Table 4.6. Li/Ca in $\mu\text{mol/mol}$, Mg/Ca in mmol/mol , and Sr/Ca in mmol/mol from *Globigerinoides sacculifer* from the Sierra Leone Rise.

EN066-1	Water Depth (m)	Li/Ca	Mg/Ca	Sr/Ca
		<i>G. sacculifer</i>		
42GGC	2666	13.1	4.2	1.29
20GGC	2756	12.4	4.0	1.29
10GGC	3527	---	---	1.25
11GGC	3695	12.9	4.1	1.22
21GGC	3792	12.2	3.8	1.23
36GGC	4095	12.1	3.5	1.21
24GGC	4518	11.7	3.9	1.23
26GGC	4745	11.7	3.7	1.23
33GGC	4848	12.9	3.7	1.24
29GGC	5105	11.9	3.6	1.21

(Rosenthal et al., 2000). The mean annual sea surface temperature at this site is around 27°C (Levitus and Boyer, 1994). Foraminiferal Mg/Ca and Sr/Ca also decrease with increasing depth by 14% and 6% respectively.

4.3.3. North Atlantic Transect

Figure 4.5 shows the latitudinal variations in Li/Ca, Mg/Ca, and Sr/Ca from the planktonic foraminifer *O. universa* for a Holocene and core top transect of the North Atlantic Ocean (Fig. 4.1). All samples along the transect are above 3700 m water depth, so the dissolution effect should be minimal. There is a 39% rise in Li/Ca, a 5% rise in Sr/Ca, and a 63% decrease in Mg/Ca in *O. universa* with increasing latitude from 12°N to 63°N (Table 4.7). The incorporation of magnesium in foraminiferal calcite is temperature dependent (Nürnberg et al., 1996; Rosenthal et al., 1997; Hastings et al., 1998; Lea et al., 1999). Li/Ca in *O. universa* along the Atlantic transect shows a general inverse relationship with Mg/Ca (Fig. 4.5). The controls on foraminiferal Sr/Ca are complex and include seawater concentration, temperature, salinity, pressure, pH, and postdepositional dissolution (e.g.; Brown and Elderfield, 1996; Rosenthal et al., 1997; Lea et al., 1999; Stoll et al., 1999; Elderfield et al., 2000; Shen et al., 2001).

4.3.4. Bahama Bank Margins

Along the Bahama Bank margins, Holocene and core top samples show that Li/Ca ratios increase with increasing water depth in *H. elegans*, *C. robertsonianus*, *P. rugosus*, *P. wuellerstorfi*, and *C. incrassatus* while there is a small mid-depth maximum present in *C. cicatricosus* and *C. pachyderma* (Fig. 4.6; Table 4.8). In contrast, foraminiferal Mg/Ca decreases with increasing water depth and decreasing temperature (Fig. 4.7) whereas Sr/Ca

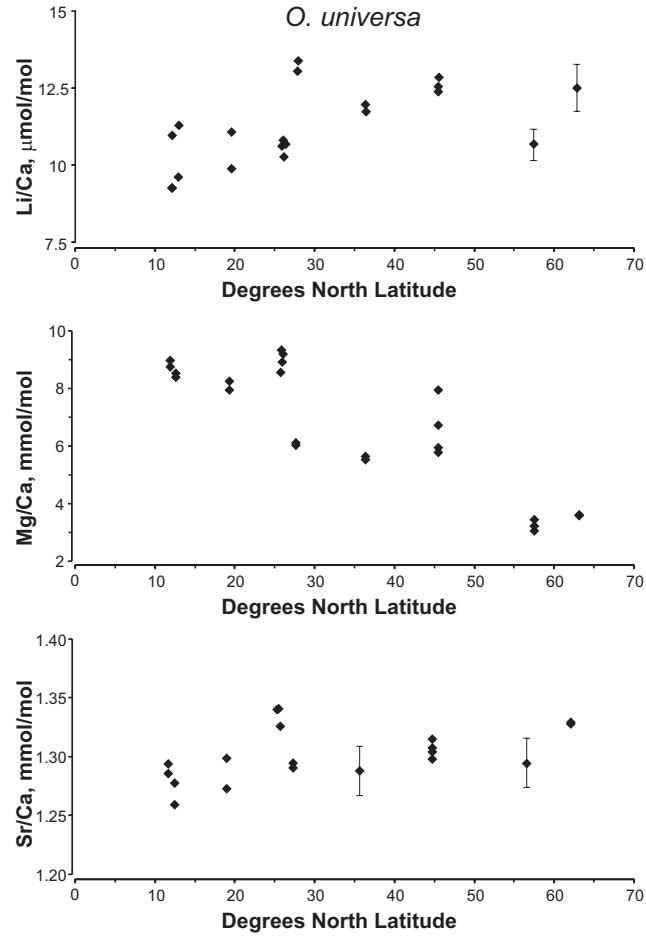


Figure 4.5. Li/Ca, Mg/Ca, and Sr/Ca from *Orbulina universa* in a core top transect of the mid-depth (1526 to 3690 m) North Atlantic from 12 to 63°N latitude. See Table 4.7 for data summary.

Table 4.7. Core top transect of Li/Ca in $\mu\text{mol/mol}$, Mg/Ca in mmol/mol , and Sr/Ca in mmol/mol from *Orbulina universa* from the North Atlantic. Bahaman cores are represented by Holocene samples.

North Atlantic	Latitude, °N	Water Depth (m)	Sample Core Depth (cm)	Li/Ca <i>O. universa</i>	Mg/Ca <i>O. universa</i>	Sr/Ca <i>O. universa</i>
KNR31-3-1-1GPC	36.45	2829	13-14	11.9	5.6	1.26
				11.7	5.5	1.32
AII94-2-91-16PC	57.49	2708	2-3	9.0	3.4	1.30
				10.3	3.2	1.25
				11.1	3.0	1.33
CHN61-10-175PC	27.88	3690	5-6	13.4	6.0	1.29
				13.0	6.1	1.29
CHN43-1-102-28PC	45.5	3012	6-7	12.5	7.9	1.32
				---	5.8	1.30
				12.4	5.9	1.31
				12.8	6.7	1.30
CHN75-2-29-19PC	12.97	3266	2-3	9.6	8.5	1.28
				11.3	8.4	1.26
CHN75-2-43-33PC	12.18	2173	2-3	9.2	9.0	1.29
				11.0	8.7	1.29
AII42-1-17-16PC	19.56	2471	3-4	9.9	8.0	1.27
				11.1	8.2	1.30
KNR54-6-100-27BC	63	1526	0-1	13.4	3.6	1.33
				11.6	3.6	1.33
			n			
OC205-2-149JPC	26.26	423	12	10.7±0.3	9.2±1.0	1.33±0.02
OC205-2-103GGC	26.07	965	13	10.3±0.5	9.3±0.9	1.34±0.04
OC205-2-97JPC	25.94	1183	16	10.6±0.4	9.0±1.4	1.35±0.05
OC205-2-7JPC	26.14	1320	5	10.9±0.5	8.9±1.0	1.44±0.03

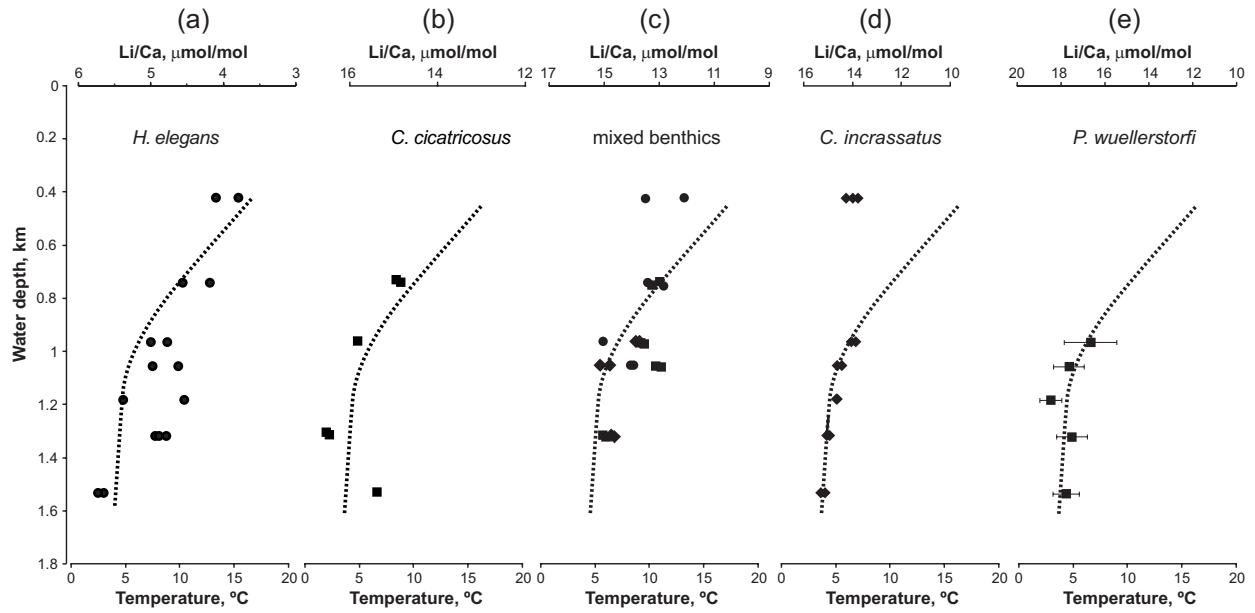


Figure 4.6. Holocene and core top measurements of Li/Ca from the Bahama Banks between 423 to 1535 m water depths in (a) *Hoeglandina elegans*, (b) *Cibicidoides cicatricosus*, (c) *Planulina rugosus* (diamond), *Cibicidoides pachyderma* (circle), *Cibicidoides robertsonianus* (square), (d) *Cibicidoides incrassatus*, and (e) *Planulina wuellerstorfi*. Bottom water temperature changes shown as dashed line. See Table 4.8 for data summary.

Table 4.8. Holocene and core top measurements of Li/Ca, Mg/Ca, and Sr/Ca in *Hoeglandina elegans*, *Cibicidoides cicatricosus*, *Cibicidoides pachyderma*, *Cibicidoides robertsonianus*, *Planulina rugosus*, *Cibicidoides incrassatus*, and *Planulina wuellerstorfi*.

Water Depth (m)	Li/Ca ($\mu\text{mol/mol}$)	Mg/Ca (mmol/mol)	Sr/Ca (mmol/mol)	Water Depth (m)	Li/Ca ($\mu\text{mol/mol}$)	Mg/Ca (mmol/mol)	Sr/Ca (mmol/mol)
<i>H. elegans</i>				■ <i>C. robertsonianus</i>			
423	3.69	1.92	2.52	743	13.2	3.71	1.46
423	4.00	2.01	2.55	743	13.0	3.71	1.46
423	---	1.95	---	965	13.7	3.03	1.44
743	4.08	1.49	2.12	965	13.7	3.40	1.47
743	4.45	1.49	2.12	1057	13.1	4.88	1.33
965	4.89	1.38	2.03	1057	12.9	4.88	1.33
965	4.67	1.38	2.17	1320	15.0	2.85	1.33
1057	4.89	1.30	1.76	1320	14.9	2.87	1.33
1057	4.53	1.30	1.76	◆ <i>P. rugosus</i>			
1183	5.28	1.31	1.78	965	13.8	2.25	1.44
1183	4.44	1.25	1.74	965	14.0	2.39	1.43
1320	4.82	1.31	1.77	965	13.8	2.54	1.49
1320	4.81	1.32	1.68	1057	15.2	3.26	1.40
1320	4.84	1.23	1.79	1057	14.8	3.26	1.40
1320	4.69	1.28	1.70	1320	14.8	1.98	1.45
1320	4.79	1.24	1.79	1320	14.7	1.99	1.45
1320	4.84	1.30	1.67	<i>C. incrassatus</i>			
1535	5.55	1.50	1.63	423	14.2	8.84	1.55
1535	5.63	1.49	1.63	423	14.0	9.53	1.61
<i>C. cicatricosus</i>				423	13.8	9.53	1.61
743	14.9	5.49	1.49	965	13.9	4.25	1.56
743	14.8	5.49	1.49	965	14.0	4.25	1.56
965	15.8	6.00	1.51	1057	14.6	4.78	1.51
965	---	4.63	1.52	1057	14.5	4.78	1.51
1320	16.5	4.02	1.30	1183	14.7	4.37	1.51
1320	16.5	4.04	1.30	1183	14.6	4.38	1.51
1535	15.4	4.40	1.38	1320	15.0	4.56	1.50
● <i>C. pachyderma</i>				1320	15.0	4.58	1.50
423	13.5	4.42	1.41	1535	15.3	4.43	1.54
423	12.1	4.42	1.41	1535	15.2	4.48	1.54
743	13.4	2.94	1.35	<i>P. wuellerstorfi</i>			
743	13.0	2.94	1.35	965	16.7 \pm 1.2	2.74 \pm 0.28	1.42 \pm 0.02
965	15.0	2.60	1.20	1057	17.7 \pm 0.7	2.62 \pm 0.23	1.41 \pm 0.05
1057	14.1	1.50	1.43	1183	18.5 \pm 0.5	2.31 \pm 0.20	1.43 \pm 0.02
1057	13.9	1.50	1.43	1320	17.5 \pm 0.7	2.33 \pm 0.14	1.38 \pm 0.05
				1535	17.8 \pm 0.6	2.20 \pm 0.17	1.36 \pm 0.03

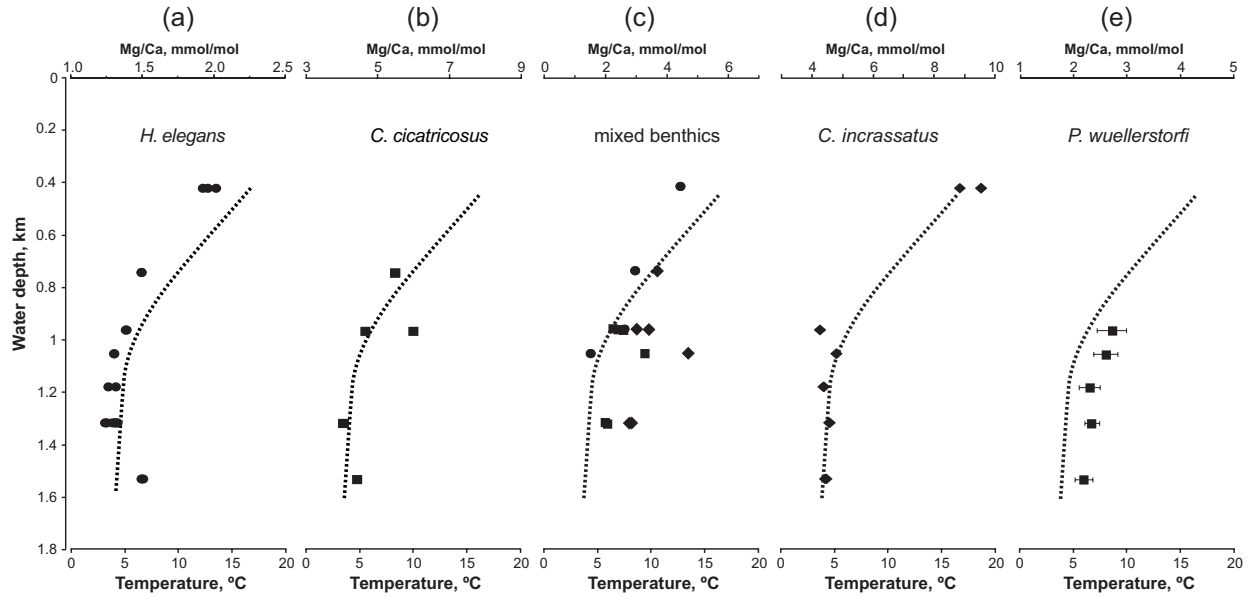


Figure 4.7. Holocene and core top measurements of Mg/Ca from the Bahama Banks between 423 to 1535 m water depths in (a) *Hoeglandina elegans*, (b) *Cibicidoides cicatricosus*, (c) *Planulina rugosus* (diamond), *Cibicidoides pachyderma* (circle), *Cibicidoides robertsonianus* (square), (d) *Cibicidoides incrassatus*, and (e) *Planulina wuellerstorfi*. Bottom water temperature changes shown as dashed line. See Table 4.8 for data summary.

decreases with increasing water depth or does not vary (Fig. 4.8). The decrease in Holocene Sr/Ca with increasing water depth is believed to be related to pressure rather than temperature effects (McCorkle et al., 1995; Elderfield et al., 1996; Rosenthal et al., 1997). Sr/Ca ratios in the aragonitic foraminifer *H. elegans* are similar to those reported in Rosenthal et al. (1997) while Mg/Ca reported in this study depicts less total variation than previously reported.

4.3.5. Interspecies Differences

Interspecies variations can be seen in down-core measurements of multiple species of benthic (*P. wuellerstorfi* and *H. elegans*) and planktonic (*O. universa*, *G. ruber*, and *G. sacculifer*) foraminifera from Bahaman core 7JPC (Fig. 4.9; Table 4.9). All species examined exhibited an increase in Li/Ca during glacial time, but the down-core distribution patterns are different among the species (Fig. 4.9). It is interesting to note that the Li/Ca incorporation in the

aragonitic species *H. elegans* is on average 60% lower than in the calcitic species *P. wuellerstorfi*. During the LGM, *P. wuellerstorfi* depicts a broad Li/Ca maximum between 67.5 and 79 cm core depth increasing by a total of 15% from the Holocene to the LGM. Aragonitic *H. elegans* shows a maximum at 77.5 cm, increasing by 25%. In contrast, *O. universa* has a maximum of Li/Ca at 63.5 cm core depth increasing by 37%, *G. ruber* depicts a broader maximum at 63.5 to 79 cm increasing by 19%, while *G. sacculifer* has no clear maximum at all but increases by 32% from the Holocene to the LGM.

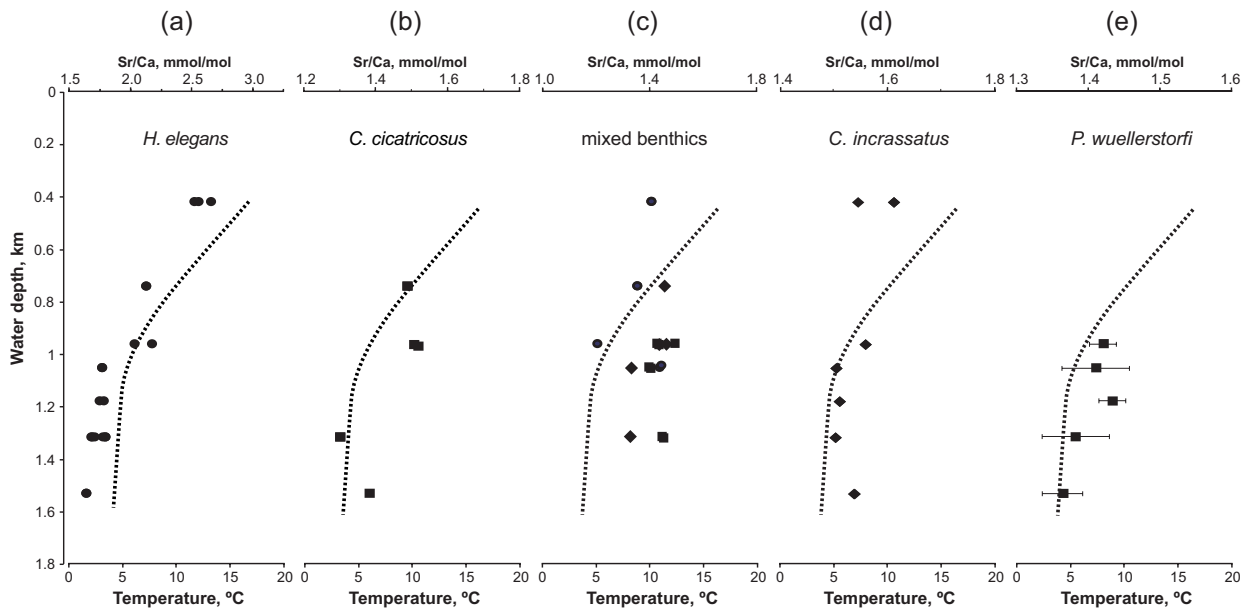


Figure 4.8. Holocene and core top measurements of Sr/Ca from the Bahama Banks between 423 to 1535 m water depths in (a) *Hoeglandina elegans*, (b) *Cibicidoides cicatricosus*, (c) *Planulina rugosus* (diamond), *Cibicidoides pachyderma* (circle), *Cibicidoides robertsonianus* (square), (d) *Cibicidoides incrassatus*, and (e) *Planulina wuellerstorfi*. Bottom water temperature changes shown as dashed line. See Table 4.8 for data summary.

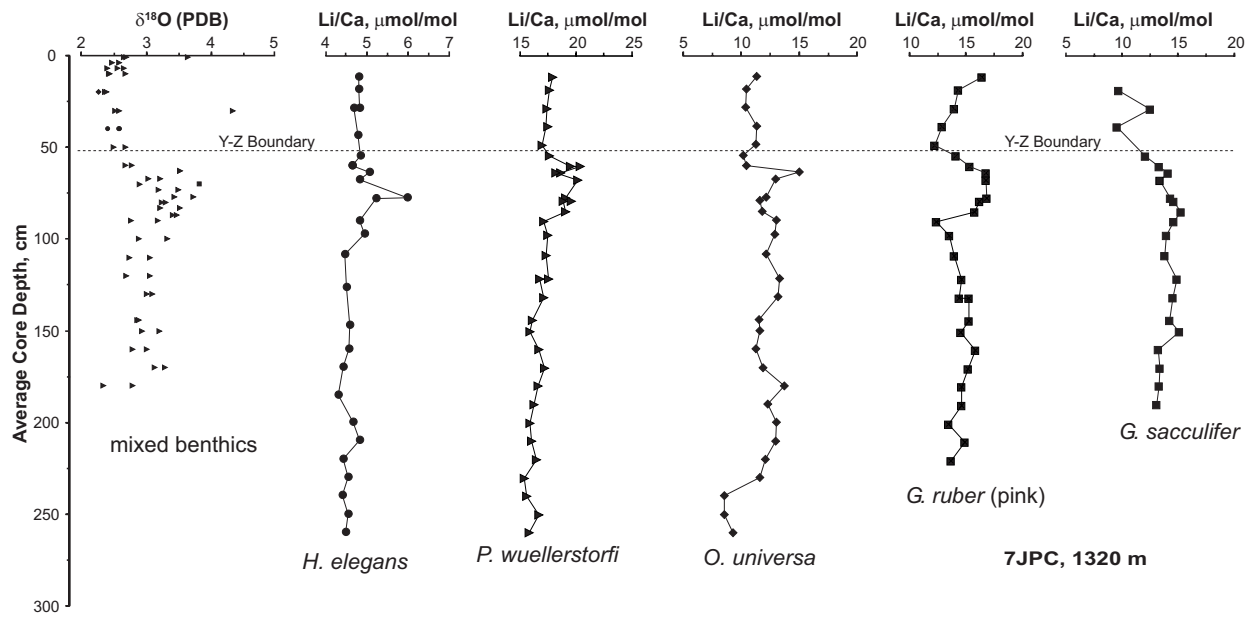


Figure 4.9. $\delta^{18}\text{O}$ from individual mixed benthic species (Slowey and Curry, 1995) from Bahaman core 7JPC and Li/Ca from *Hoeglandina elegans*, *Planulina wuellerstorfi*, *Orbulina universa*, *Globigerinoides ruber* (pink), and *Globigerinoides sacculifer*. The Y-Z boundary is based on the *Globorotalia menardii* complex (Ericson and Wollin 1956). See Table 4.9 for data summary.

Table 4.9. Li/Ca in *Hoeglandina elegans*, *Planulina wuellerstorfi*, *Orbulina universa*, *Globigerinoides ruber* (pink), and *Globigerinoides sacculifer* from Bahaman core OC205-2-7JPC.

Average Core Depth (cm)	OC205-2-7JPC, 1320 m			Li/Ca ($\mu\text{mol/mol}$)	
	<i>H. elegans</i>	<i>P. wuellerstorfi</i>	<i>O. universa</i>	<i>G. ruber</i>	<i>G. sacculifer</i>
11.5	4.8	17.9	11.3	16.4	---
18.5	4.8	17.6	10.5	14.3	9.7
28.5	4.8	17.4	10.4	14.0	12.5
28.5	4.7	---	---	---	---
38.5	---	18.6	11.3	12.8	9.6
38.5	---	16.5	---	---	---
43.5	4.8	---	---	---	---
48.5	---	17.0	11.3	12.3	---
54.5	4.8	17.7	10.2	14.1	12.1
60	4.6	19.5	10.5	15.3	13.3
60	4.6	20.4	---	---	---
63.5	5.1	18.6	15.0	16.7	14.1
63.5	---	18.2	---	---	---
67.5	4.8	20.2	13.0	16.8	13.4
77.5	6.0	19.1	12.2	16.8	14.3
78	5.2	---	---	---	---
79	---	19.6	11.6	16.2	14.6
79	---	18.9	---	---	---
85	---	19.1	11.8	15.7	15.3
90	4.8	17.1	13.0	12.4	14.6
97.5	4.9	17.5	12.9	13.5	14.0
108.5	4.5	17.3	12.2	13.9	13.8
121.5	---	17.6	13.3	14.6	14.9
121.5	---	18.9	---	---	---
126.5	4.5	---	---	---	---
131.5	---	17.1	13.1	14.4	14.5
131.5	---	---	---	15.3	---
144	---	16.1	11.5	15.2	14.2
147	4.6	---	---	---	---
150	---	15.9	11.6	14.6	15.1
160	4.6	16.7	11.3	15.8	13.2
170	4.4	17.2	11.9	15.2	13.4
180	---	16.6	13.7	14.6	13.3
185	4.3	---	---	---	---
190	---	16.3	12.3	14.6	13.1
200	4.7	15.9	13.0	13.4	---
210	4.8	16.0	12.9	14.9	---
220	4.4	16.5	12.1	13.7	---
230	4.5	15.4	11.6	---	---
240	4.4	15.6	8.6	---	---
250	4.5	16.7	8.5	---	---
260	4.5	15.9	9.3	---	---

4.4. Discussion

The sources and sinks of lithium have probably not changed during Holocene or glacial periods based on the long oceanic residence time of lithium and constant $\delta^6\text{Li}$ according the preliminary data from *O. universa* (Chapter 5). Therefore, glacial-interglacial variations in Li/Ca are likely an expression of changes in the incorporation behavior of the foraminifera due to vital or environmental effects. Li/Ca variations in multiple species of planktonic and benthic foraminifera coincident with glacial-interglacial $\delta^{18}\text{O}$ are seen consistently in the cores from this study (Fig. 4.2; Fig. 4.9). Similar findings are also reported in *G. menardii* from the northeast Indian Ocean (Burton and Vance, 2000). Burton and Vance (2000) suggest that Li/Ca variations may be caused by preferential dissolution of foraminifera in response to changes in bottom water conditions. The present data set permits evaluation of various factors that influence lithium incorporation in foraminiferal calcite.

4.4.1. Water Depth

Caribbean basin water originates from waters that flow over the sills, thus representing the properties of mid-depth Atlantic water. As such, benthic foraminiferal Li/Ca from Caribbean core VM28-129PC (3400 m depth) and the deepest Bahaman core 117JPC (1535 m depth) is used to isolate the effects of water depth on incorporation behavior. The two sites have similar bottom water temperatures of 4°C (Wüst, 1963; Slowey and Curry, 1995). During the Holocene, the average Li/Ca for *P. wuellerstorfi* from Bahaman core 117JPC is 37% higher than in the Caribbean core (Table 4.4). During the LGM, this difference is only 8%. North Atlantic Deep Water dominates water chemistry over the present day Bahama Banks between 1000 and 2000 m water depth (Slowey and Curry, 1995) while the intermediate depth water entering the Caribbean Sea consists of 85% North Atlantic Deep Water, 10% Antarctic Intermediate Water, and 5%

Mediterranean Overflow Water (deMenocal et al., 1992). At glacial time, both sites were dominated by the presence of Glacial North Atlantic Intermediate Water (Chapter 2; Boyle and Keigwin, 1987; Oppo and Fairbanks, 1987, 1990; Lea and Boyle, 1990; deMenocal et al., 1992). As Caribbean waters should be saturated with respect to calcite (Broecker and Peng, 1982; Haddad and Droxler, 1996), the relative depletion in benthic Li/Ca during both the Holocene and LGM cannot be attributed to postdepositional dissolution. While the cause of the varying degree of depletion between the Holocene and the LGM is unclear, pressure or pressure related biological effects appear to depress foraminiferal lithium incorporation. This effect may be related to a response in physiological processes under different pressure conditions.

4.4.2. Dissolution

The postdepositional dissolution of calcite is known to decrease trace element concentrations in foraminifera (McCorkle et al., 1995; Brown and Elderfield, 1996). Down-slope analyses of the planktonic foraminifer *G. sacculifer* recovered from the deep submarine Sierra Leone Rise shows the effect of increasing postdepositional dissolution with depth (Fig. 4.4). Between 2684 and 5104 m water depth, foraminiferal Li/Ca decreases by 9% under the influence of increasing dissolution (Table 4.6). The gradual decrease of foraminiferal Li/Ca with increasing water depth corresponds to a decrease in Mg/Ca and a loss in shell mass that begins to occur well above the lysocline (Rosenthal et al., 2000). This has been attributed to the magnesium content in foraminiferal calcite such that an increase in lattice bound magnesium results in a shallower Mg-calcite lysocline depth. Alternatively, it has been suggested that postdepositional dissolution may occur above the lysocline when the saturation state of sediment pore waters is less than the overlying bottom water.

4.4.3. Temperature

The calcification of foraminiferal tests is likely restricted to summer months in cold upper North Atlantic waters (Carstens and Wefer, 1992). The summer sea surface temperature at 63°N is 10°C, while the average sea surface temperature is 27°C at 12°N latitude (Levitus and Boyer, 1994). The depth habitat for *O. universa* is predominantly within 50 to 100 m water depth (Bé, 1977). Accounting for the range in habitat depth and the seasonality of the northernmost samples, the estimated range in water temperature for this transect is between 12 to 17°C (Levitus and Boyer, 1994). The latitudinal variation in foraminiferal Mg/Ca confirms the Mg-temperature association (Fig. 4.5). Using the Mg/Ca range from the northern and southern ends of the transect at 3 and 9 mmol/mol (Table 4.7) and the temperature relationship derived for *O. universa* (Lea et al., 1999), the calculated calcification temperatures are estimated at 9 to 22°C. A total change in temperature of 13°C further supports the previous estimation.

The total northward decrease in Li/Ca for this transect is 39% for a temperature change of 12 to 17°C. The estimated decrease in temperature during the LGM is at most 5°C at the sea surface (CLIMAP, 1984) and between 2 and 4°C in the thermocline (Slowey and Curry, 1995). Thus, the observed Li/Ca increase of 42% in *O. universa* between the Holocene and the LGM cannot be solely accounted for by glacial-interglacial change in temperature.

The annual sea surface temperature of the tropical Indian Ocean is similar to the Bahama Banks around 24 to 26°C (Levitus and Boyer, 1994). Planktonic *O. universa* from the Indian Ocean yields an average Li/Ca value of 10.3 ± 0.5 $\mu\text{mol/mol}$, which corresponds precisely to the Holocene values from the Bahama Banks (Table 4.2). Therefore, minor variations in temperature do not yield significant differences in Li/Ca from *O. universa*.

Benthic Li/Ca from the Bahama Banks generally increases with increasing water depth (Fig. 4.6) and decreasing temperature (from 16.5 to 4°C). The increase in Li/Ca with water depth along the Bahama Bank margins is contrary to the observed decrease in Li/Ca with increasing pressure as discussed above. Therefore, the overriding influence on the Li/Ca Bahama Bank record is not attributed to changes in pressure. An inverse relationship between Li/Ca incorporation and temperature was also observed in modern brachiopods (Delaney et al., 1989). However, temperature alone does not appear to have sufficient influence on foraminiferal lithium incorporation according to the latitudinal transect of *O. universa*. An additional factor may be temperature dependent changes in calcification rate (Lear et al., in review). Future work is needed to isolate the effects of calcification rate on lithium incorporation behavior with laboratory culture experiments.

4.4.4. Interspecies Incorporation Behavior

Li/Ca in *C. incrassatus* from the Bahama Banks shows the least variation (Fig. 4.6), while Mg/Ca shows a clear relationship with water temperature (Fig. 4.7). The lack of variation may indicate that the incorporation of lithium in this species is less susceptible to environmental conditions. In contrast, the glacial-interglacial sensitivity of Li/Ca changes in the aragonitic species *H. elegans* is 10% greater than in calcitic *P. wuellerstorfi*. However, the Li/Ca in aragonitic *H. elegans* is significantly lower than in calcitic species. Relative lithium depletion in aragonitic species is surprising because lithium is more easily coprecipitated with aragonite than with calcite in experimental inorganic mineralization of calcium carbonate (Okumura and Kitano, 1986). According to Okumura and Kitano (1986), the amount of lithium coprecipitated with calcite increases with increasing magnesium ions in the parent solution, while the amount of lithium in aragonite decreases. In addition, the amount of lithium coprecipitated with aragonite

decreases with increasing sodium chloride concentration in the parent solution. While foraminiferal lithium incorporation behavior may not be similar to inorganic mineralization, the presence of magnesium and sodium ions in seawater may enhance lithium incorporation in calcitic species and suppress it in aragonitic species.

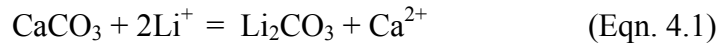
Despite these differences in interspecies variability, all species examined exhibited an increase in Li/Ca during glacial time (Fig. 4.2; Fig. 4.9). Contrary to this observation, thermodynamic calculations predict that the lithium content of calcite should decrease with decreasing temperature (Table 4.10). As foraminiferal Li/Ca increases with decreasing temperatures during glacial time, additional factors such as physiological processes must control lithium incorporation. Previous laboratory experiments suggest that the incorporation of foraminiferal trace elements may be a function of growth conditions, such as light level, food availability, and temperature dependent calcification rates (Delaney et al., 1985). This hypothesis is supported by the observed interspecies differences in down-core Li/Ca (Fig. 4.9; Table 4.9). As such, it is important to perform single species analyses for the purposes of paleoceanographic studies.

4.4.5. Calcification Rate

Monovalent cations such as lithium and sodium are non-selectively distributed in interstitial positions within the crystal structure of calcite (Onuma et al., 1979; Okumura and Kitano, 1986), but substitute for calcium in the aragonite lattice (Okumura and Kitano, 1986). The rate of precipitation significantly affects the incorporation of ions into calcium carbonate (Lorens, 1981; Lahann and Siebert, 1982; Busenberg and Plummer, 1985). Inorganic precipitation of calcium carbonate in the laboratory shows that Na/Ca (Busenberg and Plummer, 1985) and Sr/Ca (Lorens, 1981) increase with increasing precipitation rate. It is possible that

foraminiferal lithium incorporation may have increased during the LGM due to an increase in the calcification rate. This mechanism may also account for glacial-interglacial variation in Sr/Ca.

Table 4.10. The effects of temperature change on the precipitation of inorganic lithium carbonate estimated between 5 and 25°C. The thermodynamic coefficient (k_{Li}^C) in Eqn. 4.2 is determined by the ratio of the solubility products of pure calcite (K^C) and pure lithium carbonate (K^{LC}), by the ratio of the effective activity coefficients of the carbonates, and by the activity coefficients of the ions from Eqn. 4.1. Equation 4.3 is used to calculate the ratio of the solubility products, where ΔH° is the reaction enthalpy (Dean, 1992), R is the gas constant, and T is temperature in Kelvin.



$$k_{Li}^C = \frac{K^C}{K^{LC}} * \frac{\lambda_{\text{CaCO}_3}}{\lambda_{\text{Li}_2\text{CO}_3}} * \frac{\gamma_{\text{Li}^+}^2}{\gamma_{\text{Ca}^{2+}}} \quad (\text{Eqn. 4.2})$$

$$\text{Log} \left(\frac{K_{T2}}{K_{T1}} \right) = \frac{\Delta H^\circ}{2.3R} \left(\frac{1}{T_1} - \frac{1}{T_2} \right) \quad (\text{Eqn. 4.3})$$

$$\Delta H^\circ_{25^\circ\text{C}} = 5.03 \text{ kJ}$$

$$K_{5^\circ\text{C}}/K_{25^\circ\text{C}} = 0.86$$

During the LGM, there is an overall increase in Li/Ca in *P. wuellerstorfi*, with the greatest changes occurring above 1057 m water depth (Fig. 4.2). Table 4.4 shows foraminiferal Li/Ca, LGM to Holocene ratios. Although it is difficult to differentiate the effects of increasing pressure and decreasing temperature with depth, there is a noticeable decrease in the total difference in Li/Ca from the LGM to the Holocene beginning below 1057 m water depth. This may be an indication that the change in calcification rate from the LGM to the Holocene was greater in shallower waters and decreased at greater depths.

4.5. Conclusions

Li/Ca ratios vary systematically in benthic and planktonic species through the glacial-interglacial transition and are positively correlated with $\delta^{18}\text{O}$. Although different species are not all in phase with one another, all species examined exhibit an increase in Li/Ca, as high as 50%, during glacial time. Based on the long residence time calculated for lithium in the ocean and on preliminary $\delta^6\text{Li}$ data from *O. universa* (Chapter 5), the composition of Li/Ca in seawater is not expected to vary over glacial-interglacial timescales. Therefore, glacial-interglacial variations in foraminiferal Li/Ca are likely an expression of changes in incorporation behavior due to vital or environmental effects.

Future work should be directed toward the laboratory culturing of foraminiferal species to better understand the effects of calcification rate and other growth conditions on lithium incorporation behavior. Nevertheless, the following conclusions are proposed: (1) Shell mass does not appear to influence lithium incorporation in *O. universa* or *P. wuellerstorfi*. (2) Greater water depth and postdepositional dissolution cause a decrease in foraminiferal Li/Ca. (3) A latitudinal transect of *O. universa* from the North Atlantic shows that Li/Ca increases with increasing latitude and decreasing temperature. However, despite having three times the temperature variation, the total difference in Li/Ca in the transect is smaller in magnitude than the glacial-interglacial change. Therefore, glacial changes in *O. universa* Li/Ca cannot be solely attributed to temperature. (4) Benthic foraminiferal Li/Ca along the Bahama Bank margins increases with decreasing temperature but are also insufficient to account for the observed changes during glacial time. (5) Physiological factors such as calcification rate and other growth conditions may increase the Li/Ca content of foraminiferal calcite. There is a noticeable decrease in the total difference in Li/Ca from the LGM to the Holocene beginning below 1057 m

water depth in the North Atlantic. This may be an indication that the change in calcification rate from the LGM to the Holocene was greater in the surface water and decreased at intermediate depth.

4.6. References

- Bé A.W.H. (1977) An ecological zoogeographic and taxonomic review of recent planktonic foraminifera. In: *Oceanic Micropaleontology* (ed. A.T.S. Ramsay), pp. 1-100. Academic Press, London.
- Boyle E.A. (1981) Cadmium, zinc, copper, and barium in foraminifera tests. *Earth and Planetary Science Letters* **53**, 11-35.
- Boyle E.A. (1983) Manganese carbonate overgrowths on foraminifera tests. *Geochimica et Cosmochimica Acta* **47**, 1815-1819.
- Boyle E.A. and Keigwin L.D. (1987) North Atlantic thermohaline circulation during the past 20,000 years linked to high-latitude surface temperature. *Nature* **330**, 35-40.
- Broecker W.S., Ewing M., and Heezen B.C. (1960) Evidence for an abrupt change in climate close to 11,000 years ago. *American Journal of Science* **258**, 429-448.
- Broecker W.S. and Peng T.-H. (1982) *Tracers in the Sea*. Eldigio Press.
- Brown S.J. and Elderfield H. (1996) Variations in Mg/Ca and Sr/Ca ratios of planktonic foraminifera caused by postdepositional dissolution: Evidence of shallow Mg-dependent dissolution. *Paleoceanography* **11**, 543-551.
- Burton K.W. and Vance D. (2000) Glacial-interglacial variations in the neodymium isotope composition of seawater in the Bay of Bengal recorded by planktonic foraminifera. *Earth and Planetary Science Letters* **176**, 425-441.
- Busenberg E. and Plummer L.N. (1985) Kinetic and thermodynamic factors controlling the distribution of SO_4^{2-} and Na^+ in calcites and selected aragonites. *Geochimica et Cosmochimica Acta* **49**, 713-725.
- Carstens J. and Wefer G. (1992) Recent distribution of planktonic foraminifera in the Nansen Basin, Arctic Ocean. *Deep-Sea Research* **39**: S507-S524.
- Chan L.-H. and Edmond J.M. (1988) Variations of lithium isotope composition in the marine environment: A preliminary report. *Geochimica et Cosmochimica Acta* **52**, 1711-1717.
- CLIMAP Project members (1984) The last interglacial ocean. *Quaternary Research* **21**, 123-224.

- Dean J.A. (1992) *Lange's Handbook of Chemistry, fourteenth edition*. McGraw-Hill, Inc.
- Delaney M.L., Bé A.W.H., and Boyle E.A. (1985) Li, Sr, Mg, and Na in foraminiferal calcite shells from laboratory culture, sediment traps, and sediment cores. *Geochimica et Cosmochimica Acta* **49**, 1327-1341.
- Delaney M.L. and Boyle E.A. (1986) Lithium in foraminiferal shells: Implications for high-temperature hydrothermal circulation fluxes and oceanic crustal generation rates. *Earth and Planetary Science Letters* **80**, 91-105.
- Delaney M.L., Popp B.N., Lepzelter G.C., and Anderson T.F. (1989) Lithium-to-calcium ratios in modern, Cenozoic, and Paleozoic articulate brachiopod shells. *Paleoceanography* **4**, 681-691.
- deMenocal P.B., Oppo D.W., Fairbanks R.G., and Prell W.L. (1992) Pleistocene $\delta^{13}\text{C}$ variability of North Atlantic Intermediate Water. *Paleoceanography* **7**, 229-250.
- Elderfield H., Bertram C.J., and Erez J. (1996) A biomineralization model for the incorporation of trace elements into foraminiferal calcium carbonate. *Earth and Planetary Science Letters* **142**, 409-423.
- Elderfield H., Cooper M., and Ganssen G. (2000) Sr/Ca in multiple species of planktonic foraminifera: Implications for reconstructions of seawater Sr/Ca. *Geochemistry, Geophysics, Geosystems* **1**, Paper number 1999GC000031.
- Ericson D.B. and Wollin G. (1956) Micropaleontological and isotopic determinations of Pleistocene climates. *Micropaleontology* **2**, 257-270.
- Ericson D.B. and Wollin G. (1968) Pleistocene climate and chronology in deep-sea sediments. *Science* **162**, 1227-1234.
- Haddad G.A. and Droxler A.W. (1996) Metastable CaCO_3 dissolution at intermediate water depths of the Caribbean and western North Atlantic: Implications for intermediate water circulation during the past 200,000 years. *Paleoceanography* **11**, 701-716.
- Hastings D.W., Russell A.D., and Emerson S.R. (1998) Foraminiferal magnesium in *Globeriginoides sacculifer* as a paleotemperature proxy. *Paleoceanography* **13**, 161-169.
- Huh Y., Chan L.-H., Zhang L., and Edmond J.M. (1998) Lithium and its isotopes in major world rivers: Implications for weathering and the oceanic budget. *Geochimica et Cosmochimica Acta* **62**, 2039-2051.
- Lahann R.W. and Siebert R.M. (1982) A kinetic model for distribution coefficients and application to Mg-calcites. *Geochimica et Cosmochimica Acta* **46**, 2229-2237.

- Lea D.W. and Boyle E.A. (1990) Foraminiferal reconstruction of barium distributions in water masses of the glacial oceans. *Paleoceanography* **5**, 719-742.
- Lea D.W. and Boyle E.A. (1993) Determination of carbonate-bound barium in foraminifera and corals by isotope dilution plasma-mass spectrometry. *Chemical Geology* **103**, 73-84.
- Lea D.W., Mashiotta T.A., and Spero H.J. (1999) Controls on magnesium and strontium uptake in planktonic foraminifera determined by live culturing. *Geochimica et Cosmochimica Acta* **63**, 2369-2379.
- Lear C.H., Rosenthal Y., and Slowey N. (in review) Benthic foraminiferal Mg/Ca-paleothermometry: A revised core-top calibration. *Geochimica et Cosmochimica Acta*.
- Levitus S. and Boyer T.P. (1994) *World Ocean Atlas 1994 Volume 4: Temperature*. NOAA Atlas NESDIS **4**, U.S. Department of Commerce, Washington, D.C.
- Lorens R.B. (1981) Sr, Cd, Mn and Co distribution coefficients in calcite as a function of calcite precipitation rate. *Geochimica et Cosmochimica Acta* **45**, 553-561.
- Marchitto T.M., Curry W.B., and Oppo D.W. (1998) Millennial-scale changes in North Atlantic circulation since the last glaciation. *Nature* **393**, 557-561.
- McCorkle D.C., Martin P.A., Lea D.W., Klinkhammer G.P. (1995) Evidence of a dissolution effect on benthic foraminiferal shell chemistry: $\delta^{13}\text{C}$, Cd/Ca, Ba/Ca, and Sr/Ca results from the Ontong Java Plateau. *Paleoceanography* **10**, 699-714.
- Nürnberg D., Bijma J., and Hemleben C. (1996) Assessing the reliability of magnesium in foraminiferal calcite as a proxy for water mass temperature. *Geochimica et Cosmochimica Acta* **60**, 803-814.
- Okumura M. and Kitano Y. (1986) Coprecipitation of alkali metal ions with calcium carbonate. *Geochimica et Cosmochimica Acta* **50**, 49-58.
- Onuma N., Masuda F., Hirano M., and Wada K. (1979) Crystal structure control on trace element partition in molluscan shell formation. *Geochemical Journal* **13**, 187-189.
- Oppo D.W. and Fairbanks R.G. (1987) Variability in the deep and intermediate water circulation of the Atlantic Ocean during the past 25,000 years: Northern Hemisphere modulation of the Southern Ocean. *Earth and Planetary Science Letters* **86**, 1-15.
- Oppo D.W. and Fairbanks R.G. (1990) Atlantic Ocean thermohaline circulation of the last 150,000 years: Relationship to climate and atmospheric CO₂. *Paleoceanography* **5**, 277-288.
- Prell W.L. (1978) Upper Quaternary sediments of the Colombia Basin: Spatial and stratigraphic variation. *Geological Society of America Bulletin* **89**, 1241-1255.

- Rosenthal Y., Boyle E.A., and Slowey N. (1997) Temperature control on the incorporation of magnesium, strontium, fluorine, and cadmium into benthic foraminiferal shells from Little Bahama Bank: Prospects for thermocline paleoceanography. *Geochimica et Cosmochimica Acta* **61**, 3633-3643.
- Rosenthal Y., Field M.P., and Sherrell R.M. (1999) Precise determination of element/calcium ratios in calcareous samples using sector field inductively coupled plasma mass spectrometry. *Analytical Chemistry* **71**, 3248-3253.
- Rosenthal Y., Lohmann G.P., Lohmann K.C., and Sherrell R.M. (2000) Incorporation and preservation of Mg in *Globigerinoides sacculifer*: Implications for reconstructing the temperature and $^{18}\text{O}/^{16}\text{O}$ of seawater. *Paleoceanography* **15**, 135-145.
- Shen C.-C., Hastings D.W., Lee T., Chiu C.-H., Lee M.-Y., Wei K.-Y., and Edwards R.L. (2001) High precision glacial-interglacial benthic foraminiferal Sr/Ca records from the eastern equatorial Atlantic Ocean and Caribbean Sea. *Earth and Planetary Science Letters* **190**, 197-209.
- Slowey N.C. and Curry W.B. (1995) Glacial-interglacial differences in circulation and carbon cycling within the upper western North Atlantic. *Paleoceanography* **10**, 715-732.
- Stoffyn-Egli P. and Mackenzie F.T. (1984) Mass balance of dissolved lithium in the oceans. *Geochimica et Cosmochimica Acta* **48**, 859-872.
- Stoll H.M., Schrag D.P., and Clemens S.C. (1999) Are seawater Sr/Ca variations preserved in Quaternary foraminifera? *Geochimica et Cosmochimica Acta*. **63**, 3535-3547.
- Wüst G. (1963) On the stratification and the circulation in the cold water sphere of Antillean-Caribbean basins. *Deep Sea Research* **16**, 165-187.
- You C.-F. and Chan L.H. (1996) Precise determination of lithium isotopic composition in low concentration natural samples. *Geochimica et Cosmochimica Acta* **60**, 909-915.

CHAPTER 5. DETERMINATION OF THE LITHIUM ISOTOPIC COMPOSITION OF FORAMINIFERAL TESTS AND ITS APPLICATION AS A PALEO-SEAWATER PROXY

5.1. Introduction

The lithium isotopic composition of foraminifera has the potential to be used as a paleo-lithium seawater proxy. Calcareous foraminifera secrete a test from the surrounding seawater in which they live and incorporate lithium as a trace element. Lithium exhibits conservative behavior in the ocean. It has an oceanic residence time of about 1.5 Ma (Huh et al., 1998) and currently has a constant concentration (26 μM) and isotopic composition (-32‰ $\delta^6\text{Li}$) throughout the world oceans (Chan and Edmond, 1988; You and Chan, 1996; James and Palmer, 2000). The major sources of lithium to the ocean are rivers (Huh et al., 1998) and hydrothermal interaction with oceanic crust (Von Damm et al., 1985; Chan et al., 1993). Because hydrothermal and river fluxes have distinctly different isotopic signatures, at -7‰ $\delta^6\text{Li}$ (Chan et al., 1993; Bray, 2001) and -23‰ $\delta^6\text{Li}$ (Huh et al., 1998) respectively, changes in the lithium isotopic composition of seawater reflects changes in the sources of lithium to the ocean over geologic time, provided the removal rate constants do not change.

There are, as of yet, no comprehensive published results for the lithium isotopic composition of foraminiferal tests. Previous studies reporting lithium isotopic values for foraminifera failed to demonstrate precision or reproducibility and depicted unsystematic variation (You and Chan, 1996; Hoefs and Sywall, 1997; Košler et al., 2001). The difficulties associated with measuring the lithium isotopic composition of foraminiferal tests are threefold. (1) Lithium isotopes are easily fractionated due to the large relative mass difference between ^6Li and ^7Li . This mass dependent fractionation can occur during chemical separation with cation exchange columns and during instrumental analysis. (2) Current high precision techniques that

were developed to measure lithium isotopes in natural samples require a large sample size, ranging from 40 to 120 ng of lithium (Chan, 1987; Moriguti and Nakamura, 1998; Tomascak et al., 1999; James and Palmer, 2000). In comparison, several milligrams of foraminiferal shells from a sediment core horizon are required in order to yield several nanograms of lithium. Moreover, analysis of a single species is necessary to prevent the introduction of interspecies variability due to vital effects. Therefore, sample size is limited by the availability of single species foraminifera in a sediment core horizon. (3) Rigorous, labor intensive cleaning of foraminifera is necessary to remove impurities such as detrital sediments, which contain high levels of lithium compared to calcareous foraminiferal tests. Various steps are involved in the cleaning procedure to ensure that the sample has been purified of detrital, metal oxide, and organic phases in accordance with Boyle and Keigwin (1985). These phases can drastically change the lithium isotopic composition of a sample. This kind of protocol was not used in previous investigations (You and Chan, 1996; Hoefs and Sywall, 1997; Košler et al., 2001), possibly compromising the reliability of the results.

Preliminary work by You and Chan (1996) on the planktonic foraminifer *Pulleniatina obliquiloculata* from the Ontong-Java Plateau suggested large glacial-interglacial variation in the lithium inventory and isotopic composition of oceanic lithium during the past 1 Ma. Later work by Hoefs and Sywall (1997) observed large changes in the isotopic composition of mixed planktonic species from the Quaternary and Tertiary from various localities. It is possible that this variability is due in part to diagenetic alteration and interspecies variability. Using quadrupole inductively coupled plasma mass spectrometry (ICP-MS), Košler et al. (2001) investigated the planktonic foraminifers *Pulleniatina obliquiloculata* and *Globorotalia tumida* taken from the Ontong-Java Plateau and the Ceara Rise. Although the data set is limited, values

reported for *Pulleniatina obliquiloculata* are similar to the lithium isotopic composition of modern seawater, whereas *Globorotalia tumida* shows substantial variability.

Single species analyses and rigorous cleaning procedures were used in this study to investigate the potential use of lithium isotopes in foraminifera as a paleo-lithium seawater proxy. This work also expands the present body of foraminiferal $\delta^6\text{Li}$ data. Lithium measurements and isotopic analyses were conducted on seawater and the planktonic foraminifer *Orbulina universa*. The locations of the sediment and seawater samples are listed in Table 5.1. Seawater from various depths and surface sediments from the tropical Indian Ocean were collected during cruise KN162-13. Previous $\delta^6\text{Li}$ seawater studies have focused on the Atlantic and Pacific Oceans (Chan and Edmond, 1988; You and Chan, 1996; Moriguti and Nakamura, 1998; James and Palmer, 2000). This work represents the first $\delta^6\text{Li}$ seawater analyses from the Indian Ocean. A sediment core taken from the Great Bahama Bank spanning the Holocene and last glacial maximum (Slowey and Curry, 1995) was also used to investigate glacial-interglacial variation in foraminiferal $\delta^6\text{Li}$. Radiocarbon calendar ages for this core were reported by Marchitto et al. (1998).

Table 5.1. Seawater and sediment sample descriptions.

Sample	Latitude	Longitude	Water Depth (m)
<i>Bahama banks:</i>			
OC205-2-103GGC	26.07°N	78.06°W	965
<i>Indian Ocean:</i>			
KNR162-13-D7	24.50°S	69.92°E	2255
KNR162-13-CTD1	22.95°S	64.55°E	

5.2. Materials and Methods

5.2.1. Lithium Composition of Seawater

Seawater samples were collected in HCl-cleaned, polypropylene bottles from KNR162-13-CTD1 and acidified with HCl. Lithium concentrations were measured by flame emission with a Varian AA-475, atomic absorption spectrophotometer using standard additions. Salinity measurements made during the CTD cast were used to calculate chlorinity. Calcium concentrations were measured on a PerkinElmer Optima 3300DV, inductively coupled plasma-optical emission spectrometer (ICP-OES) using ICP-MS grade standards (High-Purity Standards).

5.2.2. Foraminiferal Cleaning and Li/Ca

Sediment samples of core OC205-2-103GGC taken from the Great Bahama Bank (Slowey and Curry, 1995) and dredge KNR162-13-D7 from the Indian Ocean were shaken in distilled water until disaggregated and then wet-sieved through a 150 μm polypropylene mesh. The coarse fraction remaining in the sieve was then dried in an oven for 30 minutes to an hour at 55 to 60°C. Sediments were picked for the planktonic foraminifer *O. universa*. Lithium isotopic samples were prepared from 2.5 to 5 mg of *O. universa*, containing between 40 to 70 individual tests, whereas Li/Ca samples were prepared from 0.5 mg of *O. universa*, containing between 4 to 12 individual tests. The tests were gently crushed and then purified following modified procedures from Lea and Boyle (1993). Samples were ultrasonically cleaned four times with distilled water and twice with methanol to remove detrital grains and fine clay particles. Metal oxide coatings were reduced in a solution consisting of anhydrous-hydrazine, citric-acid, and ammonium-hydroxide and organic matter was oxidized in a solution of hydrogen-peroxide and sodium-hydroxide. Sedimentary barite (BaSO_4) was dissolved in alkaline diethylenetriamine-

pentaacetic acid and then removed by rinsing with ammonium hydroxide. Any remaining adsorbed metals were leached with 0.001 N nitric acid prepared from SEASTAR™ high purity acid.

The cleaning step removing sedimentary barite was performed on Li/Ca samples only and not on $^6\text{Li}/^7\text{Li}$ samples, as lithium was later separated from the matrix for isotopic analyses. The shell material that remained in Li/Ca samples after the cleaning procedures was dissolved in 0.1 N SEASTAR™ nitric acid and simultaneously analyzed for lithium and calcium with a ThermoQuest Finnigan Element 2 inductively coupled plasma mass spectrometer at the University of Southern Mississippi.

Using the method developed by Rosenthal et al. (1999), element to calcium ratios were determined from intensity ratios with an external matrix matched standard. A multi-element standard was prepared from ICP-MS grade High-Purity Standards. This solution was standardized for lithium by isotope dilution using a Finnigan MAT 262, thermal ionization mass spectrometer (TIMS) and procedures developed by You and Chan (1996). Calcium was standardized using ICP-OES. Replicate analyses of dilute seawater were performed to monitor the reproducibility and accuracy of the method. The long-term Li/Ca values from seawater measured by ICP-MS average $2368 \pm 3.9\%$, which agrees with the average Li/Ca of $2443 \pm 1.2\%$ obtained by ICP-OES and flame emission. Precision for foraminiferal Li/Ca is about 3.5% based on replicate analyses of *O. universa* (Table 4.2).

5.2.3. Lithium Isotopic Analyses

Before loading on the ion exchange columns, the purified foraminiferal fragments were dissolved in 0.5 N HCl and diluted with sub-boiling water. Before cleaning, foraminiferal samples typically contained between 2.5 and 5 ng Li. To test the effect of sample size on

isotopic determination, a 5 ng Li sample of the lithium isotope standard L-SVEC and 100, 10, and 5 ng Li samples of seawater were processed for isotope analyses. Lithium was separated from seawater and foraminiferal samples by cation exchange chromatography based on procedures developed by You and Chan (1996).

Increased resin volume allows for a more effective separation of lithium from extraneous cations, but can also increase the amount of impurity from the resin (Moriguti and Nakamura, 1998). Two sets of cation exchange columns with different diameters were used in order to determine the effects of resin volume on isotopic separation. Both sets of columns were made of Pyrex glass and filled with Bio-Rad AG50WX8 (200-400 mesh) resin. The large columns have an internal diameter of 10 mm and were packed to a resin height of 150 mm. The small columns have an internal diameter of 8 mm and were also packed to a resin height of 150 mm. The large columns were calibrated for lithium separation with North Atlantic seawater (100 ng Li) while the small columns were calibrated with Indian Ocean seawater (100 ng Li), L-SVEC isotopic standard (50 ng Li), and 5 mg of cleaned foraminiferal tests (spiked with L-SVEC to 50 ng Li) and analyzed by flame emission. Seawater samples were processed on large columns while foraminiferal samples were analyzed on both the large and small columns.

After the sample was loaded on the columns, the resin was washed with sub-boiling water to remove anions. Samples were then eluted with 0.5 N HCl and the entire lithium fraction was collected. The separated lithium was converted to Li_3PO_4 using H_3PO_4 . Isotopic analyses were conducted on a Finnigan MAT 262 TIMS following the procedures of You and Chan, (1996). According to this technique, ${}^6\text{Li}/{}^7\text{Li}$ ratios were determined on Li^+ from the phosphate ion source using double rhenium filaments. The isotopic ratio is expressed as $\delta^6\text{Li}$ relative to the NIST lithium carbonate standard L-SVEC (Flesch et al., 1973) according to Eqn. 5.1. Using the

procedures developed by You and Chan (1996), the ${}^6\text{Li}/{}^7\text{Li}$ ratio in L-SVEC has been determined to be 0.082760. Based on repeated analyses of L-SVEC and seawater, this technique yields a precision of about $\pm 1\%$ (1σ).

$$\delta^6\text{Li} (\text{‰}) = \{ [({}^6\text{Li}/{}^7\text{Li})_{\text{sample}} / ({}^6\text{Li}/{}^7\text{Li})_{\text{L-SVEC}}] - 1 \} * 1000 \quad \text{Eqn. 5.1}$$

5.3. Results and Discussion

5.3.1. Lithium in Seawater

Lithium concentrations, Li/Cl ratios, and $\delta^6\text{Li}$ values in Indian Ocean seawater are given in Table 5.2 and their vertical distributions are shown in Fig. 5.1. The lithium concentration of Indian Ocean seawater is uniform throughout the water column with an average value of $25.4 \pm 0.2 \mu\text{mol/kg}$. Previous work by Stoffyn-Egli and Mackenzie (1984) in the North Atlantic Ocean suggests that reactions with marine sediments may cause Li/Cl ratios in deep ocean water to decrease by 2% compared to the surface water. The present study shows that there is no significant variation in Li/Cl versus depth for the tropical Indian Ocean. The Li/Cl ratio averages $9.10 \pm 0.11 \mu\text{g/g}$ throughout the water column (Table 5.2, Fig 5.1).

Indian Ocean seawater samples that were processed on the large columns and analyzed at 100 ng Li yield an average value of $-31.9 \pm 0.6\%$ $\delta^6\text{Li}$ throughout the water column (Table 5.2). Previous $\delta^6\text{Li}$ seawater analyses reported similar 1σ values at $-32.3 \pm 0.5\%$ (Chan, 1987; Chan and Edmond, 1988), $-31.4 \pm 1\%$ (You and Chan, 1996), $-29.1 \pm 0.3\%$ (Moriguti and Nakamura, 1998), $-30.84 \pm 0.9\%$ (Tomascak et al., 1999), and $-31.5 \pm 0.7\%$ (James and Palmer, 2000). Therefore, Indian Ocean seawater is statistically equivalent to Atlantic and Pacific Ocean water

values and falls within the standard seawater range suggested by James and Palmer (2000) of $-31.5 \pm 1\text{‰}$.

Table 5.2. Lithium in seawater from the tropical Indian Ocean (22°57'S, 64°33'E). The lithium isotopic composition of seawater from 201 m water depth was analyzed at 100, 10, and 5 ng Li.

Water depth (m)	Sample size Li (ng)	Temperature (°C)	Salinity (‰)	Li (μmol/kg)	Li/Cl (μg/g)	${}^6\text{Li}/{}^7\text{Li}$	$\delta^6\text{Li}$ (‰) $\pm 2\sigma_m$
23	100	26.75	35.57	25.6	9.01	0.080197	-31.0 ± 0.4
201	100	18.40	35.80	25.7	8.99	0.080090	-32.3 ± 0.9
201	10	18.40	35.80	---	---	0.080073	-32.5 ± 0.2
201	5	18.40	35.80	---	---	0.080138	-31.7 ± 0.2
1001	100	5.51	34.46	25.5	9.27	0.080076	-32.4 ± 0.2
2512	100	1.98	34.75	25.2	9.11	0.080146	-31.6 ± 0.3
4010	100	1.44	34.70	25.2	9.10	0.080102	-32.1 ± 0.7

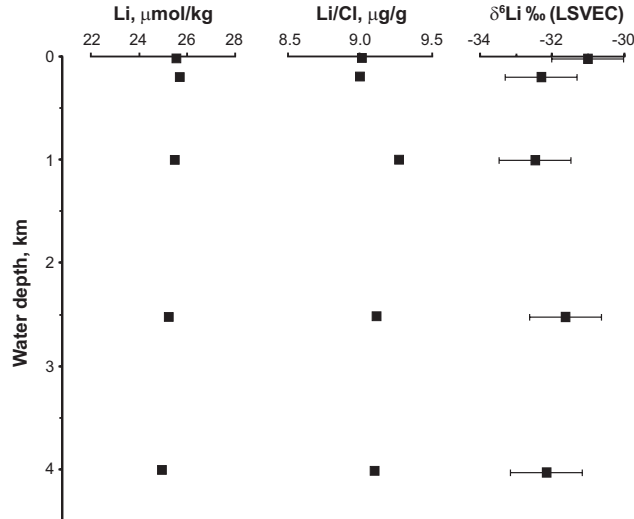


Figure 5.1. Lithium concentrations, Li/Cl ratios, and $\delta^6\text{Li}$ values in seawater from the tropical Indian Ocean (22°57'S, 64°33'E). Error bars of $\pm 1\text{‰}$ are based on external reproducibility. See Table 5.2 for data summary.

Small seawater samples containing 10 and 5 ng Li, processed on the large columns, yield $\delta^6\text{Li}$ values of $-32.5 \pm 0.2\text{‰}$ and $-31.7 \pm 0.2 \text{‰}$, respectively, which agrees with the results from 100 ng Li samples (Table 5.2). In addition, a 5 ng L-SVEC standard, passed through a large column, resulted in a $^6\text{Li}/^7\text{Li}$ ratio of 0.082684. This value falls within 1‰ of the mean value of LSVEC, based on long-term replicate analyses of 100 ng Li samples (0.082760). Hence, 5 to 10 ng Li samples are proven to yield isotopic ratios with similar precision and accuracy as 100 ng Li samples. Furthermore, this validates the use of this method on foraminiferal samples containing ≤ 5 ng Li.

5.3.2. Lithium in *O. universa*

Cleaned samples of *O. universa* were processed on the large and small columns. Samples from the Great Bahama Bank and the Indian Ocean have $\delta^6\text{Li}$ values between -29.4‰ and -32.6‰ (Table 5.3). Exceptions are samples which showed very high ^{23}Na and ^{39}K ion currents ($> 11\text{V}$) during the mass spectrometric run. These samples yielded values lower than -33‰ $\delta^6\text{Li}$. Lower $\delta^6\text{Li}$ values occurred consistently when samples were separated on the small columns and occasionally for samples processed on the large columns. Contamination with significant amounts of extraneous ions can lower the $\delta^6\text{Li}$ of the sample (Košler et al., 2001). If values from the samples with high Na and K signals are excluded from the data set, the average $\delta^6\text{Li}$ in *O. universa* is $-30.5 \pm 1.1\text{‰}$ (1σ). The mean value for the Holocene samples ($-30.7 \pm 1.4\text{‰}$) is identical within analytical uncertainty to samples from the last glacial maximum and older, thus showing no glacial-interglacial variation in lithium isotopic composition in ocean water over the last 36 ka.

Quadrupole ICP-MS data reported by Košler et al. (2001) for *P. obliquiloculata* from the Ontong-Java Plateau, range between -27.1‰ and -30.4‰ , yielding a mean of $-29.1 \pm 1.4\text{‰}$.

These values are similar to the lithium isotopic composition observed in the uncontaminated samples from the present study, suggesting that planktonic species *P. obliquiloculata* and *O. universa* may show similar isotopic fractionation during lithium incorporation.

Table 5.3. $\delta^6\text{Li}$ and Li/Ca in *Orbulina universa*. Calendar ages based on Marchitto et al. (1998).

Core depth (cm)	Calendar age (yr)	Li/Ca ($\mu\text{mol/mol}$)	$^6\text{Li}/^7\text{Li}$	$\delta^6\text{Li}$ ‰ (L-SVEC)	Comment
<i>Large column:</i>		<i>OC205-2-103GGC</i>			
8.5	434	9.3	0.080301	-29.7 ± 0.3	
17.5	1250	10.3	0.080060	-32.6 ± 0.4	
57.5	5196	10.9	0.080316	-29.5 ± 0.4	
57.5	5196	---	0.079950	-34.0 ± 0.2	Na>11V, K>11V
114	12684	11.7	0.080213	-30.8 ± 0.3	
122.5	14443	14.7	0.080313	-29.6 ± 0.3	
131	18314	14.6	0.080323	-29.4 ± 0.2	
131	18314	---	0.080242	-30.4 ± 0.1	
200	35760	13.1	0.080170	-31.3 ± 0.1	
		<i>K162-13-D7</i>			
0	0	10.5	0.079958	-33.9 ± 0.3	Na>11V, K>11V
0	0	9.9	0.080152	-31.5 ± 0.1	
0	0	10.9	0.079653	-37.5 ± 0.2	Na>11V, K>11V
---	---	10.0	---	---	
<i>Small column:</i>					
0	0	---	0.079794	-35.8 ± 0.2	Na>11V, K>11V
0	0	---	0.079841	-35.3 ± 0.1	Na>11V, K>11V
0	0	---	0.079831	-35.4 ± 0.1	Na>11V, K>11V

Only one Indian Ocean *O. universa* sample was free of contamination, yielding a $\delta^6\text{Li}$ value within analytical uncertainty of the mean value measured in the Great Bahama Bank samples. This is consistent with the homogeneous lithium isotopic composition of the oceans. Additionally, *O. universa* shells from the Indian Ocean yield an average Li/Ca value of $10.3 \pm$

0.5 $\mu\text{mol/mol}$, which corresponds precisely to the Holocene values from the Great Bahama Bank.

Based on the determinations from this work and previous studies cited above, the existing data set for seawater yields a mean $\delta^6\text{Li}$ of $-31.0 \pm 1.2\text{‰}$ (1σ), ($n = 38$). The mean $\delta^6\text{Li}$ for *O. universa* from uncontaminated samples is $30.5 \pm 1.1\text{‰}$. Thus, the fractionation factor between *O. universa* and seawater is 1.0005 ± 0.0012 , showing virtually no isotopic fractionation accompanying the formation of foraminiferal calcite. The constancy in $\delta^6\text{Li}$ is indicative that the sources and sinks of lithium in the ocean did not change significantly over the last 36 ka. Given our current understanding of lithium behavior in the ocean, the concentration and isotopic composition of lithium in foraminiferal tests are not expected to change over this glacial-interglacial timescale. These results corroborate the hypothesis that foraminiferal $\delta^6\text{Li}$ can be used as a reliable proxy of paleo-seawater lithium isotopic composition. In contrast, the average value for Li/Ca in *O. universa* during the last glacial maximum in the Bahamas is $14.8 \pm 0.3 \mu\text{mol/mol}$ and decreases to $10.3 \pm 0.5 \mu\text{mol/mol}$ in the Holocene (Fig. 5.2). Therefore, glacial-interglacial variation in Li/Ca in *O. universa* appears to be influenced by factors other than seawater composition alone (Chapter 4).

The sources of Na and K contamination are unknown. The blanks for these elements in the sub-boiling water and high purity acids are very low. A potential source is the ion exchange resin or impurities introduced during sample preparation. Although extreme care was taken throughout the sample preparation process, the effect of a slight Na or K contamination will be magnified in the ionization process in the mass spectrometer because the lithium sample is so small. Fundamental developmental work remains to be done before the lithium isotopic composition of foraminifera can be used as a proxy of seawater composition in the past.

Problems with sample contamination must be solved to improve the reproducibility of isotopic determinations. As the ion exchange resin is a potential source of contamination, further experiments with varying resin volume and elution technique may help to elucidate these uncertainties. In addition, the influences of temperature and interspecies differences need to be investigated through live culture and field experiments. The effects of postdepositional dissolution and diagenesis also need to be assessed in order to meaningfully evaluate ancient samples.

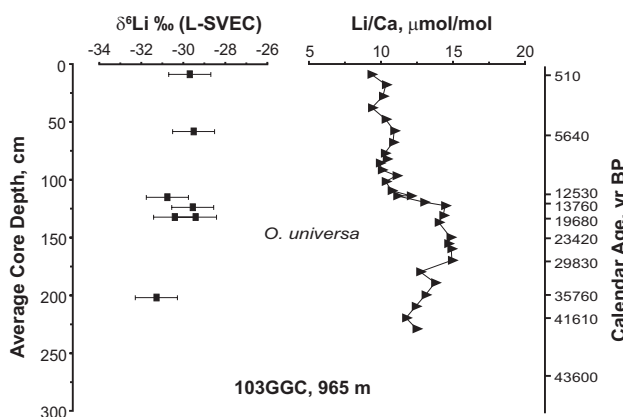


Figure 5.2. $\delta^6\text{Li}$ and Li/Ca in *Orbulina universa* from the Great Bahama Bank. Error bars of $\pm 1\text{‰}$ are based on external reproducibility. Calendar ages were reported by Marchitto et al. (1998). See Table 5.3 for data summary.

5.4. Conclusions

This investigation represents the first lithium analyses of Indian Ocean seawater. The results indicate that lithium concentrations, Li/Cl ratios, and $\delta^6\text{Li}$ values are uniform throughout the water column. The accuracy and precision of the $\delta^6\text{Li}$ method used were maintained even when very small samples (5 ng) were used. Indian Ocean seawater $\delta^6\text{Li}$ is statistically equivalent ($-31.9 \pm 0.6\text{‰}$) to Atlantic and Pacific Ocean water values ($-31.0 \pm 1\text{‰}$), confirming that lithium

isotopic composition is homogeneous in the world oceans. In contrast to previous work, a depletion of lithium in deep water by reactions with marine sediments is not seen at this site.

The isotopic fractionation accompanying the precipitation of foraminiferal calcite appears to be small. The lithium isotopic composition in down-core measurements of *O. universa* from the North Atlantic remains constant for the last 36 ka at $-30.5 \pm 1.1\%$, corresponding to $\delta^6\text{Li}$ in *O. universa* from surface sediments from the Indian Ocean. These preliminary results suggest that $\delta^6\text{Li}$ in foraminiferal tests is a potentially useful proxy for seawater composition in the past. Contamination by Na and K occurred in random samples preventing consistent high-precision measurements. Further developmental work toward high purity sample preparation is required before lithium isotopes can be confidently applied to paleoceanographic studies.

5.5. References

- Boyle E. A. and Keigwin L. D. (1985) Comparison of Atlantic and Pacific paleochemical records for the last 215,000 years: Changes in deep ocean circulation and chemical inventories. *Earth and Planetary Science Letters* **76**, 135-150.
- Bray A. (2001) The geochemistry of boron and lithium in mid-ocean ridge hydrothermal vent fluids. Ph.D. dissertation, University of New Hampshire.
- Chan L.-H. (1987) Lithium isotope analysis by thermal ionization mass spectrometry of lithium tetraborate. *Analytical Chemistry* **59**, 2662-2665.
- Chan L.-H. and Edmond J.M. (1988) Variation of lithium isotope composition in the marine environment: A preliminary report. *Geochimica et Cosmochimica Acta* **52**, 1711-1717.
- Chan L.-H., Edmond J.M., and Thompson G. (1993) A lithium isotope study of hot springs and metabasalts from mid-ocean ridge hydrothermal systems. *Journal of Geophysical Research* **98**, 9653-9659.
- Flesch G.D., Anderson A.R., and Svec H.J. (1973) A secondary isotopic standard for $^6\text{Li}/^7\text{Li}$ determinations. *International Journal of Mass Spectrometry and Ion Physics* **12**, 265-272.
- Hoefs J. and Sywall M. (1997) Lithium isotope composition of Quaternary and Tertiary biogenic carbonates and a global lithium isotope balance. *Geochimica et Cosmochimica Acta* **13**, 2679-2690.

- Huh Y., Chan L.-H., Zhang L., and Edmond J.M. (1998) Lithium and its isotopes in major world rivers: Implications for weathering and the oceanic budget. *Geochimica et Cosmochimica Acta* **62**, 2039-2051.
- James R.H. and Palmer M.R. (2000) The lithium isotope composition of internal rock standards. *Chemical Geology* **166**, 319-326.
- Košler J., Kučera M., and Sylvester P. (2001) Precise measurement of Li isotopes in planktonic foraminiferal tests by quadrupole ICPMS. *Chemical Geology* **181**, 169-179.
- Lea D.W. and Boyle E.A. (1993) Determination of carbonate-bound barium in foraminifera and corals by isotope dilution plasma-mass spectrometry. *Chemical Geology* **103**, 73-84.
- Marchitto T.M., Curry W.B., and Oppo D.W. (1998) Millennial-scale changes in North Atlantic circulation since the last glaciation. *Nature* **393**, 557-561.
- Moriguti T. and Nakamura E. (1998) High-yield lithium separation and the precise isotopic analysis for natural rock and aqueous samples. *Chemical Geology* **145**, 91-104.
- Rosenthal Y., Field M.P., and Sherrell R. M. (1999) Precise determination of element/calcium ratios in calcareous samples using sector field inductively coupled plasma mass spectrometry. *Analytical Chemistry* **71**, 3248-3253.
- Stoffyn-Egli P. and Mackenzie F.T. (1984) Mass balance of dissolved lithium in the oceans. *Geochimica et Cosmochimica Acta* **48**, 859-872.
- Tomascak P.B., Carlson R.W., and Shirey S.B. (1999) Accurate and precise determination of Li isotopic compositions by multi-collector sector ICP-MS. *Chemical Geology* **158**, 145-154.
- Von Damm K.L., Edmond J.M., Grant B., Measures C.I., Walden B., and Weiss R.F. (1985) Chemistry of submarine hydrothermal solutions at 21°N, East Pacific Rise. *Geochimica et Cosmochimica Acta* **49**, 2197-2220.
- You C.-F. and Chan L.H. (1996) Precise determination of lithium isotopic composition in low concentration natural samples. *Geochimica et Cosmochimica Acta* **60**, 909-915.

CHAPTER 6. SUMMARY AND CONCLUSIONS

6.1. Benthic Ba/Ca Record of North Atlantic Circulation Changes

The barium content of the benthic foraminifer *Planulina wuellerstorfi* was used as a refractory nutrient proxy to reconstruct changes in thermocline ventilation and mid-depth watermass circulation in the western North Atlantic during the last glacial cycle. This investigation represents the first paleo-barium data from the thermocline layer and elucidates the changes that occurred during the last deglacial transition.

Today the basal thermocline and mid-depth waters of the North Atlantic are dominated by the presence of North Atlantic Deep Water (NADW), with a minor contribution of Antarctic Intermediate Water. During the last glacial maximum (LGM), the production of NADW was greatly reduced whereas Glacial North Atlantic Intermediate Water (GNAIW) was enhanced. This resulted in an increase in ventilation of the thermocline, causing a decrease in nutrients as shown by foraminiferal $\delta^{13}\text{C}$, Cd/Ca, and Ba/Ca. The benthic record from the Bahama Banks shows that lower thermocline waters had less than 20% barium depletion during the LGM compared to the Holocene. These results indicate that, as the difference in barium concentration between the surface water and the lower thermocline is relatively small, an increase in ventilation rate had relatively little effect on barium distribution compared to $\delta^{13}\text{C}$ and Cd/Ca. This also implies that GNAIW may not have been as depleted in barium compared to cadmium depletion.

During the LGM, southern component water filled the Atlantic basin up to 2000 m water depth while NADW was replaced by GNAIW in the intermediate depth North Atlantic. Determination of Ba/Ca in benthic foraminifera from the Bahama Banks and the deep Caribbean Sea suggests that the intermediate waters between 1400 and 1800 m were between 0 to 20%

depleted in barium during the LGM. These results are consistent with previous observations in the glacial Atlantic.

During deglacial time, an increase in iceberg and meltwater discharge caused the production of GNAIW to cease. This resulted in an overall decrease in ventilation as seen by an enrichment of nutrients in the lower thermocline. GNAIW was subsequently replaced by southern component water in the mid-depth North Atlantic. The foraminiferal Ba/Ca record indicates a 38% contribution from southern component water during deglacial time at 1475 m and a 14% contribution at 1123 m water depth. Therefore, the influence of southern component water extended to shallower depths in the North Atlantic when northern watermasses were unable to form due to the presence of meltwater in the surface ocean during deglacial time.

6.2. Planktonic Ba/Ca Record of Arctic Meltwater Discharge

Ba/Ca in the planktonic foraminifer *Neogloboquadrina pachyderma* sinistral was used as a new proxy of deglacial meltwater discharge into the Arctic Ocean. Planktonic foraminifera can be used to reconstruct freshwater input because rivers are concentrated in barium compared to the surface ocean. Samples from a core taken from the Mendeleev Ridge in the western Arctic Ocean were analyzed for Ba/Ca and $\delta^{18}\text{O}$ in *Neogloboquadrina pachyderma* sinistral. *N. pachyderma* sin. incorporates barium from seawater with an apparent distribution coefficient of 0.22 ± 0.02 . Two deglacial meltwater events are identified, characterized by high foraminiferal Ba/Ca compared to core top values and corresponding low $\delta^{18}\text{O}$. These two meltwater events coincide with rapid sea level rise associated with meltwater pulses mwp-IB (9.5 ka) and mwp-IA (12 ka). The high barium concentrations calculated for the freshwater endmember during deglacial time are indicative of a continental source. The concentration of barium released between 12 ka and 11.3 ^{14}C ka BP exceeds that of the current Mackenzie River,

suggesting enhanced weathering and erosion of the bedrock during glaciation. Reconstruction of the meltwater endmember at 9.4 ^{14}C ka BP yields a concentration that is equivalent to the modern Mackenzie River value.

The reconstruction of surface water barium concentrations can be directly correlated to the ice sheet retreat and evolution of the Mackenzie River drainage basin. Expansion of the Mackenzie River drainage basin due to retreating ice caused an increase in meltwater discharge to the western Arctic Ocean, corresponding to maximum barium concentrations in the Arctic surface water at 11.8 ^{14}C ka BP. The subsequent increase in the export of freshwater from the Arctic Ocean may have led to a freshening of North Atlantic surface waters and the shutdown of GNAIW production during deglacial time (Chapter 2). The reduction in deepwater formation in the North Atlantic in turn triggered the onset of the Younger Dryas cold interval beginning around 11 ^{14}C ka BP. Although there is some question regarding the timing and magnitude, a second meltwater event at 9.4 ^{14}C ka BP may be the result of glacial Lake Agassiz flooding through the Clearwater spillway to the Mackenzie River.

6.3. Lithium in Foraminifera: A New Paleocean Tracer?

To evaluate lithium as a tracer of paleocean chemistry, factors influencing its incorporation into foraminiferal tests were systematically investigated. The parameters studied include interspecies differences, temperature, pressure, dissolution, and shell mass. Benthic and planktonic foraminifera show a systematic variation in Li/Ca through the last glacial-interglacial transition coincident with $\delta^{18}\text{O}$. Shell mass does not appear to influence lithium incorporation in *Orbulina universa* or *Planulina wuellerstorfi*. Whereas different species are not all in phase with one another, all species examined exhibit an increase (up to 50%) in Li/Ca during glacial time. In view of the long residence time of lithium in the ocean and the preliminary $\delta^6\text{Li}$ data from

Orbulina universa (Chapter 5), the composition of Li/Ca in seawater is not expected to vary over glacial-interglacial timescales. Therefore, glacial-interglacial variations in foraminiferal Li/Ca are likely an expression of changes in incorporation behavior due to vital and environmental effects.

Postdepositional dissolution and increasing water depth are shown to decrease foraminiferal Li/Ca, and do not account for glacial-interglacial variations. A latitudinal transect of planktonic *Orbulina universa* in the North Atlantic shows that Li/Ca generally increases with increasing latitude and decreasing temperature. However, the temperature dependent variation is smaller in magnitude than that observed in glacial-interglacial samples. Foraminiferal Li/Ca increases with decreasing temperature and increasing water depth in all benthic species on the slope of the Bahama Banks. This increase is attributed to temperature changes as well as biological factors that may include changes in calcification rate with depth. There is also a noticeable decrease in the difference in Li/Ca from the LGM to the Holocene beginning below 1057 m water depth in the North Atlantic. However, all of the physical parameters studied were insufficient to account for the large increase in planktonic and benthic Li/Ca observed during glacial time. Therefore, it is speculated that physiological factors such as calcification rate and other growth conditions may influence the lithium content of foraminiferal calcite.

6.4. Foraminiferal Lithium Isotopic Composition

The lithium isotopic composition of seawater and the planktonic foraminifer *Orbulina universa* were determined to investigate the use of foraminifera as a proxy for paleo-lithium seawater composition. This investigation represents the first lithium seawater analyses from the Indian Ocean showing that seawater Li/Cl ratios and $\delta^6\text{Li}$ values are uniform throughout the water column. Contrary to previous work, a depletion of lithium in seawater from reactions with

marine sediments is not seen at this site. Indian Ocean seawater $\delta^6\text{Li}$ at $-31.9 \pm 0.6\text{‰}$ is statistically equivalent to Atlantic and Pacific Ocean water values at $-31.5 \pm 1\text{‰}$. These findings are consistent with a homogeneous lithium isotopic composition for the world oceans.

The lithium isotopic composition of *Orbulina universa* from the North Atlantic remained constant over the last 36 ka at $-30.5 \pm 1.1\text{‰}$. The isotopic fractionation associated with the precipitation of foraminiferal calcite from seawater at 1.0005 ± 0.0012 appears to be small. The $\delta^6\text{Li}$ value for the Atlantic is consistent with that in *Orbulina universa* from Indian Ocean surface sediments and is indicative of the homogeneous isotopic composition between ocean basins. These preliminary results suggest that $\delta^6\text{Li}$ in foraminiferal tests can be a useful proxy for past seawater composition. However, small lithium samples (2 to 5 ng Li) are prone to contamination by extraneous ions. Contamination by Na and K occurred in some foraminiferal samples preventing high precision measurements. Therefore, the preparation of high-purity samples for isotopic determination of foraminiferal tests remains a challenge.

6.5. Future Work

The results of this dissertation demonstrate that planktonic foraminiferal Ba/Ca is a powerful tracer of meltwater discharge. As discussed in Chapter 2, the high flux of deglacial meltwater from the Laurentide Ice Sheet may have had a significant impact on ocean circulation and climate change by interrupting deepwater formation in the North Atlantic. For a more comprehensive understanding of the timing and effects of meltwater discharge from the Laurentide Ice Sheet, future work should include high resolution measurement of cores from all five of the major meltwater routes (i.e.; the Mississippi River, the Hudson River, the St. Lawrence River, the Hudson Strait, and the Arctic Ocean). Changes in nutrient distribution based on benthic foraminiferal Ba/Ca could also be reconstructed using cores from the eastern

and southern Atlantic Ocean in order to produce a three dimensional representation of glacial-interglacial changes.

The physical parameters examined in this work failed to explain the enrichment of lithium in foraminiferal tests during glacial time, suggesting the involvement of physiological factors. To better understand the effects of calcification rate and other growth conditions on foraminiferal Li/Ca incorporation behavior, future work should be directed toward laboratory culturing and field experiments.

Further developmental work in high purity sample preparation should be done to improve analytical reproducibility in lithium isotope analysis of foraminiferal shells. As the ion exchange resin is a potential source of contamination, future experimentation with resin volume and the elution technique may help to elucidate the uncertainty. The influences of temperature and interspecies differences on the lithium isotopic composition need to be investigated through live culture and field experiments. The effects of postdepositional dissolution and diagenesis should also be assessed in order to meaningfully evaluate down-core $\delta^6\text{Li}$ variations.

APPENDIX 1. FORAMINIFERAL MN/CA DATA SUMMARY

OC205-2-97JPC, 1183 m			OC205-2-117JPC, 1535 m		VM28-129PC, 3400 m	
Average Core Depth (cm)	Mn/Ca ($\mu\text{mol/mol}$)	Mn/Ca ($\mu\text{mol/mol}$)	Average Core Depth (cm)	Mn/Ca ($\mu\text{mol/mol}$)	Average Core Depth (cm)	Mn/Ca ($\mu\text{mol/mol}$)
	<i>O. universa</i>	<i>P. wuellerstorfi</i>		<i>P. wuellerstorfi</i>		<i>P. wuellerstorfi</i>
4.5	2.0	---	17	72.3	3.5	66.9
4.5	2.2	---	24.5	79.1	9	24.5
4.5	2.4	---	30	52.1	13	26.5
4.5	1.6	---	30	53.7	17	45.9
4.5	2.1	---	40	45.9	21	78.8
4.5	2.3	---	50	60.9	25	126.7
12.5	3.3	---	53	45.8	25	137.4
19.5	8.5	---	53	74.2	29	156.9
24.5	7.4	---	55.5	68.6	33	156.1
29.5	7.1	---	59	74.0	33	155.8
34.5	16.6	---	61.5	67.7	37	165.6
39.5	12.4	77.2	65.5	57.0	37	158.3
43	16.9	86.3	67.5	57.0	37	199.5
43	9.6	43.8	74	71.9	41	200.5
47	12.8	62.5	81	83.2	41	178.5
50	14.3	56.8	87	51.6	41	166.2
53	10.7	61.6	87	69.6	45	187.5
57	9.6	---	92.5	76.0	45	190.6
57	7.9	66.3	103.5	65.7	45	187.5
60	25.1	48.9	110	83.3	49	203.8
63	10.9	---	120	85.3	49	221.4
70	7.4	84.7	130	69.6	49	216.2
73	11.2	50.0	140	59.4	49	222.8
77	9.1	---	150	69.9	53	243.7
77	11.0	69.0	160	81.8	53	415.8
80	47.8	---	170	39.4	53	264.1
80	18.5	53.6	180	40.8	53	237.2
83	12.8	40.8	190	43.3	57	272.8
87	17.7	44.4	200	81.1	57	244.7
90	32.8	50.0	220	61.5	57	243.5
94.5	21.3	47.2	230	38.0	61	299.8
99.5	22.7	---	240	71.2	67	268.7
99.5	29.6	42.7	247	82.2	75	312.4
104.5	23.1	46.8			83	347.7
110	26.8	68.8			89	293.0
					93	290.6
					97	267.7
					101	279.2

Appendix 1 continued

OC205-2-149JPC, 423 m		OC205-2-100GGC, 1057 m		OC205-2-103GGC, 965 m		
Average Core	Mn/Ca	Average Core	Mn/Ca	Average Core	Mn/Ca	Mn/Ca
Depth (cm)	($\mu\text{mol/mol}$)	Depth (cm)	($\mu\text{mol/mol}$)	Depth (cm)	($\mu\text{mol/mol}$)	($\mu\text{mol/mol}$)
<i>O. universa</i>		<i>P. wuellerstorfi</i>		<i>O. universa</i>	<i>P. wuellerstorfi</i>	
3	2.4	43.5	72.2	8.5	0.8	---
19	1.2	90	76.8	17.5	5.3	---
38.5	1.5	90	100.0	27.5	6.9	---
58.5	1.4	100	97.3	37.5	10.0	---
79.5	1.1	100	116.9	47.5	8.7	---
99.5	2.4	110	56.8	57.5	12.9	---
119.5	1.0	110	55.4	67.5	18.6	---
139.5	4.6	114.5	58.2	77	8.5	176.7
159.5	1.8	114.5	56.7	82	11.9	109.2
179.5	2.3	118.5	85.7	85.5	9.6	---
199.5	7.0	118.5	70.8	91.5	10.9	---
209.5	2.1	118.5	69.5	96.5	15.4	---
219.5	4.3	123	43.5	101.5	10.1	66.5
230	5.9	126	68.1	109.5	7.7	56.4
240	10.7	129	69.1	114	5.2	73.2
247	9.5	131.5	51.6	114	10.1	---
		134.5	62.2	119.5	10.4	119.5
		137	59.6	122.5	14.2	---
		137	68.9	131	11.7	62.2
		147.5	45.0	137	18.0	---
		156	72.6	150	11.9	58.5
		156	75.3	155.5	16.4	66.6
		167	62.1	160	31.9	62.8
		167	50.7	170	15.7	56.3
		176.5	65.9	180	36.4	61.6
		190	49.1	189.5	41.2	68.7
		199.5	210.6	200	20.2	178.5
		210	56.5	210	36.5	154.7
		220	194.5	220	50.0	287.9
		230	54.7	220	---	706.1
		230	79.2	229.5	54.3	178.9
		240	79.4	240	---	49.6
		250	62.7	250	---	80.3
		260.5	95.8	259.5	---	73.6
		271	67.9	259.5	---	330.9
		280.5	75.6	259.5	---	396.2
				270	---	72.5
				280	---	335.3
				280	---	72.0

Appendix 1 continued

Average Core Depth (cm)	OC205-2-7JPC, 1320 m			Mn/Ca ($\mu\text{mol/mol}$)	
	<i>H. elegans</i>	<i>P. wuellerstorfi</i>	<i>O. universa</i>	<i>G. ruber</i>	<i>G. sacculifer</i>
11.5	0.16	18.5	17.4	18.5	---
18.5	0.24	26.9	3.4	5.4	5.7
28.5	0.16	25.6	4.6	10.9	15.9
28.5	0.20	---	---	---	---
38.5	---	36.9	11.6	25.0	19.3
38.5	---	107.4	---	---	---
43.5	0.28	---	---	---	---
48.5	---	23.3	6.8	12.9	---
54.5	0.27	54.8	8.8	18.0	47.3
60	0.34	25.7	6.7	19.6	32.7
60	0.26	29.7	---	---	---
63.5	0.23	32.7	7.7	38.8	73.6
63.5	---	37.0	---	---	---
67.5	0.20	35.4	9.4	23.6	69.1
77.5	0.47	31.4	11.4	56.5	76.0
78	0.33	---	---	---	---
79	---	36.6	9.3	37.0	90.6
79	---	36.1	---	---	---
85	---	125.4	8.2	26.3	14.3
90	0.19	76.3	8.1	20.1	36.8
97.5	0.18	46.7	8.1	11.2	12.8
108.5	0.18	86.7	9.3	9.4	16.2
121.5	---	66.2	15.7	12.4	17.3
121.5	---	42.0	---	---	---
126.5	0.16	---	---	---	---
131.5	---	35.1	5.9	11.9	12.8
131.5	---	---	---	16.3	---
144	---	93.9	18.7	33.1	117.8
147	0.12	---	---	---	---
150	---	201.9	24.5	87.4	215.5
160	0.12	276.0	46.6	185.6	331.7
170	0.15	42.5	26.7	182.8	257.9
180	---	191.8	60.8	127.9	305.5
185	0.26	---	---	---	---
190	---	45.0	82.1	143.3	303.6
200	0.14	198.9	33.7	124.6	---
210	0.28	54.4	24.6	42.8	---
220	0.25	81.1	19.9	57.4	---
230	0.24	228.9	7.5	---	---
240	0.42	37.6	9.8	---	---
250	0.40	72.9	19.5	---	---
260	0.25	33.7	25.5	---	---

Appendix 1 continued

North Atlantic transect		94B-17, 2217 m		Bahama Banks	
Core	Mn/Ca ($\mu\text{mol/mol}$)	Average Core Depth (cm)	Mn/Ca ($\mu\text{mol/mol}$)	Water Depth (m)	Mn/Ca ($\mu\text{mol/mol}$)
<i>O. universa</i>		<i>N. pachyderma</i> sinstral		<i>C. cicatricosus</i>	
KNR31-3-1-1GPC	0.7	0.5	5.9	743	47.4
	0.6	1.5	3.5	743	153.6
AII94-2-91-16PC		2.5	3.4	965	42.1
	10.2	3.5	7.0	965	63.9
	17.2	4.5	3.4	1320	20.4
	12.8	5.5	3.8	1535	32.5
CHN61-10-175PC		6.5	3.5	<i>C. robertsonianus</i>	
	18.7	7.5	5.9		
	27.3	8.5	4.7	743	1.7
CHN43-1-102-28PC		9.5	2.5	965	10.0
	11.4	10.5	2.4	965	18.2
	12.5	11.5	2.5	1057	26.9
	8.5	12.5	1.5	1320	9.0
	11.5	13.5	1.0	<i>C. incrassatus</i>	
CHN75-2-29-19PC		14.5	2.0		
	0.7	15.5	1.7	423	3.9
	1.1	16.5	1.7	423	4.4
CHN75-2-43-33PC		17.5	2.1	965	36.1
	46.4	18.5	2.6	1057	18.3
	55.1	19.5	2.0	1183	11.2
		20.5	2.0	1320	9.3
AII42-1-17-16PC	1.0			1535	62.3
	1.0			<i>C. pachyderma</i>	
KNR54-6-100-27BC	3.5			423	6.2
	1.9			743	26.9
				1057	9.1

Appendix 1 continued

APPENDIX 2. DETERMINATION OF THE Y-Z BOUNDARY

OC205-2-103GGC, 965 m				OC205-2-100GGC, 1057 m			
Average Core Depth (cm)	Sample Weight (g)	Number of <i>G. menardii</i>	Frequency	Average Core Depth (cm)	Sample Weight (g)	Number of <i>G. menardii</i>	Frequency
8.5	0.59	245	0.42	15.5	0.72	211	0.29
17.5	0.68	247	0.36	20	0.49	185	0.37
27.5	0.35	238	0.67	28.5	0.95	301	0.32
37.5	0.65	341	0.52	40.5	0.52	225	0.43
47.5	0.68	385	0.57	50	0.49	194	0.39
57.5	0.63	273	0.43	60	0.74	184	0.25
67.5	1.11	246	0.22	71.5	0.56	126	0.23
77	1.07	208	0.19	80	0.49	159	0.32
82	0.93	288	0.31	90	0.50	48	0.10
85.5	0.90	235	0.26	100	0.77	56	0.07
91.5	0.69	105	0.15	110	1.02	52	0.05
96.5	0.99	86	0.09	114.5	0.90	1	0
101.5	2.59	192	0.07	118.5	1.40	4	0
109.5	1.48	25	0.02	123	0.92	2	0
114	2.26	22	0.01	126	1.38	0	0
119.5	2.22	18	0.01	129	1.41	0	0
122.5	1.75	9	0.01	131.5	0.67	0	0
131	1.63	0	0	134.5	0.82	0	0
137	0.68	0	0	137	1.19	1	0
150	0.79	0	0	147.5	0.52	0	0
155.5	1.01	0	0	156	1.14	0	0
160	1.43	0	0	167	1.13	0	0
170	1.11	0	0	176.5	0.74	0	0
180	1.34	0	0	190	0.86	1	0
189.5	0.90	1	0	199.5	0.77	0	0
200	0.95	1	0	210	0.93	0	0
210	1.21	0	0	220	1.59	0	0
220	1.19	0	0	230	1.02	0	0
229.5	0.96	0	0	240	1.28	0	0
240	1.63	0	0	250	0.83	0	0
250	1.21	0	0	260.5	0.85	3	0
259.5	1.61	1	0	271	0.67	0	0
270	1.38	3	0	280.5	0.80	1	0
280	1.13	1	0				
Y-Z boundary = 106 cm				Y-Z boundary = 110 cm			

Appendix 2 continued

OC205-2-7JPC, 1320 m				OC205-2-117JPC, 1535 m			
Average Core Depth (cm)	Sample Weight (g)	Number of <i>G. menardii</i>	Frequency	Average Core Depth (cm)	Sample Weight (g)	Number of <i>G. menardii</i>	Frequency
11.5	1.42	278	0.20	8.5	1.29	210	0.16
18.5	0.97	231	0.24	17	0.81	181	0.22
28.5	1.45	423	0.29	24.5	0.77	225	0.29
38.5	1.66	231	0.14	30	1.01	246	0.24
48.5	1.34	132	0.10	40	1.13	65	0.06
54.5	2.30	68	0.03	50	1.84	24	0.01
60	5.14	72	0.01	53	1.65	1	0
63.5	6.33	22	0	55.5	1.52	4	0
67.5	5.05	23	0	59	1.24	0	0
77.5	2.20	16	0.01	61.5	0.67	0	0
79	2.72	22	0.01	65.5	1.29	0	0
85	2.84	29	0.01	67.5	0.71	0	0
90	2.06	84	0.04	74	0.84	1	0
97.5	2.08	72	0.03	81	1.03	0	0
108.5	2.48	72	0.03	87	1.22	0	0
121.5	2.45	437	0.18	92.5	1.09	0	0
131.5	1.49	316	0.21	110	1.60	0	0
144	2.19	360	0.16	120	2.04	0	0
150	1.20	350	0.29	103.5	1.44	0	0
160	1.37	395	0.29	130	0.72	0	0
170	1.56	400	0.26	140	1.35	1	0
180	1.59	570	0.36	150	1.96	0	0
190	2.71	902	0.33	160	2.07	0	0
200	1.85	354	0.19	170	0.70	0	0
210	2.11	281	0.13	180	1.13	5	0
220	1.49	243	0.16	190	0.81	1	0
230	1.90	270	0.14	200	1.22	6	0
240	1.30	371	0.28	210	0.57	6	0.01
250	1.60	247	0.15	220	0.87	13	0.01
260	2.05	488	0.24	230	1.22	7	0.01
270	3.70	284	0.08	240	1.02	4	0
280	4.13	237	0.06	247	1.87	1	0
288	4.21	740	0.18				
Y-Z boundary = 52 cm				Y-Z boundary = 45 cm			

Appendix 2 continued

OC205-2-149JPC, 423 m				OC205-2-97JPC, 1183 m			
Average Core Depth (cm)	Sample Weight (g)	Number of <i>G. menardii</i>	Frequency	Average Core Depth (cm)	Sample Weight (g)	Number of <i>G. menardii</i>	Frequency
3	1.25	120	0.10	4.5	2.65	164	0.06
19	0.63	26	0.04	12.5	1.46	85	0.06
38.5	0.27	20	0.07	19.5	2.95	153	0.05
58.5	0.43	54	0.12	24.5	0.50	198	0.40
79.5	0.20	21	0.10	29.5	0.63	87	0.14
99.5	0.47	43	0.09	34.5	0.89	288	0.32
119.5	0.39	39	0.10	39.5	0.55	127	0.23
139.5	0.27	33	0.12	43	0.99	98	0.10
159.5	0.54	55	0.10	47	1.03	125	0.12
179.5	1.13	35	0.03	50	1.60	195	0.12
199.5	2.34	65	0.03	53	1.32	21	0.02
209.5	2.20	43	0.02	57	2.05	4	0
219.5	6.26	15	0	60	1.65	0	0
230	4.12	1	0	63	1.40	0	0
240	4.20	1	0	70	2.05	0	0
247	1.86	0	0	77	2.87	0	0
				83	1.55	0	0
				73	3.52	0	0
				80	3.88	0	0
				87	3.27	0	0
				90	2.12	0	0
				94.5	1.93	0	0
				99.5	3.56	0	0
				104.5	5.21	0	0
				110	7.09	0	0
				115	16.98	0	0
Y-Z boundary = 170 cm				Y-Z boundary = 52 cm			

Appendix 2 continued

VITA

Jenney M. Hall was born on October 2, 1975, in Alpine, Utah. She graduated from Highland High School in 1992 and went on to graduate from Southern Utah University in 1996 with a Bachelor of Science in geology and a minor in chemistry. She then left Utah to pursue graduate study at the University of Kansas, graduating with a Master of Science in geology in 1998. She entered the doctoral program at Louisiana State University in the fall of 1998 as a Board of Regents Fellow, defended in June 2002, and will graduate in August 2002. She is currently working as a post-doctoral researcher at Yale University as a Donnelley Environmental Fellow.